รายงานวิจัยฉบับสมบูรณ์

โครงการการพัฒนาตัวเร่งปฏิกิริยาแบบใช้แสงสำหรับกระบวนการแยกน้ำเพื่อผลิตพลังงานไฮโดรเจน

โดย ดร. ธรรมนูญ ศรีทะวงศ์ และคณะ

มิถุนายน 2551

สัญญาเลขที่ MRG4980030

รายงานวิจัยฉบับสมบูรณ์

โครงการการพัฒนาตัวเร่งปฏิกิริยาแบบใช้แสงสำหรับกระบวนการแยกน้ำเพื่อผลิตพลังงานไฮโดรเจน

คณะผู้วิจัย		สังกัด
1.	ดร. ธรรมนูญ ศรีทะวงศ์	วิทยาลัยปิโตรเลียมและปิโตรเคมี จุฬาลงกรณ์มหาวิทยาลัย
2.	รศ. ดร. สุเมธ ชวเดช	วิทยาลัยปิโตรเลียมและปิโตรเคมี จุฬาลงกรณ์มหาวิทยาลัย

สนับสนุนโดยสำนักงานคณะกรรมการการอุดมศึกษา และสำนักงานกองทุนสนับสนุนการวิจัย

บทคัดย่อ

==========

รหัสโครงการ : MRG4980030

ชื่อโครงการ : การพัฒนาตัวเร่งปฏิกิริยาแบบใช้แสงสำหรับกระบวนการแยกน้ำเพื่อผลิตพลังงานไฮโดรเจน

ชื่อนักวิจัย : ดร. ธรรมนูญ ศรีทะวงศ์ วิทยาลัยปิโตรเลียมและปิโตรเคมี จุฬาลงกรณ์มหาวิทยาลัย

E-mail Address : thammanoon.s@chula.ac.th

ระยะเวลาโครงการ : 2 ปี ตั้งแต่วันที่ 1 กรกฎาคม พ.ศ. 2549 ถึงวันที่ 30 มิถุนายน พ.ศ. 2551

งานวิจัยนี้แบ่งเป็นสองส่วนหลักได้แก่ ส่วนแรก ได้ทำการศึกษาการผลิตพลังงานไฮโดรเจนจากการแยกโมเลกุลน้ำด้วยปฏิกิริยาแบบใช้แสงร่วมภายใต้ระบบที่ให้แสงในช่วงอัลตราไวโอเลต โดยใช้ตัวเร่งปฏิกิริยาไททาเนียที่มีขนาดผลึกในระดับนาโนเมตร, มีรูพรุนในระดับเมโซพอร์, และถูกใส่ตัวเร่งปฏิกิริยาร่วมแพลทินัม 0.6 เปอร์เซ็นต์โดยน้ำหนัก ซึ่งถูกสังเคราะห์โดยวิธีโซล-เจลแบบขั้นตอนเดียวแบบใช้สารลดแรงตึงผิวเป็นสารชี้นำโครงสร้าง โดยทำการศึกษาผลของตัวแปรต่างๆได้แก่ ชนิดของสารเอื้อให้เกิดปฏิกิริยา, ค่าความเป็นกรด-ด่างของสารละลายเริ่มต้น, ความเข้มข้นของตัวเร่งปฏิกิริยา, ความเข้มข้นเริ่มต้นของสารเอื้อให้เกิดปฏิกิริยา (ชนิดที่ดีที่สุด), และระยะเวลาที่ให้แสงแก่ระบบ จากการศึกษาพบว่าตัวแปรต่างๆที่กล่าวมาทั้งหมดส่งผลกระทบอย่างมากต่อการผลิตพลังงานไฮโดรเจน ซึ่งจากผลการทดลองทำให้ค้นพบค่าที่เหมาะสมของแต่ละตัวแปร จากการศึกษาในส่วนแรกนี้แสดงให้เห็นว่าการเลือกค่าตัวแปรที่เหมาะสมซึ่งส่งผลกระทบต่อการดำเนินระบบสำหรับการผลิตพลังงานไฮโดรเจนโดยใช้ตัวเร่งปฏิกิริยาดังกล่าว จะส่งผลให้ได้ค่าความสามารถในการทำปฏิกิริยาสูงเป็นที่น่าพอใจ สำหรับส่วนที่สองนั้น ได้ทำการศึกษาการปรับปรุงความสามารถของตัวเร่งปฏิกิริยาไททาเนียให้สามารถทำปฏิกิริยาภายใต้ระบบที่ให้แสงในช่วงตามองเห็นได้ โดยทำการโด๊ปไนโตรเจนลงบนตัวเร่งปฏิกิริยาไททาเนียที่มีขนาดผลึกในระดับนาโนเมตรและมีรูพรุนในระดับเมโซพอร์ซึ่งถูกสังเคราะห์โดยวิธีโซล-เจลแบบใช้สารลดแรงตึงผิวเป็นสารชี้นำโครงสร้าง เปรียบเทียบกับตัวเร่งปฏิกิริยาไททาเนียที่ไม่มีรูพรุนในระดับเมโซพอร์ซึ่งใช้ในทางการค้า (ดีกัสซา พี-25) ซึ่งการโด๊ปไนโตรเจนถูกทำโดยการเผาส่วนผสมของตัวเร่งปฏิกิริยาไททาเนียกับยูเรียซึ่งใช้เป็นแหล่งของธาตุไนโตรเจนภายใต้สภาวะที่มีปริมาณของธาตุไนโตรเจนและอุณหภูมิในการเผาค่าต่างๆ จากการศึกษาพบว่า ตัวเร่งปฏิกิริยาไททาเนียที่สังเคราะห์ขึ้นและถูกโด๊ปด้วยไนโตรเจนโดยใช้ปริมาณโดยโมลของยูเรียต่อไททาเนียและอุณหภูมิที่ใช้ในการเผาที่เหมาะสม ให้ค่าความสามารถในการทำปฏิกิริยาสูงที่สุด จากการศึกษาในส่วนที่สองนี้แสดงให้เห็นถึงความสำคัญของโครงสร้างรูพรุนในระดับเมโซพอร์ของตัวเร่งปฏิกิริยาต่อการเพิ่มความสามารถในการทำปฏิกิริยา เนื่องมาจากการเพิ่มขึ้นของพื้นที่ผิวและการเพิ่มขึ้นของความสามารถในการโด๊ปไนโตรเจน

คำหลัก : การเร่งปฏิกิริยาแบบใช้แสง, กระบวนการแยกน้ำ, การผลิตไฮโดรเจน, ไททาเนีย

Abstract

==========

Project Code : MRG4980030

Project Title : Photocatalyst Development for Photocatalytic Water Splitting Reaction for Hydrogen Evolution

Investigator : Dr. Thammanoon Sreethawong

The Petroleum and Petrochemical College, Chulalongkorn University

E-mail Address : thammanoon.s@chula.ac.th

Project Period : 2 Years from July 1, 2006 to June 30, 2008

This research was divided into two main parts. For the first part, the photocatalytic H_2 production from water splitting was investigated under various conditions over 0.6 wt% Pt-loaded nanocrystalline mesoporous TiO_2 photocatalyst prepared by a single-step sol-gel process with a structure-directing surfactant under UV light irradiation. The influence of the following operational parameters, namely sacrificial reagent type, initial solution pH, photocatalyst concentration, initial sacrificial reagent concentration (of the best sacrificial reagent studied), and irradiation time, was the main focus. The hydrogen production was found to be strongly affected by all of the above parameters. The optimum values of all of the above parameters were obtained. The results showed that the use of the photocatalyst with the proper selection of optimum operational conditions could lead to considerably high photocatalytic H_2 production activity. For the second part, N-doped mesoporous TiO_2 and N-doped non-mesoporous commercial TiO_2 (Degussa P-25) nanocrystals were comparatively investigated for photocatalytic H_2 production from water splitting under visible light irradiation. The nanocrystalline mesoporous TiO_2 was synthesized by a sol-gel process with a structure-directing surfactant. The N-doping process was performed by calcining the mixture of TiO_2 photocatalysts and urea, as a N source, at different N contents and calcination temperatures. From the experimental results, it was found that N-doped mesoporous TiO_2 prepared at a proper urea:TiO_2 molar ratio and a proper calcination temperature exhibited the highest photocatalytic activity. The results indicated the importance of the mesoporous characteristic of the photocatalyst in enhancing the photocatalytic activity by increasing the specific surface area and N-doping capability.

Keywords : Photocatalysis, Water Splitting, Hydrogen Production, Titania

Executive Summary

This research was divided into two main parts as follows. For the first part, the use of 0.6 wt.% Pt-loaded nanocrystalline mesoporous TiO_2 photocatalyst with high surface area and narrow monomodal pore size distribution, which was synthesized by a single-step sol-gel process with the aid of structure-directing surfactant, for photocatalyzing H_2 production from water under UV light irradiation was studied under various reaction conditions. Several operational parameters were investigated in order to determine the optimum conditions exhibiting the maximum H_2 production activity. The experimental results showed that methanol was found to be the most efficient sacrificial reagent among several types of sacrificial reagents investigated. Mild acidic pH values in the range of 5-6 were favorable for the reaction. The optimum photocatalyst and initial methanol concentration were found to be 0.91 g/l and 2.25 M, respectively. For the second part, two types of N-doped TiO_2 photocatalysts, namely synthesized mesoporous TiO_2 and non-mesoporous commercial TiO_2, were comparatively studied for their photocatalytic H_2 production activity under visible light irradiation. The nanocrystalline mesoporous TiO_2 photocatalyst was synthesized by a sol-gel process with the aid of structure-directing surfactant. To modify the visible light absorption ability of the TiO_2 photocatalysts, N-doping was performed. The urea, as a source of N, was mixed with both TiO_2 photocatalysts at various urea:TiO_2 molar ratios and calcined at various calcination temperatures. The optimum preparation conditions of the N-doped mesoporous TiO_2 and N-doped commercial TiO_2 for achieving the highest photocatalytic H_2 production activity were a urea:TiO_2 molar ratio of 1:1 at a calcination temperature of 250ºC and 0.5:1 at a calcination temperature of 250ºC, respectively. However, the N-doped mesoporous TiO_2 prepared at such the optimum conditions relatively exhibited the best photocatalytic activity.

เนื้อหางานวิจัย

==========

This research was divided into two main parts, as aforementioned. The details of each part can be described as follows.

Part 1: Investigation of Influence of Operational Parameters on Photocatalytic H_2 Production under UV Light Irradiation over Pt-Loaded Nanocrystalline Mesoporous TiO_2 Photocatalyst

1.1 Objective

The objective was to optimize all relevant reaction parameters for photocatalytic H_2 production from water splitting under UV light irradiation over single-step sol-gel-prepared 0.6 wt.% Pt-loaded mesoporous TiO_2 photocatalyst, aiming at obtaining maximum H_2 production activity.

1.2 Experimental Procedure

1.2.1 Materials

Tetraisopropyl orthotitanate (TIPT), hydrogen hexachloroplatinate(IV) hydrate, laurylamine hydrochloride (LAHC), acetylacetone (ACA), and methanol were used for the synthesis of Pt-loaded mesoporous TiO_2. LAHC was used as a structure-directing surfactant, behaving as a mesopore-forming agent. ACA, serving as a modifying agent, was applied to moderate the hydrolysis and condensation processes of titanium precursor. HCl and NaOH were used for the adjustment of the reaction solution pH. Various sacrificial reagents, including methanol, ethanol, 1-propanol, 2-propanol, 1-butanol, acetic acid, acetone, ethylene glycol, diethylene dioxide (1,4-dioxane), and dimethyl formamide were comparatively utilized for the photocatalytic reaction study. All chemicals were analytical grade and were used without further purification.

1.2.2 Photocatalyst synthesis procedure

Single-step sol-gel 0.6 wt.% Pt-loaded nanocrystalline mesoporous TiO_2 photocatalyst was synthesized via a combined sol-gel with the aid of structure-directing surfactant in the LAHC/TIPT modified with ACA system. In a typical synthesis, a specified amount of analytical grade ACA was first introduced into TIPT with a molar ratio of unity. The mixed solution was

then gently shaken until homogeneous mixing. Afterwards, a 0.1 M LAHC aqueous solution of pH 4.2 was added to the ACA-modified TIPT solution, in which the molar ratio of TIPT to LAHC was tailored to a value of 4:1. The mixture was continuously stirred at room temperature for an hour and was then aged at 40ºC for 10 h to obtain transparent yellow sol-containing solution as a result of the complete hydrolysis of the TIPT precursor. To the aged TiO_2 sol solution, a specific amount of hydrogen hexachloroplatinate(IV) hydrate in methanol was incorporated for a desired Pt loading of 0.6 wt.%, and the final mixture was further aged at 40ºC for one day to acquire a homogeneous solution. Then, the condensation reaction-induced gelation was allowed to proceed by placing the sol-containing solution into an oven at 80ºC for a week to ensure complete gelation. Subsequently, the gel was dried overnight at 80ºC to eliminate the solvent, which was mainly the distilled water used in the preparation of the surfactant aqueous solution. The dried sample was calcined at 500ºC for 4 h to remove the LAHC template and to consequently produce the desired photocatalyst.

1.2.3 Photocatalyst characterizations

X-ray diffraction (XRD) was used to identify the crystalline phases present in the sample. An XRD system generating monochromated Cu K_{α} radiation with a continuous scanning mode at a rate of 2º/min and operating conditions of 40 kV and 40 mA was used to obtain an XRD pattern. A nitrogen adsorption system was employed to create adsorption-desorption isotherm at the liquid nitrogen temperature of -196ºC. The Brunauer-Emmett-Teller (BET) approach, using adsorption data over the relative pressure ranging from 0.05 to 0.35, was utilized to determine the surface area of the photocatalyst sample. The Barrett-Joyner-Halenda (BJH) approach was used to determine pore size distribution from the desorption data. The sample was degassed at 200ºC for 2 h to remove physisorbed gases prior to the measurement. The sample morphology was observed by a transmission electron microscope (TEM) and a scanning electron microscope (SEM) operated at 200 and 15 kV, respectively. The elemental mappings over the desired region of the photocatalyst were detected by an energy-dispersive X-ray spectrometer (EDS) attached to the SEM.

1.2.4 Photocatalytic H_2 production experiments

The photocatalytic H_2 production reaction was performed in a closed gas-circulating system. In a typical run, a specified amount of the photocatalyst was suspended in an aqueous sacrificial reagent solution by using a magnetic stirrer within an inner irradiation reactor made of Pyrex glass. A high-pressure Hg lamp (300 W, λ_{max} of 365 nm) emitting UV light was utilized as

the light source. The initial solution pH was adjusted to a desired value by adding a few drops of either HCl or NaOH aqueous solution with an appropriate concentration. Prior to the reaction, the mixture was left in the dark while being simultaneously thoroughly deaerated by purging the system with Ar gas for 30 min. Afterwards, the photocatalytic reaction system was closed, and the reaction was started by exposing the photoreactor to the light irradiation. To avoid heating of the solution during the course of the reaction, water was circulated through a cylindrical Pyrex jacket located around the light source. The gaseous H_2 evolved was collected at different intervals of irradiation time and was analyzed by an on-line gas chromatograph, which was connected to a circulation line and equipped with a thermal conductivity detector (TCD). Different operational parameters were quantitatively varied in order to obtain the optimum conditions for the maximum photocatalytic H_2 production over the Pt-loaded mesoporous TiO_2 photocatalyst. These operational parameters included sacrificial reagent type, initial solution pH, photocatalyst concentration, initial sacrificial reagent concentration (of the best sacrificial reagent), and irradiation time.

1.3 Results and Discussion

1.3.1 Photocatalyst characterizations

Figure 1.1 shows the nitrogen adsorption-desorption isotherm and pore size distribution of the 0.6 wt.% Pt-loaded mesoporous TiO_2 photocatalyst. The isotherm in Figure 1.1(a) is of typical type IV pattern with hysteresis loop, which is a marked characteristic of mesoporous materials, according to the IUPAC classification. The well-defined hysteresis loop with a sloping adsorption branch and a relatively steep desorption branch belongs to H2 type. It is well known that a distribution of various sized cavities, but with the same entrance diameter, would be attributed to this type of hysteresis loop. As can be seen from Figure 1.1(b), a narrow monomodal pore size distribution, centered at a pore diameter in the mesopore region of 2-50 nm, can be obtained from the material synthesized by the synthesis system, suggesting its exquisite quality. The textural properties of the photocatalyst are listed as follows: BET surface area = 89 m^2/g, mean pore diameter = 5.06 nm, and total pore volume = 0.162 cm^3/g.

(a)

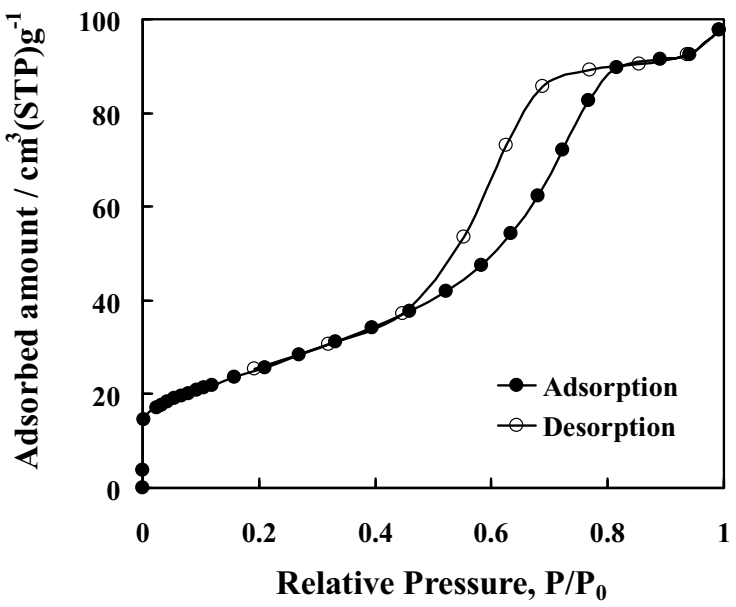

(b)

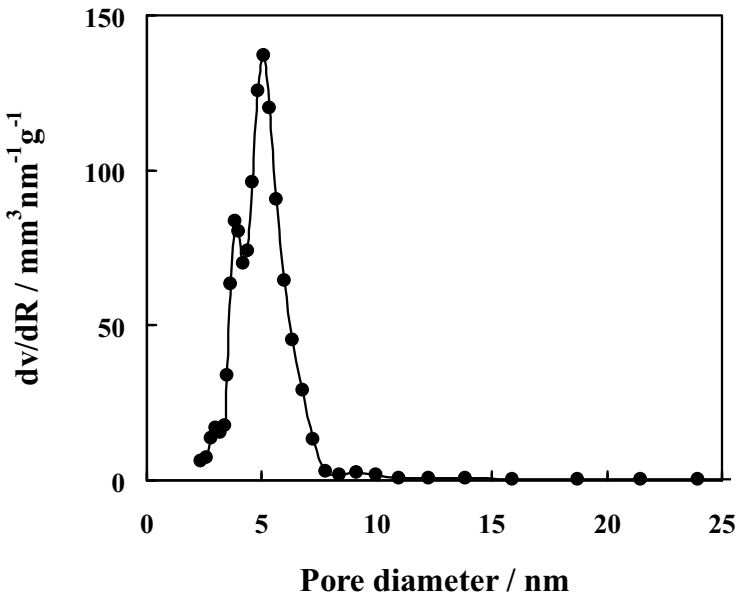

Figure 1.1 N_2 adsorption-desorption isotherm (a) and pore size distribution (b) of the synthesized mesoporous Pt/TiO_2 photocatalyst.

The crystalline structure of the synthesized mesoporous Pt/TiO_2 photocatalyst revealed by XRD analysis is shown in Figure 1.2. The diffractrogram is indexed to pure anatase TiO_2 (JCPDS Card No.21-1272) with high crystallinity. From the XRD result, the indistinguishable presence of the diffraction peaks of Pt indicates that the Pt particles were in a very high dispersion degree. As the minimum detection limit of the XRD technique is around 5 nm, it is inferred that the crystallite size of the Pt particles was below that value. The crystallite size of TiO_2 particles, estimated from line broadening of anatase (101) diffraction peak using Sherrer

formula, was approximately 11 nm. The particle sizes of Pt and TiO_2 from the TEM analysis are in the region of 1-2 and 10-15 nm, respectively, as depicted by the TEM image in Figure 1.3. The observed particle size of TiO_2 is in good accordance with the crystallite size calculated from the XRD result. In addition, homogeneously dispersed Pt nanoparticles on the TiO_2 surface are clearly seen from the TEM image.

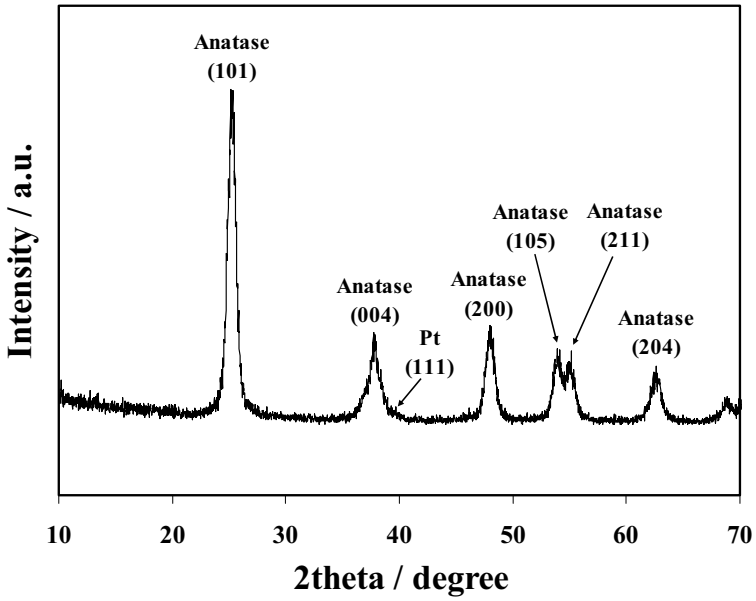

Figure 1.2 XRD pattern of the synthesized mesoporous Pt/TiO_2 photocatalyst.

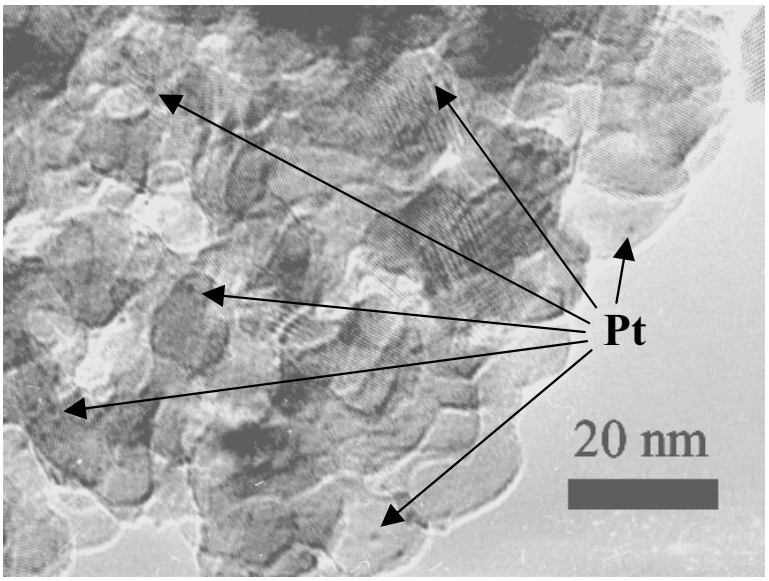

Figure 1.3 TEM image of the synthesized mesoporous Pt/TiO_2 photocatalyst.

The surface morphology of the synthesized photocatalyst was further investigated by using SEM. The acquired image is presented in Figure 1.4. In the photocatalyst micrograph, particles with quite uniform size can be observed in aggregated clusters consisting of many nanoparticles. It can be seen that the photocatalyst was highly mesoporous, which is apparent by the SEM image. EDS analysis also provided useful information about the elemental distribution on the photocatalyst, as included in Figure 1.4 by the elemental mapping of each component. The existence of dots in the elemental mapping images reveals the presence of all the investigated (Ti, O, and Pt) species. The EDS mappings reveal that all elements in the Pt-loaded TiO_2 were well distributed throughout the bulk photocatalyst, especially the investigated Pt species. This is another good verification of the high dispersion state of the deposited Pt nanoparticles. According to the N_2 adsorption-desorption, TEM, and SEM results, it is additionally worthwhile to emphasize that the mesoporous structure of the synthesized photocatalyst can be attributed to the pores formed between the nanocrystalline TiO_2 particles due to their aggregation.

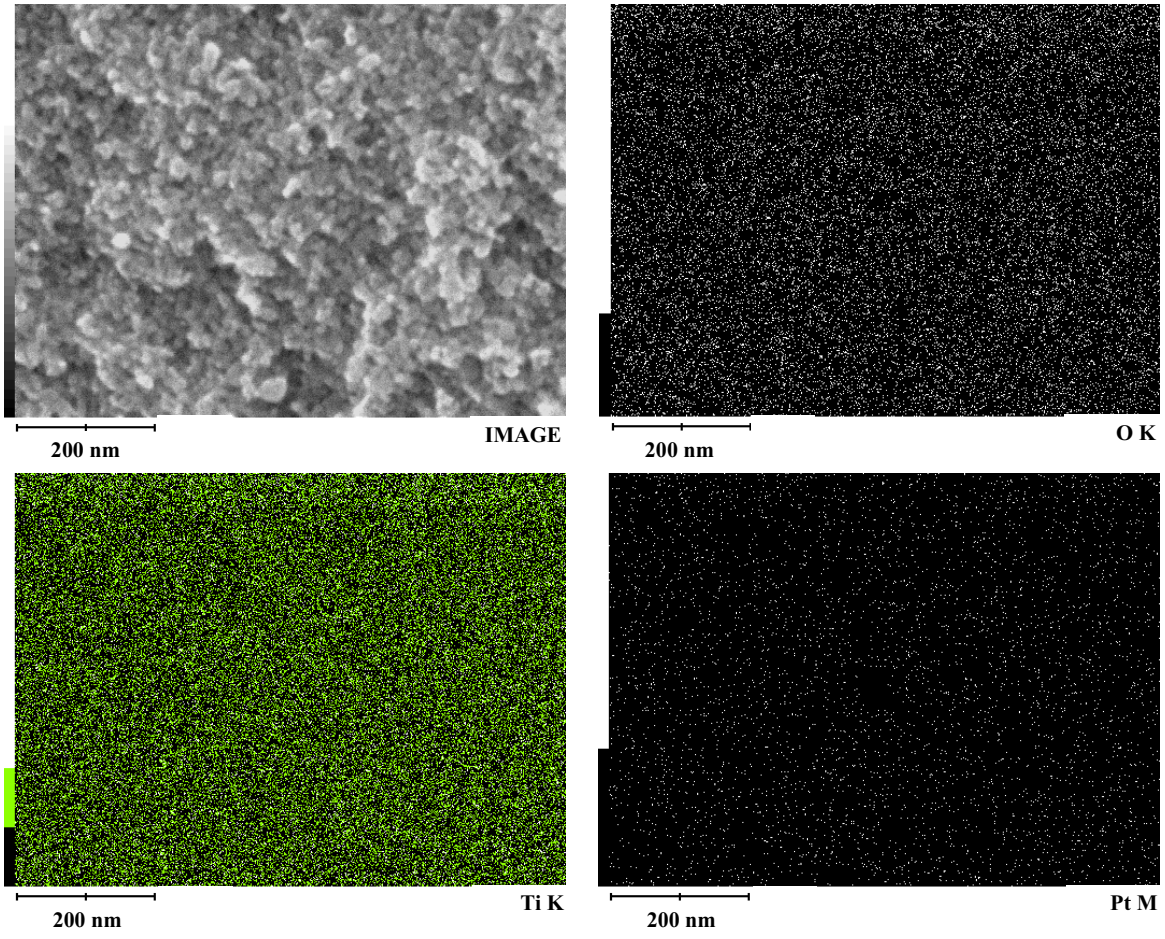

Figure 1.4 SEM image and elemental mappings of the mesoporous Pt/TiO_2 photocatalyst.

1.3.2 Photocatalytic H_2 production activity

1.3.2.1 Effect of sacrificial reagent type

In photocatalytic water splitting for H_2 production, the oxidation of water by holes is a much slower process than the reduction by electrons. In order to smooth the progress of the oxidation, sacrificial reagents or hole scavengers are often introduced, especially for the principal purpose of preventing the mutual electron-hole recombination process. Once the holes are scavenged from the photocatalyst surface, the longer decay time of surface electrons would certainly facilitate the reduction of protons in the solution to form hydrogen on the Pt active sites. It is also definitely important to first mention that no hydrogen production activity was experimentally observed for the blank tests (without photocatalyst or without sacrificial reagent).

Initially, various types of sacrificial reagents were tested for the photocatalytic H_2 production to find which type of sacrificial reagent is the most effective in assisting the photocatalytic reaction. An aqueous solution containing the same amount of various sacrificial reagents was thus illuminated under identical reaction conditions. Table 1.1 shows the photocatalytic H_2 production activity of the synthesized nanocrystalline mesoporous Pt/TiO_2 photocatalyst using various sacrificial reagents, and Figure 1.5 also shows the photocatalytic H_2 production profiles and activity using different sacrificial reagent types in an alcohol series. The results show that among the investigated sacrificial reagents, those in the alcohol series exhibited considerably higher photocatalytic activity than others. This might be attributable to the ease in donating lone-pair electrons to the valence band hole upon the photocatalyst excitation, as compared to other types of sacrificial reagents. Among the alcohol series itself, methanol was found to be the most effective and strongest sacrificial reagent to yield the highest photocatalytic H_2 production activity. It appears that compounds possessing very high polarity, such as acids and ketones, are unable to effectively suppress the electron-hole recombination, probably due to their stable electronic configuration. Apart from that, the carbon-to-carbon bond breaking also plays an important role in differentiating photocatalytic activity, since it directly involves the lone-pair electron donation. The extent of the carbon-to-carbon bond breaking decreases with the increase in chain elongation and complexity, as these factors contribute to enhancing the steric hindrance in the molecule. Since methanol was experimentally verified to be the most effective sacrificial reagent for the investigated system using the synthesized mesoporous Pt/TiO_2 photocatalyst, it was used as the main studied sacrificial reagent in further experiments.

Table 1.1 Effect of various sacrificial reagent types on photocatalytic H_2 production activity of the synthesized mesoporous Pt/TiO_2 photocatalyst (Reaction conditions: photocatalyst amount, 0.2 g; distilled water amount, 200 ml; sacrificial reagent amount, 20 ml; irradiation time, 5 h)

Type of sacrificial reagent	Molecular structure of sacrificial reagent	H_2 production activity (μmol/h)
Methanol	CH_3OH	1,385
Ethanol	CH_3CH_2OH	1,123
1-Propanol	$CH_3CH_2CH_2OH$	775
2-Propanol	$CH_3CH(OH)CH_3$	599
1-Butanol	$CH_3\ CH_2CH_2CH_2OH$	629
Acetic acid	CH_3COOH	78
Acetone	CH_3COCH_3	22
Ethylene glycol	$OHCH_2CH_2OH$	451
Diethylene dioxide (1,4-Dioxane)	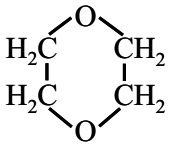	292
Dimethyl formamide	$HCON(CH_3)_2$	87

(a)

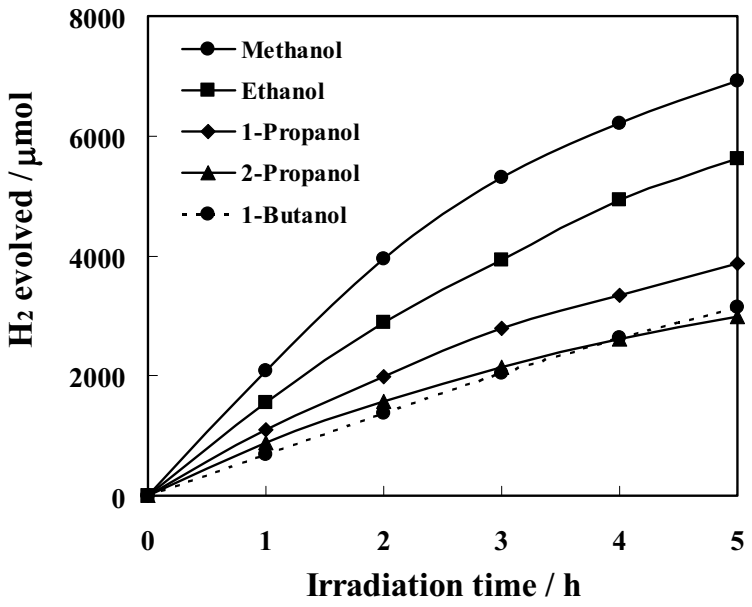

(b)

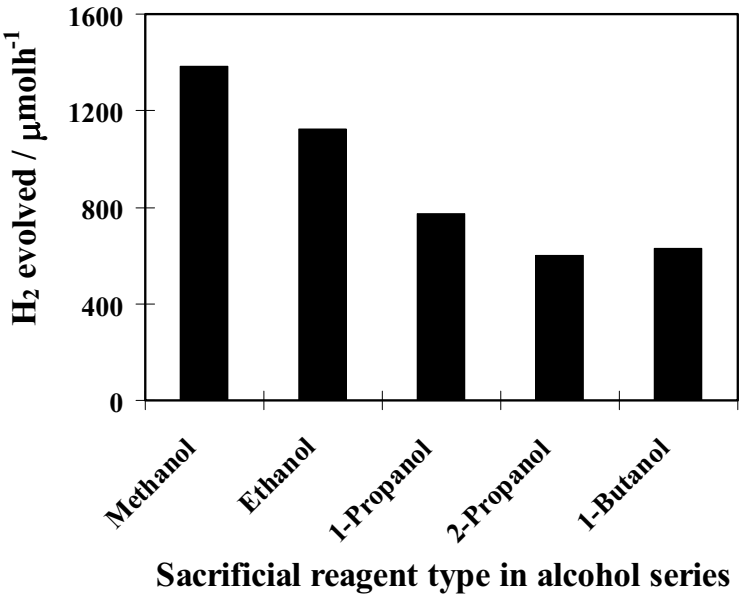

Figure 1.5 Effect of sacrificial reagent type in alcohol series on (a) time course of H_2 evolved and (b) dependence of photocatalytic H_2 production activity of the synthesized mesoporous Pt/TiO_2 photocatalyst (Reaction conditions: photocatalyst amount, 0.2 g; distilled water amount, 200 ml; sacrificial reagent amount, 20 ml; and irradiation time, 5 h).

1.3.2.2 Effect of initial solution pH

One of the important parameters affecting the photocatalytic reactions taking place on the photocatalyst surfaces is the solution pH, since it primarily dictates the surface charge properties of the photocatalyst. In addition, the solution pH can affect the states of both reactant

in solution and photocatalyst surface, which ultimately changes the electrostatic interaction between the reactant and the TiO_2 surface. The role of initial solution pH on the photocatalytic H_2 production activity was studied over a broad pH range of 2-10.5 using methanol as a sacrificial reagent, noting that the initial pH of the original solution containing 200 ml distilled water and 20 ml methanol (2.25 M) is 5.8, and insignificant changes of solution pH were observed after the course of the photocatalytic reaction. The experimental results shown in Figure 1.6 indicate that the efficiency of the H_2 production activity increases with an increase in solution pH from 2 to a range of 5-6, and a further increase in solution pH greater than 6 led to a drastic decrease in the H_2 production activity. The results imply that the H_2 production activity of the studied photocatalyst is favorable at mild acidic conditions, and the optimum initial solution pH is around 6.

The effect of solution pH on the efficiency of the photocatalytic H_2 production process is quite complicated since it contributes to several roles. It is first related to the ionization state of the photocatalyst surface according to the following reactions:

$$Ti^{IV}—OH + H^{+} \rightarrow Ti^{IV}—OH_2^{+} \quad , pH < pH_{PZC} \tag{1.1}$$

$$Ti^{IV}—OH + OH^{-} \rightarrow Ti^{IV}—O^{-} + H_2O \quad , pH > pH_{PZC} \tag{1.2}$$

As known, a pH change can influence the adsorption of these species onto the TiO_2 photocatalyst surfaces, an important step for the photocatalytic reactions to take place. The point of zero charge (PZC) of the TiO_2 is approximately at pH 5.8-6.0. Therefore, at a pH < pH_{PZC}, the TiO_2 surface is positively charged, whereas at a pH > pH_{PZC}, the TiO_2 surface is negatively charged. At acidic pHs (pH < 5), an electrostatic repulsion between the positively charged surface of the photocatalyst and the hydronium cations (H^{+}) present in the solution retards the adsorption of the hydronium cations so as to accordingly be reduced to form hydrogen, resulting in a lower photocatalytic H_2 production activity. In the opposite manner, at alkaline pHs (pH > 7), an electrostatic repulsion between the negatively charged surface of the photocatalyst and the molecules of the sacrificial reagent (lone-pair electron donor) also inhibits the adsorption of the sacrificial reagent as to scavenge the valence band holes for preventing electron-hole recombination. Besides, the photogenerated electrons cannot easily transfer to the photocatalyst surface, plausibly because of the negative charge repulsion, and subsequently transfer to outer system via the photocatalytic reduction reaction. Therefore, the electrons moving inside the bulk photocatalyst have high probability to recombine with holes at both bulk trap and defect sites. A higher rate of mutual recombination also consequently results in a lower photocatalytic H_2 production activity. These basically imply that complicated interactions between the species/molecules and the photocatalyst are taking place at acidic or alkaline

conditions. When the photocatalyst contains no charge, the species/molecules are probably allowed to much more easily reach the photocatalyst surface and achieve higher photocatalytic reaction activity, thus experimentally obtaining the highest H_2 production activity at the initial solution pHs near the point of zero charge.

(a)

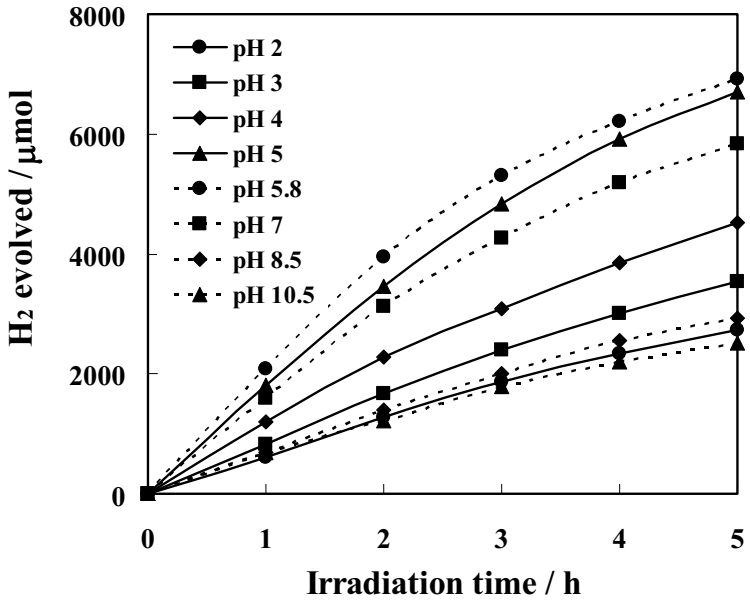

(b)

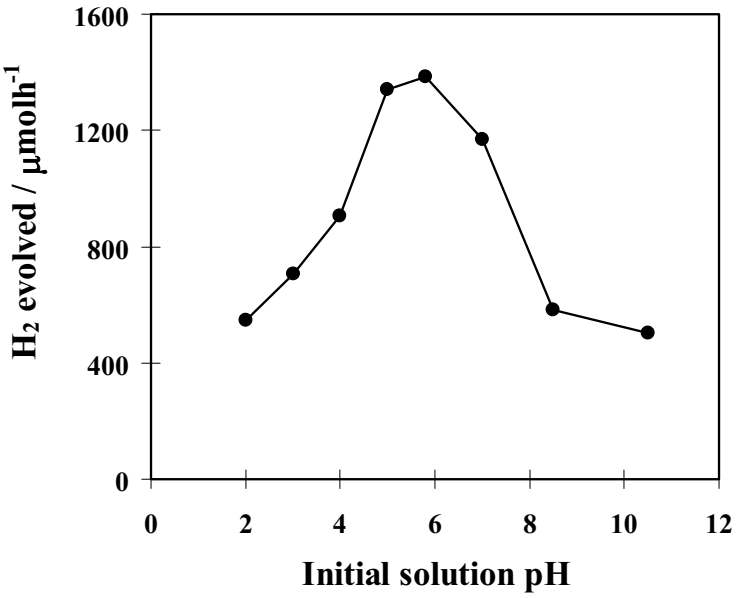

Figure 1.6 Effect of initial solution pH on (a) time course of H_2 evolved and (b) dependence of photocatalytic H_2 production activity of the synthesized Pt/TiO_2 photocatalyst (Reaction conditions: photocatalyst amount, 0.2 g; distilled water amount, 200 ml; sacrificial reagent type, methanol; sacrificial reagent amount, 20 ml; and irradiation time, 5 h).

The TiO_2 particles, moreover, tend to agglomerate under acidic conditions. This agglomeration can result in a lower surface area available for reactant adsorption and photon absorption, leading to a decrease in the photocatalytic activity; whereas another reason for the decrease in the photocatalytic activity under alkaline conditions can be attributed to the UV screening of the TiO_2 particles due to a higher concentration of OH^- present in the solution. Hence, the solution pH plays an important role both in the characteristics of reactant species-containing solutions and in the reaction mechanisms that can contribute to the H_2 production.

1.3.2.3 Effect of photocatalyst concentration

The effect of the concentration of the synthesized nanocrystalline mesoporous Pt/TiO_2 photocatalyst on the photocatalytic H_2 production was investigated in the range of 0-1.82 g/l by varying the amount of photocatalyst added to the reactor containing an original aqueous 2.25 M methanol solution (pH 5.8) without pH adjustment. Figure 1.7 illustrates the photocatalytic H_2 production activity as a function of photocatalyst concentration. The H_2 production activity first increased and then decreased with an increase in the photocatalyst amount added to the reactor. A higher concentration of the photocatalyst is expected to correspond to a greater absorption of UV energy, leading to a higher photocatalytic H_2 production activity. However, the activity began to decline when the concentration of the photocatalyst exceeded 0.91 g/l, indicating that the addition of the photocatalyst has to be optimized.

The obtained experimental results can be rationalized in terms of the availability of active sites on the TiO_2 surface and the light penetration of photoactivating light into the suspension. The availability of active sites increases with the increase in photocatalyst concentration in the suspension, but the light penetration and the consequent photoactivated volume of the suspension shrink. The penetration of light is cloaked in the reactor by the large quantity of the photocatalyst in the aqueous solution. When the photocatalyst concentration is very high, after traveling a certain distance on an optical path, turbidity impedes the further penetration of light in the reactor, indicating the block of the illuminating light. Although the light absorption of the outer photocatalyst increases, the capability of generating hydrogen from the inner photocatalyst decreases due to the lack of photoexcitation, signifying the screening effect of excess photocatalyst particles in the solution. Consequently, the overall H_2 production activity decreases with a very high concentration of the photocatalyst. Moreover, the decrease in the photocatalytic activity at a higher photocatalyst concentration may be due to the deactivation of activated TiO_2 molecules by the collision with ground-state TiO_2 molecules (inactive TiO_2). The deactivation due to the shielding by TiO_2 can be explained according to the following reaction:

$TiO_2^* + TiO_2 \rightarrow TiO_2^{\#} + TiO_2$ (1.3)

where TiO_2^* is the TiO_2 with active species adsorbed on its surface, and $TiO_2^{\#}$ is the deactivated form of TiO_2.

(a)

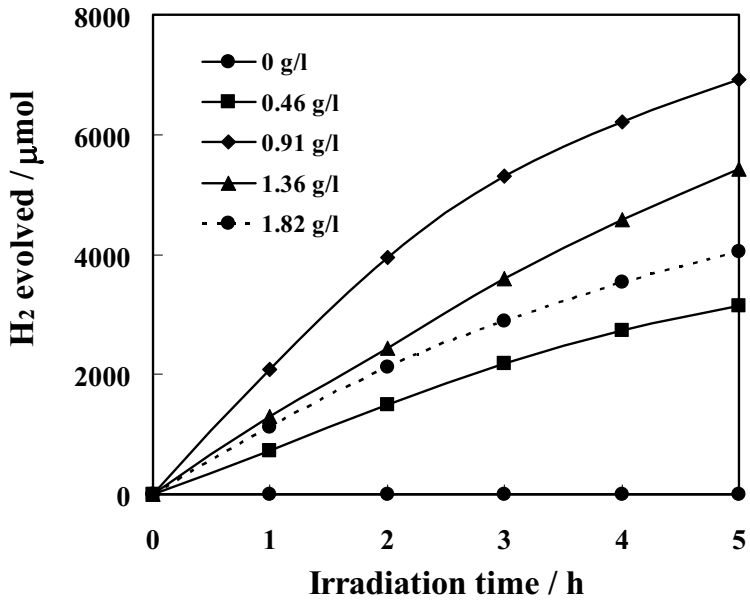

(b)

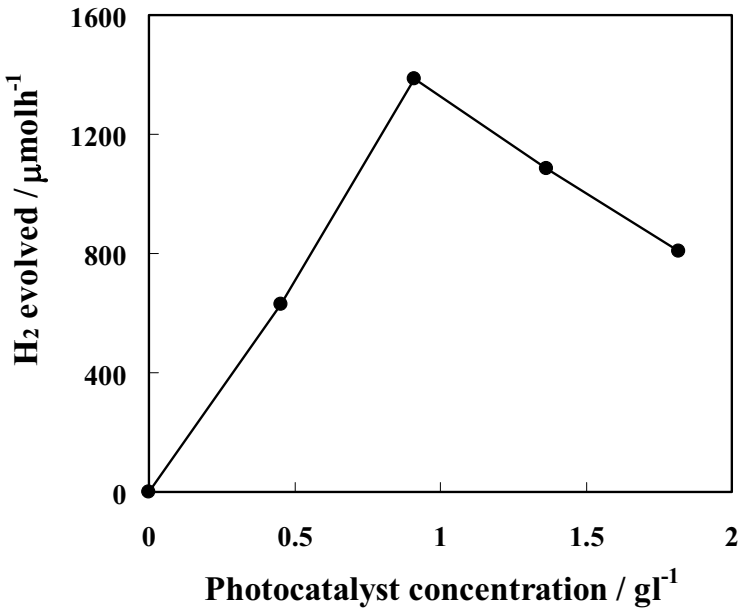

Figure 1.7 Effect of photocatalyst concentration on (a) time course of H_2 evolved and (b) dependence of photocatalytic H_2 production activity of the synthesized mesoporous Pt/TiO_2 photocatalyst (Reaction conditions: distilled water amount, 200 ml; sacrificial reagent type, methanol; sacrificial reagent amount, 20 ml; initial solution pH, 5.8; and irradiation time, 5 h).

At a considerably high photocatalyst concentration, agglomeration and sedimentation of the photocatalyst particles have also been reported. Under this condition, it leads to a reduction of the photocatalyst surface available for photon absorption and reactant adsorption, thus bringing lower stimulation to the photocatalytic reaction. An optimum photocatalyst concentration also greatly depends on the photoreactor geometry, the working conditions of the photoreactor, the degree of mixing, the UV lamp power, and the lamp geometry. The optimum amount of the photocatalyst has to be introduced into the system in order to avoid unnecessary excess photocatalyst and also to ensure total absorption of light photons for the efficient photocatalytic H_2 production reaction.

1.3.2.4 Effect of initial methanol concentration

It is important, both from mechanistic and application points of view, to study the dependence of the photocatalytic H_2 production reaction on the concentration of methanol, the most effective sacrificial reagent. The influence of initial methanol concentration on the photocatalytic H_2 production activity over the synthesized photocatalyst is shown in Figure 1.8. With an increase in the methanol concentration, the photocatalytic activity dramatically increased and reached a maximum at the methanol concentration of 2.25 M. Beyond this optimum methanol concentration, a further increase in methanol concentration led to a decrease in the photocatalytic activity. Under the studied conditions, the optimum methanol concentration was about 2.25 M. At relatively high concentrations of methanol beyond the optimum point, although the surface active sites remain constant for a fixed catalyst concentration, the number of adsorbed methanol molecules accommodated on the photocatalyst surface increases. Because the generation of valence band holes on the surface of the photocatalyst required for reacting with methanol molecules does not increase as the intensity of light and amount of catalyst are unchanged, there was an observed decrease in the photocatalytic H_2 production activity, probably due to the blockage of the adsorption of hydronium cations at surface active sites, so as to be reduced to produce hydrogen. Besides, as the photocatalytic reaction is an ion and radical reaction, and methanol can also somewhat behave as a quenching agent of ions and radicals, more ions and radicals can be quenched with the increase in methanol concentration. These mentioned reasons consequently lead to the decrease of H_2 production activity, after methanol concentration is over the optimum level.

(a)

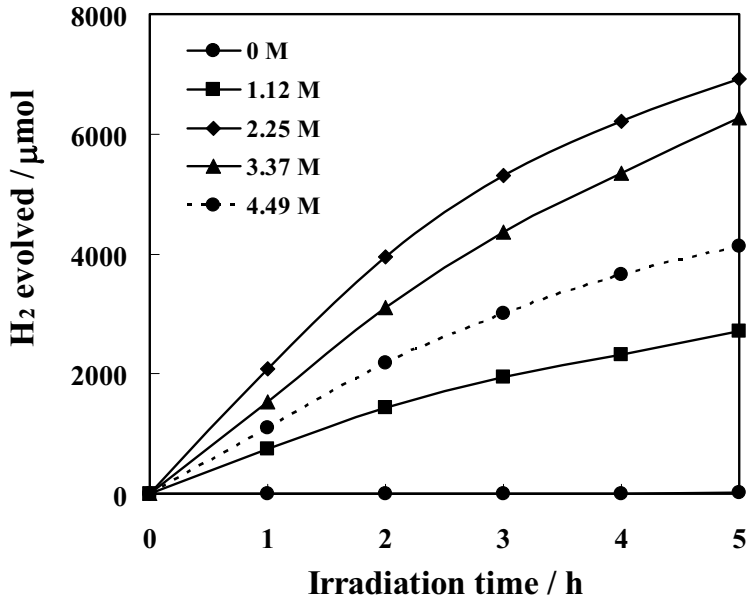

(b)

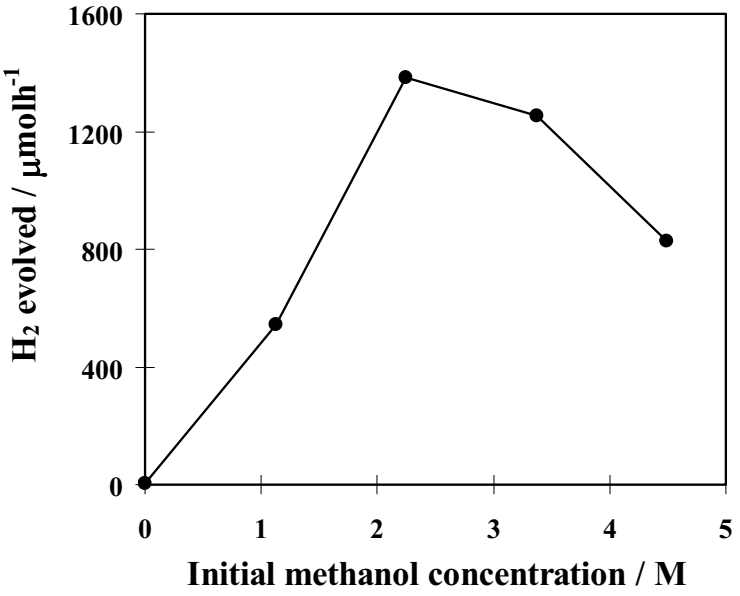

Figure 1.8 Effect of initial methanol concentration on (a) time course of H_2 evolved and (b) dependence of photocatalytic H_2 production activity of the synthesized mesoporous Pt/TiO_2 photocatalyst (Reaction conditions: photocatalyst amount, 0.2 g; solvent: distilled water; sacrificial reagent type, methanol; total solution volume, 220 ml; initial solution pH, 5.8; and irradiation time, 5 h).

1.3.2.5 Effect of irradiation time

The time courses of the photocatalytic H_2 production over the synthesized mesoporous Pt/TiO_2 photocatalyst at various reaction conditions are given in part (a) of Figures 1.5-1.8. It can be clearly seen that under light radiation, with increasing the time of irradiation up to 5 h,

the amount of H_2 evolved increased almost proportionally to the irradiation time in the investigated period. This is because, with an increase in irradiation time, the photons absorbed on the surface of the photocatalyst become greater, which, in turn, helps in the photocatalytic process. However, a slight decrease in the H_2 production rate at a long irradiation time was observed. This can be explained that in a photocatalytic batch system, a long irradiation time regularly causes a progressive decline in the H_2 production rate due to the back reactions of products generated in the reaction system, as well as the pressure buildup in the gas phase. Additionally, the active site deactivation due to the strong absorption of some molecular species might also be another cause of the decrease in the H_2 production activity after a long illumination time.

Conclusions

The use of single-step sol-gel-prepared 0.6 wt.% Pt-loaded nanocrystalline mesoporous TiO_2 photocatalyst with high surface area and narrow monomodal pore size distribution for photocatalyzing H_2 production from water under UV light irradiation was studied under various reaction conditions. Several operational parameters were investigated in order to determine the optimum conditions exhibiting the maximum H_2 production activity. The experimental results showed that methanol was found to be the most efficient sacrificial reagent among several types of sacrificial reagents investigated. Mild acidic pH values in the range of 5-6 were favorable for the reaction. The optimum photocatalyst and initial methanol concentration were found to be 0.91 g/l and 2.25 M, respectively.

Recommendations

The synthesized nanocrystalline mesoporous TiO_2 photocatalyst should be applied for photocatalytic H_2 production from water splitting under visible light irradiation because visible light accounts for approximately 42% of solar light exposed to the earth surface while only 8% for UV light. To achieve the TiO_2 photocatalyst with visible light response, some modifications of photocatalyst must be performed. The N-doping is a potential modification method, which was investigated in the second part, as described next.

Part 2: Comparative Investigation of Nanocrystalline Mesoporous and Non-Mesoporous TiO_2 Photocatalysts for Photocatalytic H_2 Production over N-Doped TiO_2 under Visible Light Irradiation

2.1 Objective

The objective was to investigate the influences of the urea:TiO_2 molar ratio and the calcination conditions on the N-doping capability and consequent photocatalytic activity of both mesoporous and non-mesoporous TiO_2 photocatalysts for H_2 production under visible light irradiation.

2.2 Experimental Procedure

2.2.1 Materials

Tetraisopropyl orthotitanate (TIPT) as a Ti precursor and acetylacetone (ACA) as a modifying ligand were used for synthesizing a mesoporous TiO_2 photocatalyst. Laurylamine hydrochloride (LAHC) was used as a structure-directing surfactant to control the mesoporosity of the synthesized TiO_2 photocatalyst. Urea (NH_2CONH_2) and hydrogen hexachloroplatinate (IV) hexahydrate ($H_2PtCl_6 \cdot 6H_2O$) were used as N and Pt sources, respectively, for doping and loading on the TiO_2 photocatalyst. Methanol was used as a hole scavenger or electron donor for the photocatalytic H_2 production. All chemicals were analytical grade and were used as received without further purification. Commercial Degussa P-25 TiO_2 was selected for the comparative studies of the photocatalytic H_2 production.

2.2.2 Synthesis procedure of mesoporous TiO_2 and preparation of N-doped TiO_2

A nanocrystalline mesoporous TiO_2 photocatalyst was synthesized via a sol-gel process with the aid of structure-directing surfactant for a system of LAHC/TIPT modified with ACA. In the typical synthesis, a specified amount of ACA was first introduced into TIPT with a molar ratio of unity. The mixed solution was then gently shaken until it was homogeneously mixed. Afterwards, a 0.1 M LAHC aqueous solution with a pH of 4.2 was added into the ACA-modified TIPT solution, in which the molar ratio of TIPT to LAHC in the mixed solution was tailored to 4:1. The mixture was continuously stirred at room temperature for 1 h and was further aged at 40°C overnight to obtain a transparent yellow sol. Then, the condensation reaction-induced gelation was allowed to proceed by placing the sol-containing solution into an oven at 80ºC for a week to ensure complete gelation. The gel was subsequently dried at 80°C overnight to eliminate the solvent, which was mainly the distilled water used in the preparation of the surfactant aqueous

solution, and the dried gel was further calcined at 500°C for 4 h to remove the LAHC template and to consequently produce the nanocrystalline mesoporous TiO_2 photocatalyst. Afterwards, the synthesized mesoporous TiO_2 was thoroughly mixed with urea at various urea:TiO_2 molar ratios, and the mixture was ground by using an agate mortar. The resulting powder was finally calcined at different temperatures, between 200 and 300°C, for 2 h to acquire N-doped TiO_2 photocatalysts. The same procedure was also used to prepare N-doped commercial TiO_2 photocatalysts. In order to improve the photocatalytic activity of the obtained N-doped TiO_2 photocatalyst with comparatively high photocatalytic activity, Pt with various contents was loaded via incipient wetness impregnation method by using aqueous solution of hydrogen hexachloroplatinate (IV) hexahydrate and then calcined at 200°C for 6 h.

2.2.3 Photocatalyst characterizations

A nitrogen sorption system was employed to measure the adsorption-desorption isotherms at a liquid nitrogen temperature of -196°C. The photocatalyst sample was degassed at 150°C for 2 h to remove the physisorbed gases prior to measurement. The Brunauer-Emmett-Teller (BET) approach using adsorption data over the relative pressure ranging from 0.05 to 0.35 was utilized to determine the specific surface areas of all studied photocatalysts. The Barrett-Joyner-Halenda (BJH) approach was used for the calculation of the mean pore sizes and pore size distributions of the photocatalyst samples. X-ray diffraction (XRD) was used to identify the crystalline structure and composition of the photocatalysts. An XRD system generating monochromated CuK_{α} radiation with continuous scanning mode at a rate of 2°/min and operating at 40 kV and 40 mA was used to obtain the XRD patterns of all the photocatalysts. A UV-visible spectrophotometer was used to record the diffuse reflectance spectra of the photocatalyst samples at room temperature with $BaSO_4$ as the reference. The oxidation state and surface composition were analyzed by an X-ray photoelectron spectroscope (XPS). A MgK_{α} source emitting an X-ray energy of 1,253.6 eV was used as the X-ray source. The relative surface charging of the samples was removed by referencing all the energies to the C1s level as an internal standard at 285 eV.

2.2.4 Photocatalytic H_2 production experiments

Photocatalytic H_2 production experiments were performed in a closed-gas system. In a typical run, a specified amount of all prepared photocatalysts (0.2 g), namely N-doped synthesized TiO_2 and N-doped commercial TiO_2, was suspended in an aqueous methanol solution (methanol 50 ml and distilled water 150 ml) by using a magnetic stirrer within a reactor

made of Pyrex glass. The mixture was initially deaerated by purging with Ar gas for 45 min in a dark environment. The photocatalytic reaction was then started by exposing the mixture with visible light irradiation from a 300 W Xe arc lamp emitting light with a wavelength longer than 400 nm using a UV cut-off glass filter. The gaseous samples from the headspace of the reactor were periodically collected and analyzed for hydrogen by a gas chromatograph equipped with a thermal conductivity detector (TCD).

2.3 Results and Discussion

2.3.1 Mesoporous TiO_2 photocatalyst synthesis results

In this study, the nanocrystalline mesoporous TiO_2 photocatalyst was synthesized via the sol-gel process with the aid of structure-directing surfactant by using TIPT as the Ti precursor modified with an ACA agent and LAHC as the structure-directing surfactant. Firstly, TIPT was mixed with ACA, resulting in a change of the co-ordination number of the Ti atoms from 4 to 5, as shown in Eq. (2.1). This also causes the change of solution color from colorless to yellow. The obtained ACA-modified TIPT is comparatively less active to the moisture in air than the TIPT itself, and is more suitable for the sol-gel synthesis.

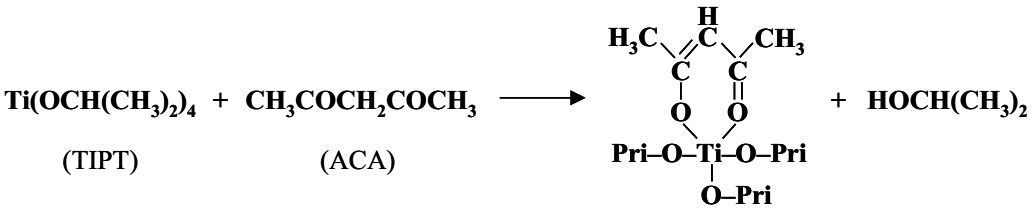

(2.1)

Ti coordination number: 4 Ti coordination number: 5

In order to control the mesoporous structure of the TiO_2, the LAHC aqueous solution was added into the TIPT/ACA solution. The precipitation of a yellow solution occurred immediately after the aqueous solution addition, owing to the partial hydrolysis of the modified TIPT molecules. Then, the solution was continuously stirred at 40°C to dissolve the precipitates. Consequently, a transparent yellow sol was obtained, which resulted from the interaction between the hydrolyzed TIPT molecules and the hydrophilic head groups of micellar LAHC and the suspension of these interacted species in the solution as infinitesimally colloidal solid particles. After placing the transparent yellow sol in an oven at 80°C, a white gel was formed via the condensation process of the modified TIPT molecules attached to the LAHC head groups, and ACA was eliminated, as evidenced by the existence of a transparent yellow liquid layer on the gel. Complete gel formation was observed after a week, and the gel was then dried at 80°C

to obtain dried TiO_2 (zero gel). The mesoporous TiO_2 photocatalyst was eventually obtained when the dried gel was calcined at 500°C, which was a sufficiently high temperature for both removing the LAHC template and crystallizing the photocatalyst.

2.3.2 Photocatalyst characterization results

To improve the visible light absorption ability of the TiO_2 photocatalysts, N-doping was carried out by mixing urea, a simple N-containing molecule, with the synthesized TiO_2 and the commercial TiO_2 at various urea:TiO_2 molar ratios and various calcination temperatures. It was experimentally found that after the N-doping, the color of both TiO_2 photocatalysts clearly changed from white to yellow.

2.3.2.1 Pore structures of photocatalysts

The N_2 adsorption-desorption isotherms of the as-synthesized TiO_2 and N-doped synthesized TiO_2 exhibit the typical IUPAC type IV pattern with the presence of a hysteresis loop, as shown in Figure 2.1. The hysteresis loop is ascribed to the existence of the mesoporous structure (mesopore size between 2-50 nm) in the sample. A sharp increase in the adsorption volume of N_2 was observed and located in the P/P_0 range of 0.5-0.9. This sharp increase can be assigned to the capillary condensation, indicating good homogeneity of the samples and fairly small pore sizes, since the P/P_0 position of the inflection point is pertaining to pore dimension. As illustrated in the inset of Figure 2.1, the pore size distribution of the sample is quite narrow and monomodal, owing to the single hysteresis loop, implying that the synthesis technique used in this study can yield a mesoporous TiO_2 nanocrystal with a narrow pore size distribution. In contrast, for the commercial TiO_2 and N-doped commercial TiO_2, the N_2 adsorption-desorption isotherms corresponded to the IUPAC type II pattern, as depicted in Figure 2.2. It is apparent that the commercial TiO_2 exhibits non-mesoporous characteristic due to the absence of the hysteresis loop. No capillary condensation of N_2 into the pore was observed since the desorption isotherm was insignificantly different from the adsorption one. The pore size distribution of the commercial TiO_2, as shown in the inset of Figure 2.2, is quite broad. The average pore sizes of the commercial TiO_2 and N-doped commercial TiO_2 are quite large, and their pore size distributions not only exist in the mesoporous region but also mostly cover the macropore region (macropore size > 50 nm).

(a)

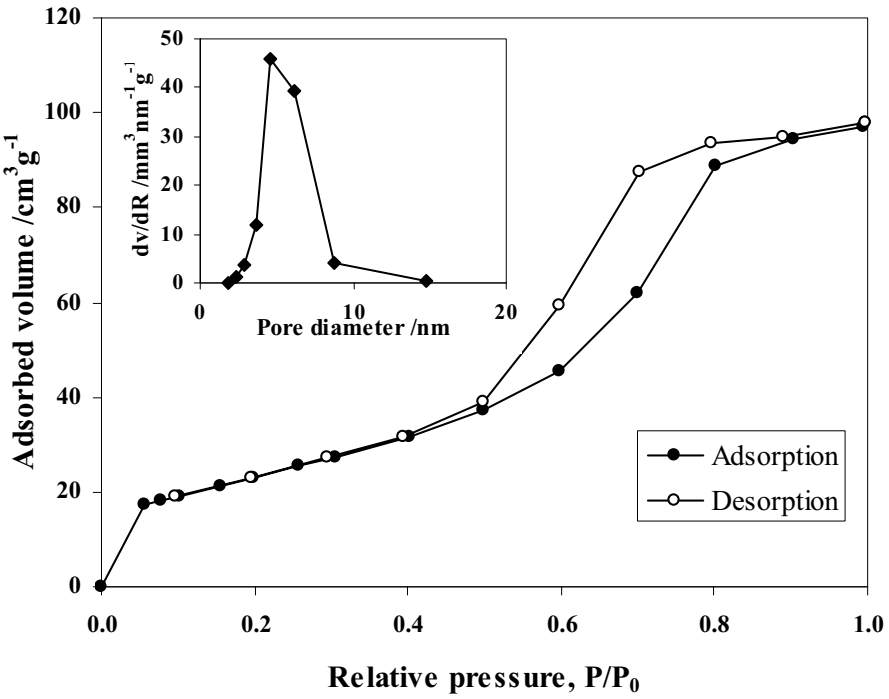

(b)

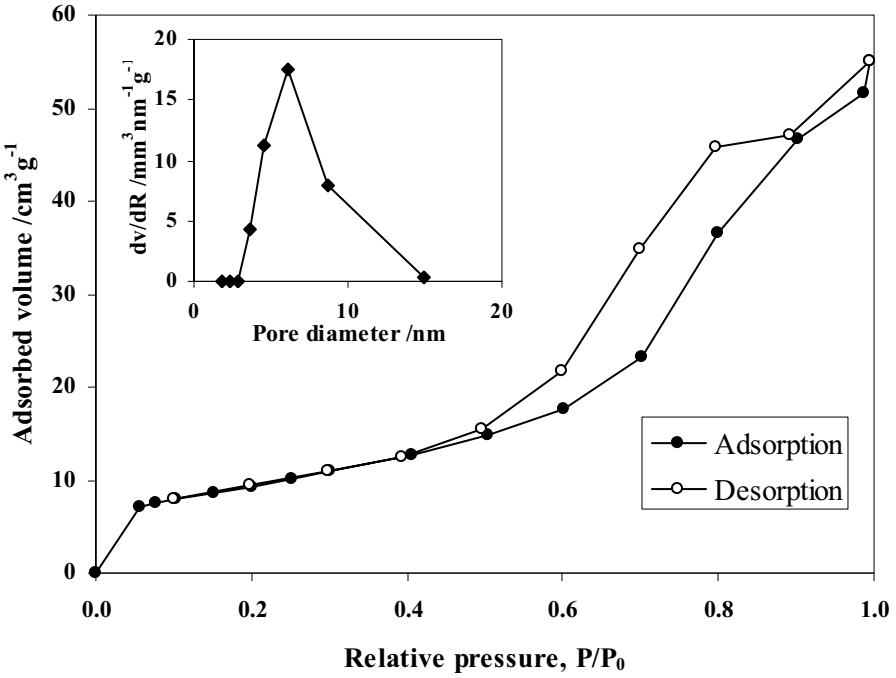

Figure 2.1 N_2 adsorption-desorption isotherm and pore size distribution (inset) of (a) the as-synthesized mesoporous TiO_2 and (b) the N-doped synthesized TiO_2 prepared at a urea:TiO_2 molar ratio of 1:1 and calcined at 250°C.

(a)

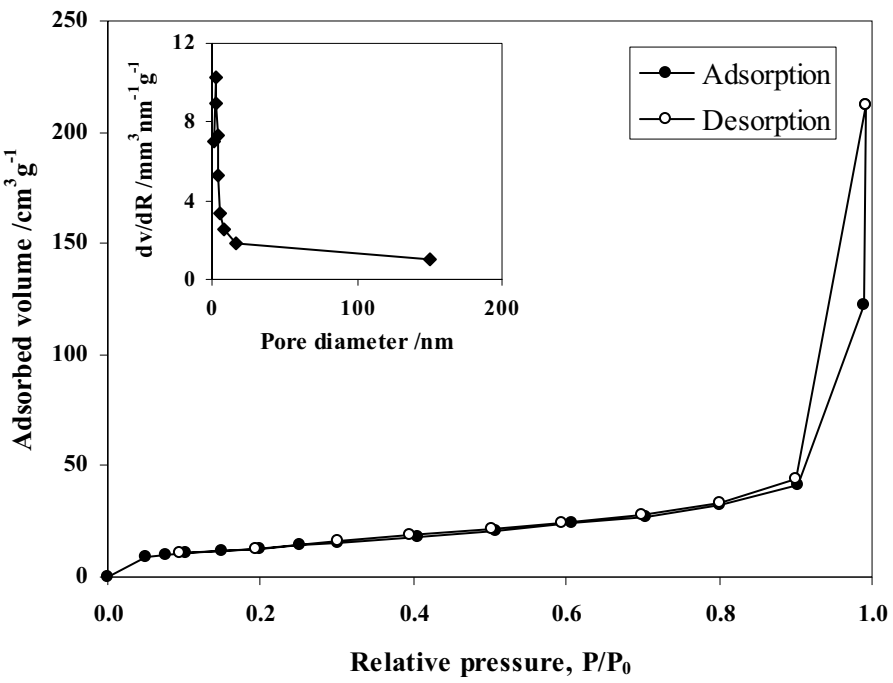

(b)

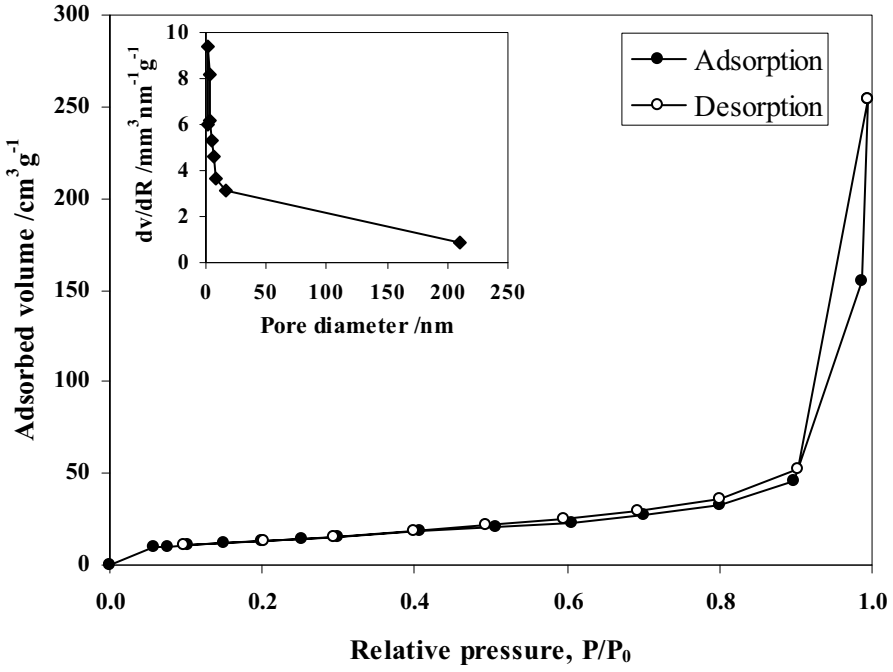

Figure 2.2 N_2 adsorption-desorption isotherm and pore size distribution (inset) of (a) the commercial TiO_2 and (b) the N-doped commercial TiO_2 prepared at a urea:TiO_2 molar ratio of 0.5:1 and calcined at 250°C.

2.3.2.2 Textural properties of photocatalysts

The experimental results of the textural property characterization of the photocatalysts, including BET surface area, mean pore diameter, and total pore volume, are shown in Table 2.1. For any given N-doped mesoporous or N-doped commercial TiO_2 photocatalyst, the surface area tended to decrease with increasing urea:TiO_2 molar ratio at all calcination temperatures. For the N-doped mesoporous TiO_2, of which the isotherm exhibited typical IUPAC type IV, the mean pore diameter was quite similar to the pure mesoporous TiO_2, however the total pore volume decreased with increasing urea:TiO_2 molar ratio. For the commercial TiO_2, the mean pore diameter and total pore volume are usually not reported because it contains a large portion of macropores, which has a very broad pore size distribution with the pore diameters larger than 50 nm up to 200-250 nm.

2.3.2.3 Light absorption capability of photocatalysts

UV-visible spectroscopy was used to investigate the light absorption capability of the studied photocatalysts. The changes in the absorption spectra of N-doped mesoporous TiO_2 nanocrystal with different urea:TiO_2 molar ratios are exemplified in Figure 2.3. The absorption band of pure mesoporous TiO_2 is in the range of 200-400 nm. The high light absorption band at low wavelengths in the spectra indicates the presence of the Ti species as tetrahedral Ti^{4+}. This light absorption band is generally associated with the electronic excitation of the valence band O2p electron to the conduction band Ti3d level. Its light absorption onset is approximately at 385 nm, which corresponds to the energy band gap of anatase TiO_2, 3.2 eV. For the N-doped mesoporous TiO_2, as also shown in Figure 2.3, the light absorption band shifts to a wavelength longer than 400 nm (red shift), which is in the range of the visible light region. From the light absorption results, the N-doping technique can improve the visible light absorption capability of the mesoporous TiO_2 synthesized in this study.

Table 2.1 Summary of textural properties of the TiO_2 photocatalysts without and with N-doping prepared at various conditions

Calcination temperature (ºC)	Urea:TiO_2 molar ratio	BET surface area ($m^2 g^{-1}$)	Mean pore diameter (nm)	Total pore volume ($cm^3 g^{-1}$)
-	Pure mesoporous TiO_2	110.30	6.114	0.185
200	0.5:1	78.14	6.150	0.136
	1:1	35.36	6.156	0.070
	3:1	22.12	4.619	0.044
250	0.5:1	82.83	6.146	0.155
	1:1	38.52	6.129	0.080
	3:1	23.45	6.140	0.049
300	0.5:1	75.78	6.150	0.147
	1:1	73.98	6.161	0.137
	3:1	22.86	6.104	0.053
-	Pure Degussa P-25 TiO_2	69.35	- [(a)]	- [(a)]
200	0.5:1	54.96	- [(a)]	- [(a)]
	1:1	53.26	- [(a)]	- [(a)]
	3:1	17.63	- [(a)]	- [(a)]
250	0.5:1	50.66	- [(a)]	- [(a)]
	1:1	44.63	- [(a)]	- [(a)]
	3:1	20.77	- [(a)]	- [(a)]
300	0.5:1	51.40	- [(a)]	- [(a)]
	1:1	26.21	- [(a)]	- [(a)]
	3:1	24.22	- [(a)]	- [(a)]

[(a)] N_2 adsorption-desorption isotherms correspond to IUPAC type II pattern.

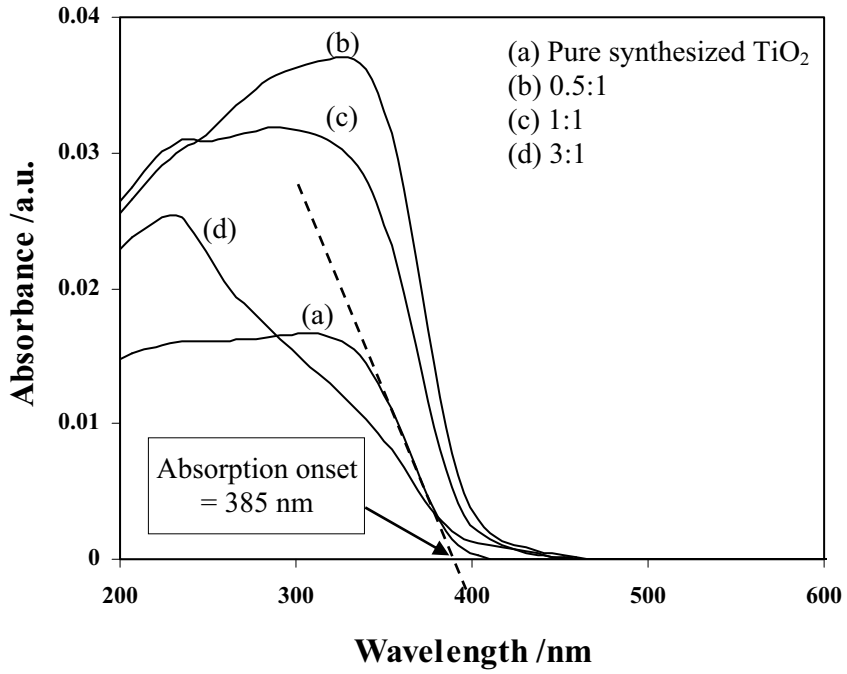

Figure 2.3 UV-visible spectra of (a) pure nanocrystalline mesoporous TiO_2 and (b)-(d) N-doped mesoporous TiO_2 with different urea:TiO_2 molar ratios of 0.5:1, 1:1, and 3:1, respectively, prepared at a calcination condition of 250°C.

The light absorption spectra of the N-doped commercial TiO_2 at different urea:TiO_2 molar ratios are shown in Figure 2.4. The light absorption onset of the pure commercial TiO_2 begins at the wavelength longer than 400 nm, indicating that it can absorb visible light by itself without N-doping. This is because the commercial TiO_2 possesses both anatase and rutile phases, as shown by XRD patterns in the next part. Their energy band gap is approximately 3.2 and 3.0 eV for anatase and rutile TiO_2, respectively, which can originally absorb both UV and visible ranges. It was therefore experimentally found that the N-doping cannot much enhance the visible light absorption capability of the commercial TiO_2. As shown later from the XPS results, because the commercial TiO_2 possesses less capability of allowing the N-doping owing to its comparatively low surface N content, its visible light absorption is not obviously improved. By comparing between Figures 2.3 and 2.4, the N-doping process gave the positive effect on the absorbance intensity, especially in UV light region, for the synthesized TiO_2 while giving the negative effect for the commercial TiO_2, however the absorption of UV light with wavelength shorter than 400 nm requires no extensive consideration due to the utilization of only visible light for photocatalytic study. As shown later for the photocatalytic activity results, since both N-doped TiO_2 photocatalysts showed potential performance for photocatalytic H_2 production under visible

light irradiation, it means that the photocatalysts can effectively capture the irradiated visible light for generating the excited electrons necessary for reducing protons to H_2 molecules. The possible reasons for these observations of absorbance intensity changes are still in doubt and need further clarified investigation.

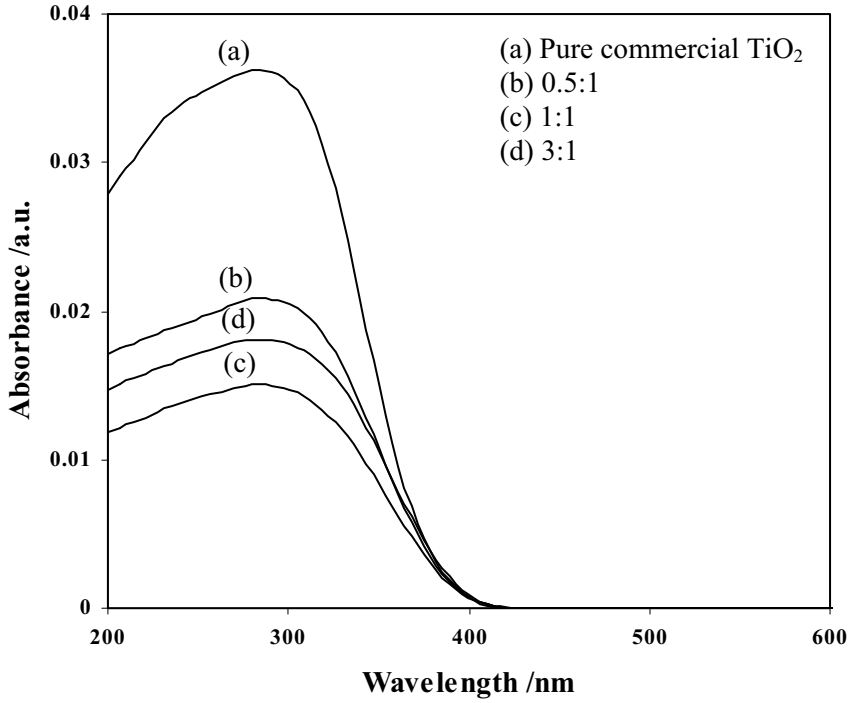

Figure 2.4 UV-visible spectra of (a) commercial TiO_2 and (b)-(d) N-doped commercial TiO_2 with different urea:TiO_2 molar ratios of 0.5:1, 1:1, and, 3:1, respectively, prepared at a calcination condition of 250°C.

2.3.2.4 Crystallinity and purity of photocatalysts

The XRD patterns of the N-doped mesoporous TiO_2 nanocrystal prepared at different urea:TiO_2 molar ratios and calcination temperatures are shown in Figure 2.5, compared with that of the pure mesoporous TiO_2 photocatalyst, whereas those of the N-doped commercial TiO_2 prepared at different urea:TiO_2 molar ratios and calcination temperatures are shown in Figure 2.6, also compared with that of the pure commercial TiO_2.

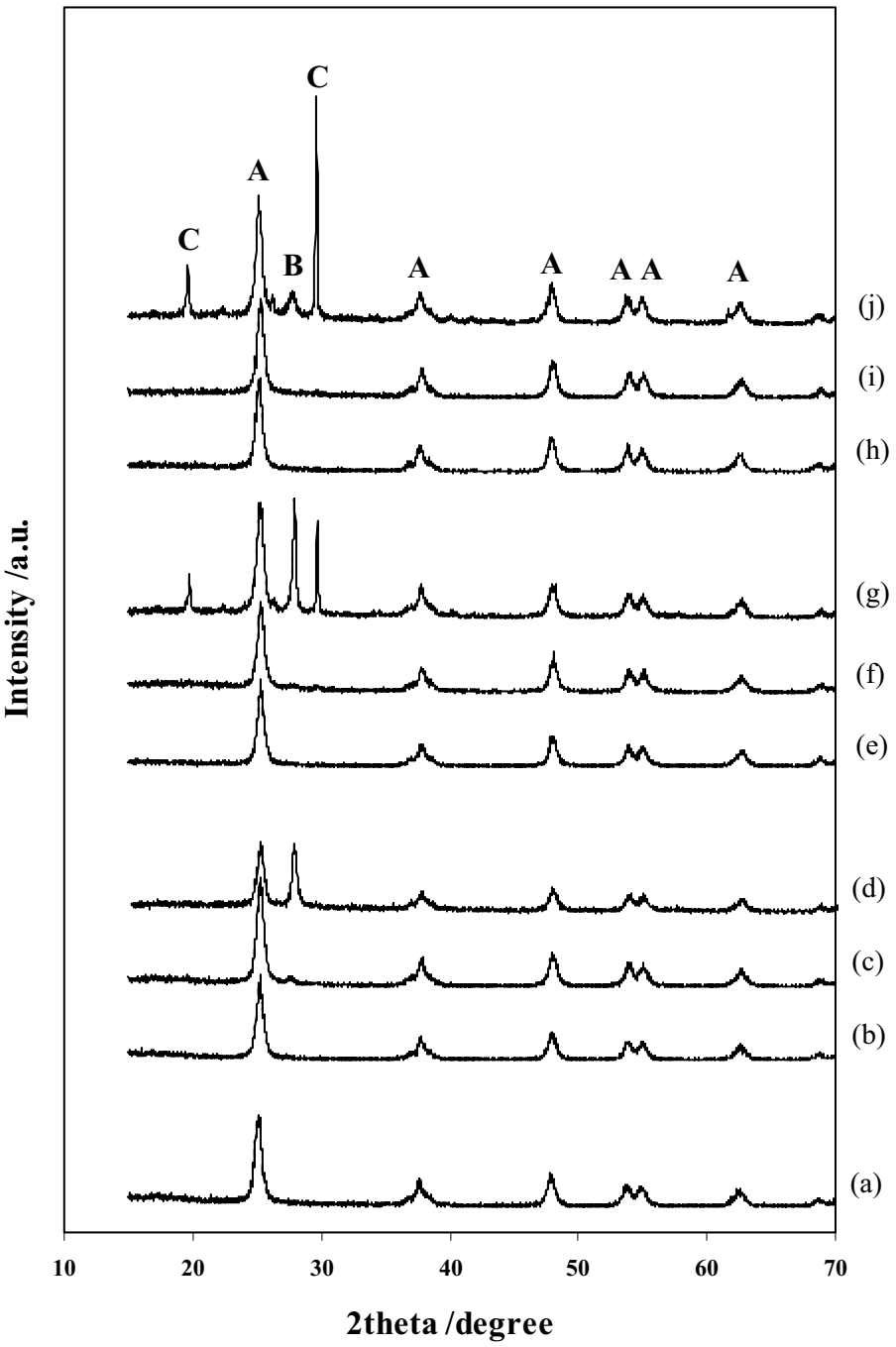

Figure 2.5 XRD patterns of (a) pure mesoporous TiO_2, and (b)-(d) N-doped mesoporous TiO_2 with different urea:TiO_2 molar ratios of 0.5:1, 1:1, and, 3:1, respectively, prepared at a calcination condition of 200°C, (e)-(g) urea:TiO_2 molar ratios of 0.5:1, 1:1, and, 3:1, respectively, at 250°C, and (h)-(j) urea:TiO_2 molar ratios of 0.5:1, 1:1, and, 3:1, respectively, at 300°C (A: Anatase TiO_2, B: Biuret, C: Cyanuric acid).

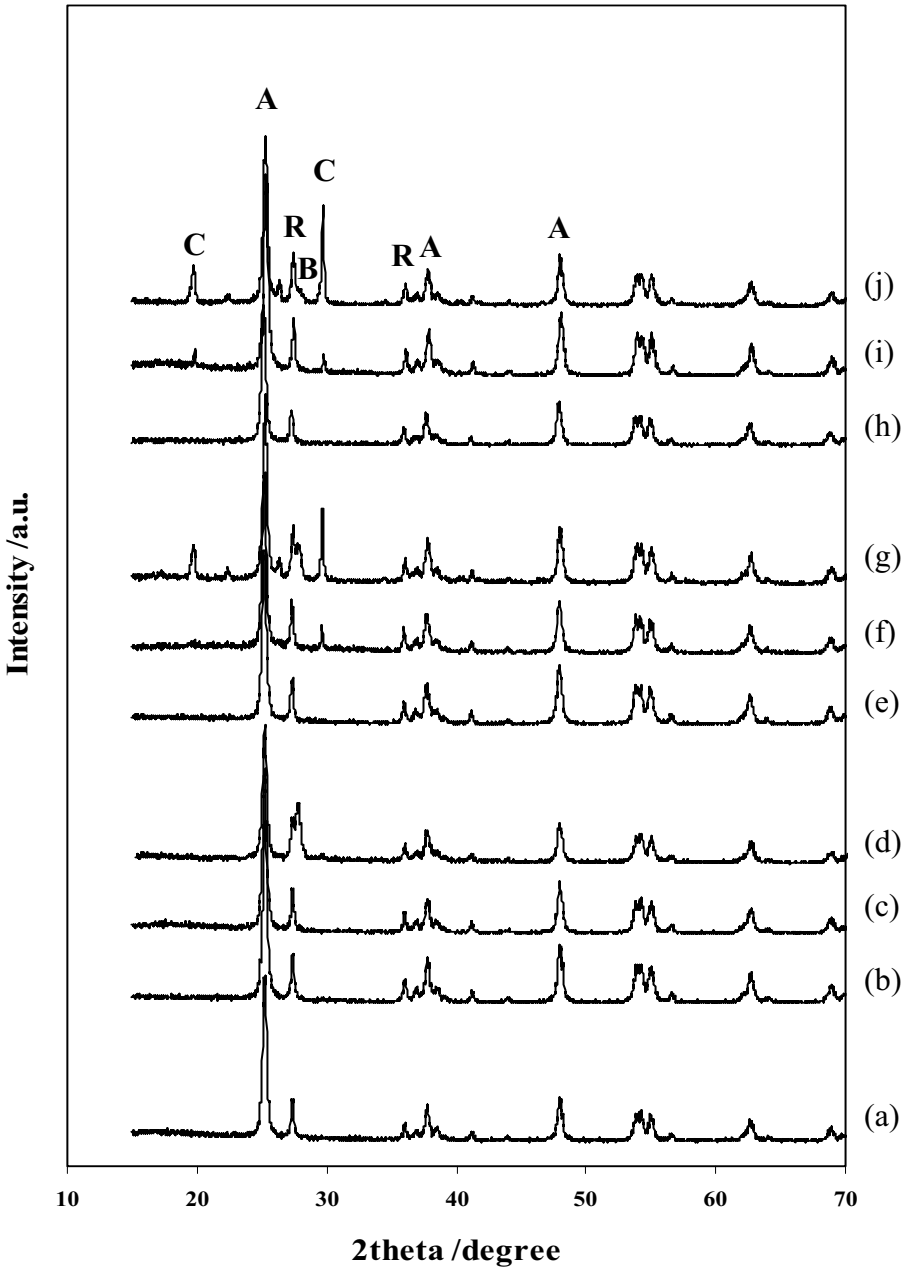

Figure 2.6 XRD patterns of (a) commercial TiO_2, (b)-(d) N-doped commercial TiO_2 with different urea:TiO_2 molar ratios of 0.5:1, 1:1, and, 3:1, respectively, prepared at a calcination condition of 200°C, (e)-(g) urea:TiO_2 molar ratios of 0.5:1, 1:1, and, 3:1, respectively, at 250°C, and (h)-(j) urea:TiO_2 molar ratios of 0.5:1, 1:1, and, 3:1, respectively, at 300°C (A: Anatase TiO_2, R: Rutile TiO_2, B: Biuret, C: Cyanuric acid).

As shown in Figure 2.5, all samples of N-doped mesoporous TiO_2 prepared at a urea:TiO_2 molar ratio of 0.5:1, regardless of calcination temperature, show quite a similar XRD diffractogram with the pure mesoporous TiO_2. The dominant peaks at 2θ at about 25.2, 37.9, 47.8, 53.8, and 55.0°, which represent the indices of (101), (004), (200), (105), and (211) planes (JCPDS Card No. 21-1272), respectively, conform to the crystalline structure of anatase TiO_2. At a temperature of 200°C, the biuret formation was first clearly observed at a urea:TiO_2 molar ratio of 3:1, as shown in Figure 2.5. The biuret was also found at the urea:TiO_2 molar ratio of 1:1 in a very small amount due to the comparatively low peak intensity at this temperature ((c) in Figure 2.5). A similar tendency of biuret formation was observed at a temperature of 250°C for the urea:TiO_2 molar ratios of both 1:1 and 3:1 ((f) and (g) in Figure 2.5), but in extremely low amounts at the molar ratio of 1:1. In addition, cyanuric acid was apparently formed at this temperature. At 300°C, biuret formation was not observed at a molar ratio of 1:1 ((i) in Figure 2.5), suggesting that biuret is decomposed at this temperature. At a molar ratio of 3:1 ((j) in Figure 2.5), a large amount of cyanuric acid was observed, and biuret was observed in relatively low amounts when compared to 250°C at the same molar ratio. These results indicate that biuret starts to decompose to form cyanuric acid at temperatures higher than 200°C. For the decomposition of urea to produce many compounds, it is temperature-dependent, and two main products are biuret and cyanuric acid. Upon increasing temperature, biuret is formed at approximately 150 to 250°C. Cyanuric acid then appears in consecutive order at approximately 190 to 350°C. The formation of biuret and cyanuric acid due to the urea composition is shown in the following decomposition reactions.

At temperatures between 150 and 250°C,

$$\underset{\text{urea}}{H_2N\text{-}CO\text{-}NH_2\ (l)} + \text{heat} \longrightarrow \underset{\text{ammonium iso-cyanate}}{NH_4^+NCO^-\ (l)} \qquad (2.2)$$

$$\underset{\text{ammonium iso-cyanate}}{NH_4^+NCO^-\ (l)} \longleftrightarrow \underset{\text{ammonia}}{NH_3\ (g)} + \underset{\text{iso-cyanic acid}}{HNCO\ (g)} \qquad (2.3)$$

$$\underset{\text{urea}}{H_2N\text{-}CO\text{-}NH_2\ (l)} + \underset{\text{iso-cyanic acid}}{HNCO\ (g)} \longleftrightarrow \underset{\text{biuret}}{H_2N\text{-}CO\text{-}NH\text{-}CO\text{-}NH_2\ (s)} \qquad (2.4)$$

and, at temperatures between 190 and 350°C,

$$\underset{\text{iso-cyanic acid}}{3HNCO\ (g)} \longrightarrow \underset{\text{cyanuric acid}}{C_3O_3N_3H_3\ (s)} \qquad (2.5)$$

$$\underset{\text{biuret}}{2H_2N\text{-}CO\text{-}NH\text{-}CO\text{-}NH_2\ (l)} \longrightarrow \underset{\text{cyanuric acid}}{C_3O_3N_3H_3\ (s)} + \underset{\text{iso-cyanic acid}}{HNCO\ (g)} + \underset{\text{ammonia}}{NH_3\ (g)} \qquad (2.6)$$

where s, l, and g represent solid, liquid, and gas phases, respectively.

The decomposition reactions of urea as described above exactly correspond to the effect of calcination temperature on the formation of impurities (biuret and cyanuric acid) at a high urea:TiO_2 molar ratio of 3:1 where the peak responsible for biuret formation was first observed at 200°C, and its intensity increased when increasing the calcination temperature to 250°C. With further increasing to 300°C, the amount of biuret formed was found to decrease substantially. In the meantime, cyanuric acid was first denoted at 250°C and increased significantly at 300°C. For the XRD patterns of N-doped commercial TiO_2, as shown in Figure 2.6, the dominant peaks at 2θ of about 27.4, 36.1, 41.2, and 54.3°, which represent the indices of (110), (101), (111), and (211) planes (JCPDS Card No. 21-1276), respectively, indicate the presence of the rutile phase, in addition to the presence of the anatase phase. Both biuret and cyanuric acid were observed in the same trend as the N-doped mesoporous TiO_2. The main difference between the mesoporous TiO_2 and the commercial TiO_2 photocatalysts was that the synthesized mesoporous TiO_2 is in only anatase form, whereas the commercial TiO_2 possesses the mixed phases of anatase (76.5%) and rutile (23.5%), of which the phase composition is calculated by the following equations:

$$W_R = [1 + 0.8I_A/I_R]^{-1} \qquad (2.7)$$

$$W_A = 1 - W_R \qquad (2.8)$$

where I_A and I_R represent integrated intensities of anatase (101) and rutile (110) diffraction peaks, respectively, and W_A and W_R represent phase compositions of anatase and rutile, respectively.

2.3.2.5 Oxidation state and surface N content of photocatalysts

The oxidation states and surface compositions of N, O, and Ti of the N-doped mesoporous TiO_2 and N-doped commercial TiO_2 nanocrystals were analyzed by XPS. The XPS results of the N-doped mesoporous TiO_2 prepared at a urea:TiO_2 molar ratio of 1:1 and calcination temperature of 250°C are exemplified in Figure 2.7. Figure 2.7(a) represents a typical XPS spectrum of Ti. The peaks of the Ti2p spectrum appeared with their centers at 458.4 and 464.0 eV, which correspond to the $Ti2p_{3/2}$ and $Ti2p_{1/2}$ levels, respectively. The peaks can denote the Ti^{4+} oxidation state, which agree well with the light absorption results. Figure 2.7(b) shows the peak of the N1s spectrum centered at 400.8 eV, which can be ascribed to the molecularly chemisorbed nitrogen. Figure 2.7(c) shows the deconvoluted peaks of the O1s (mesoporous TiO_2) spectrum with one centered at 529.7 eV, which is typical for the Ti-O-Ti environment and agrees with the O1s binding energy for TiO_2 molecule, and the other centered at 532.5 eV, which is typical for the Ti-O-H environment of the hydroxyl group on the photocatalyst surface.

It has been reported about the N-doped TiO_2 photocatalyst investigation with the XPS technique and observed that the peaks of the N1s spectrum appeared with their centers approximately at both 396 and 401 eV, correspondingly representing atomically substitutional nitrogen and molecularly chemisorbed nitrogen with comparatively low signal for the former. Although the N1s with a binding energy centered at 396 eV was not clearly observed for the samples in this study, it is believed to exist in a low amount. It has been analyzed that the peak centered at 396 eV is typical for N bound to Ti atoms, and the signal centered at 401 eV is typical for N bound to O, C, or N atoms. In combining with the light absorption results, it can be inferred that the molecularly chemisorbed nitrogen could contribute to the extended absorption into visible light region. The surface nitrogen compositions of all the investigated N-doped TiO_2 samples are summarized in Table 2.2. The presence of surface nitrogen on the as-synthesized mesoporous TiO_2 may be due to the imperfect removal of LAHC used as the surfactant template during the calcination step. For the pure commercial TiO_2, the presence of surface nitrogen is plausibly because of their production technique via spray combustion. During the combustion step, which is generally carried out with air, the commercial TiO_2 can inevitably be N-doped.

(a)

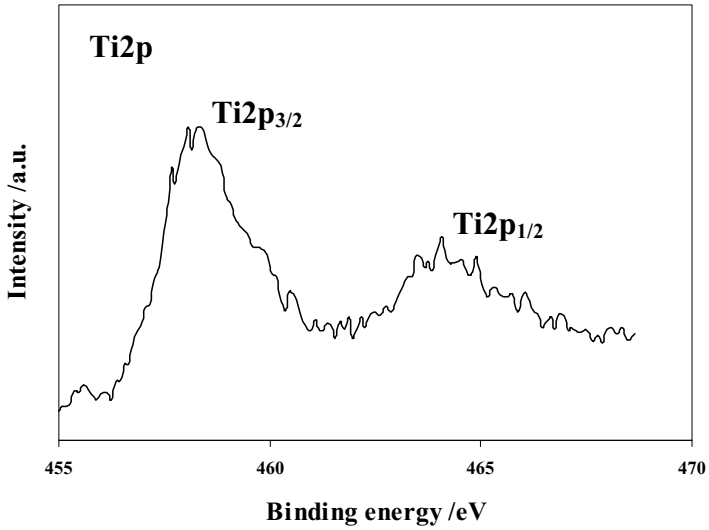
Ti2p
Ti2p3/2
Ti2p1/2
Intensity /a.u.
455
460
465
470
Binding energy /eV

(b)

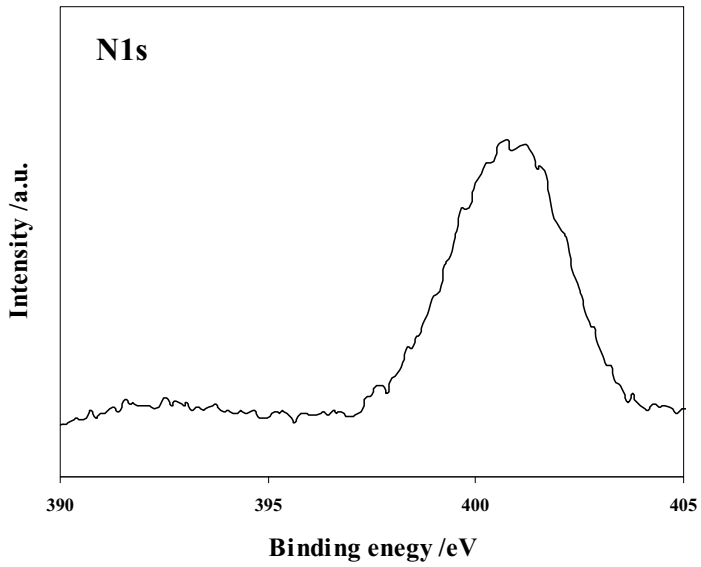
N1s
Intensity /a.u.
390
395
400
405
Binding enegy /eV

(c)

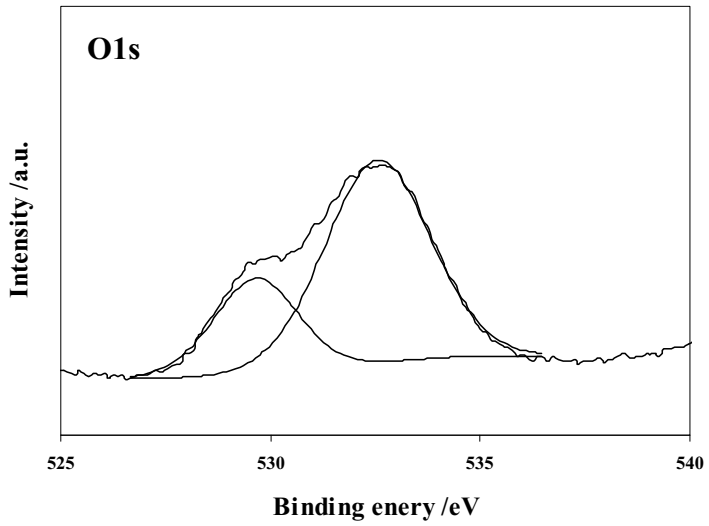
O1s
Intensity /a.u.
525
530
535
540
Binding enery /eV

Figure 2.7 XPS spectra of (a) Ti2p, (b) N1s, and (c) O1s of N-doped mesoporous TiO_2 prepared at a urea:TiO_2 molar ratio of 1:1 and a calcination temperature of 250°C.

Table 2.2 Summary of surface N content of the TiO_2 photocatalysts prepared at different conditions

Calcination temperature (ºC)	Urea:TiO_2 molar ratio	Surface N content (wt.%)	
		Mesoporous TiO_2	Commercial TiO_2
-	0:1	4.72 [(a)]	2.59 [(a)]
200	0.5:1	5.77	3.96
	1:1	20.11	5.01
	3:1	21.28	7.73
250	0.5:1	8.70	3.21
	1:1	26.23	4.68
	3:1	32.61	7.93
300	0.5:1	7.11	2.35
	1:1	11.23	2.91
	3:1	30.25	7.17

[(a)] Pure TiO_2

For the N-doped mesoporous TiO_2 prepared at any given urea:TiO_2 molar ratio, the surface N content increases with increasing calcination temperature from 200 to 250°C, but decreases with further increasing to 300°C, as shown in Table 2.2. The trend of the surface N content for N-doped mesoporous TiO_2 is quite different from that for N-doped commercial TiO_2, of which at all urea:TiO_2 molar ratios, the surface N content tended to decrease with increasing the calcination temperature from 200 to 300°C. These results can probably be related to their pore characteristics. As the pore size of the synthesized TiO_2 exists entirely in the mesopore region, the formed N-containing compounds at 250°C, i.e. biuret and cyanuric acid, are easily trapped inside the pores due to the pore size limitation. However, with increasing the temperature to 300°C, biuret further decomposes to smaller compounds, and so they can be more thermally released from the pore structure at this high temperature. In contrast to the pore size of the commercial TiO_2, which is mostly in the large macropore region, any compounds formed can be simultaneously released by the thermal removal process. At a higher temperature, this thermal removal phenomenon becomes more significant due to the greater amount of applied energy, resulting in less surface N content. Moreover, at any given

calcination temperature, the surface N content increased with increasing urea:TiO_2 molar ratio for both the mesoporous TiO_2 and commercial TiO_2, due to the presence of a higher amount of available urea molecules so as to increase the doping capability. When comparing these two types of TiO_2, it is obvious that the surface N content of the mesoporous TiO_2 was considerably higher than that of the commercial TiO_2 at all preparation conditions, because of the higher surface area of the mesoporous TiO_2, as well as other physical surface properties originating from the specific preparation technique.

2.3.3 Photocatalytic H_2 production activity results

The results of photocatalytic H_2 production over the photocatalysts are shown in Figure 2.8. The photocatalytic activity in the absence of either light irradiation, photocatalyst, or methanol was also comparatively studied. It was found that there was no detectable H_2 production in their absence, indicating that all of them are very important for the photocatalytic H_2 production from water splitting. Moreover, without N-doping, on both types of TiO_2 photocatalysts, extremely poor photocatalytic H_2 production activity was observed. As shown in Figure 2.8, the N-doped mesoporous TiO_2 prepared at a urea:TiO_2 molar ratio of 1:1 and a calcination temperature of 250°C exhibits the highest H_2 production activity. For the series of the widely-known high photocatalytic activity commercial TiO_2, the best N-doping conditions were at a urea:TiO_2 molar ratio of 0.5:1 and a calcination temperature of 250°C.

At both calcination temperatures, 200 and 250°C, the photocatalytic H_2 production activity of the N-doped mesoporous TiO_2 tended to increase with increasing urea:TiO_2 molar ratio from 0.5:1 to 1:1 and then to decrease with further increasing molar ratio. It seems that for the N-doped mesoporous TiO_2 with a urea:TiO_2 molar ratio of 3:1, a huge amount of urea was decomposed to biuret (at 200 and 250°C) and further to cyanuric acid (250°C), and they could not be completely removed; consequently they remained inside the mesoporous structure, as shown in the XRD patterns (Figure 2.5). Since both biuret and cyanuric acid are comparatively large molecules, they are easily trapped inside the pores of the synthesized mesoporous TiO_2, resulting in the decreased H_2 production activity due to less accessibility of the reactants to the photocatalyst surface (Table 2.1 and Figure 2.8) despite the higher surface N content (Table 2.2). For any given urea:TiO_2 molar ratio, the photocatalytic activity of the N-doped mesoporous TiO_2 prepared at 300°C was different from those prepared at the other two calcination temperatures, 200 and 250°C. The H_2 production reached a maximum at a urea:TiO_2 molar ratio of 0.5:1 and gradually decreased as the molar ratio further increased. A possible explanation might be that at this high temperature, the biuret formed can be easily decomposed

to cyanuric acid, iso-cyanic acid, and ammonia (Eq. (2.6)). The surface nitrogen may then also be released more, resulting in less surface N content (Table 2.2) and subsequently lowering the photocatalytic activity, as shown in Figure 2.8. In addition, although the cyanuric acid formation at a molar ratio of 1:1 was not observed from XRD, the decreased pore volume and increased amount of surface N content can be confirmed, as shown in Tables 2.1 and 2.2.

(a)

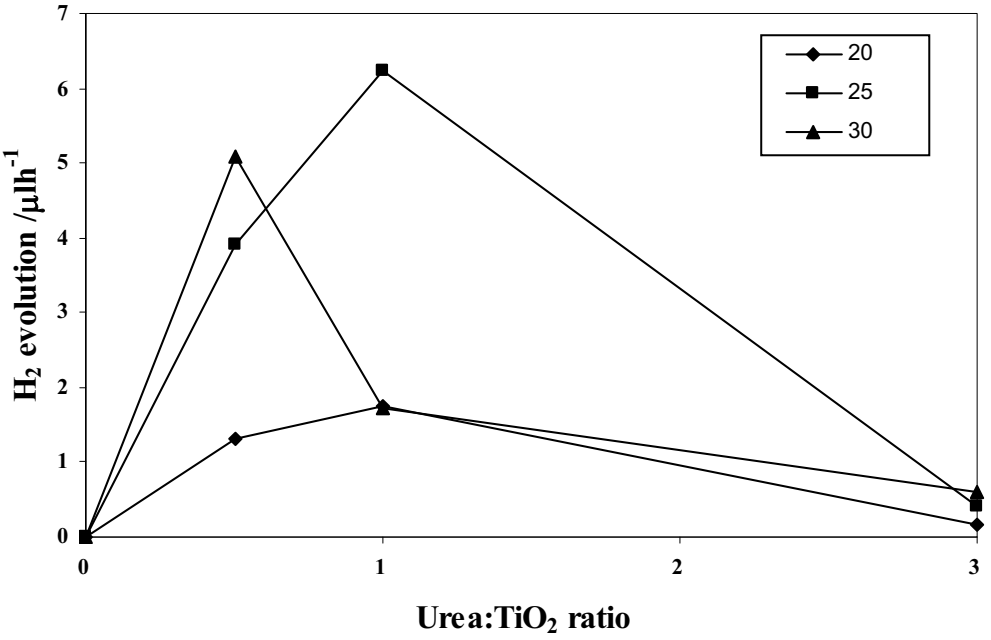

(b)

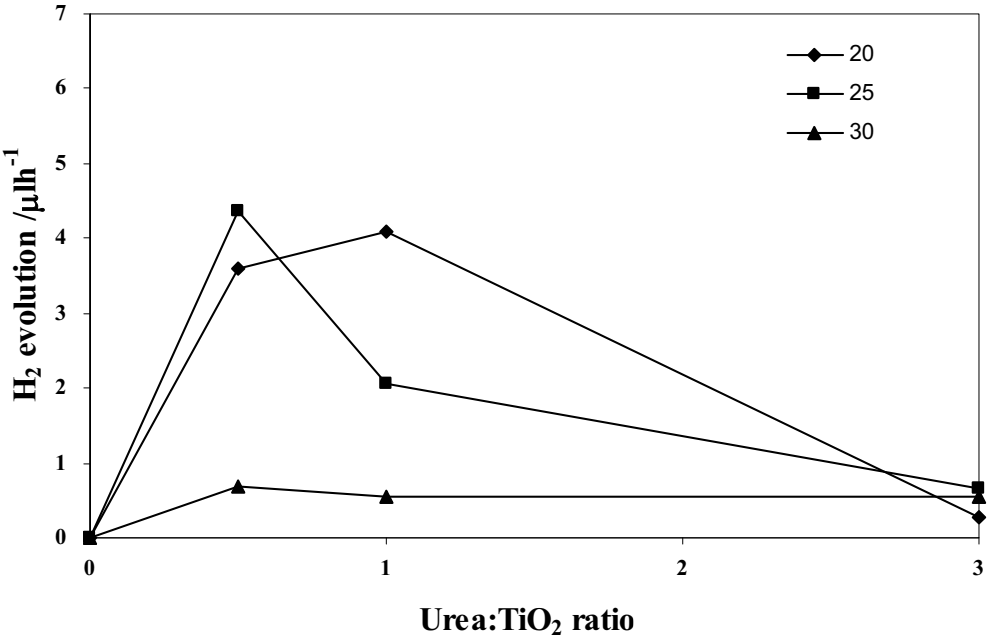

Figure 2.8 Photocatalytic H_2 production activity of (a) N-doped mesoporous TiO_2 and (b) N-doped commercial TiO_2 prepared with different urea:TiO_2 molar ratios of 0.5:1, 1:1, and, 3:1 and

at different calcination temperatures of 200, 250, and 300°C (Reaction conditions: 0.2 g photocatalyst, 150 ml distilled water, 50 ml methanol, and 5 h irradiation time).

For the N-doped commercial TiO_2 photocatalyst calcined at 200°C, the photocatalytic H_2 production activity tended to increase with increasing urea:TiO_2 molar ratio from 0.5:1 to 1:1 and then to decrease with further increasing the molar ratio. At 250°C, the photocatalytic activity reached a maximum at a urea:TiO_2 molar ratio of 0.5:1 and gradually decreased as the urea:TiO_2 molar ratio further increased. At 300°C, the photocatalytic activity remained almost unchanged, even though the urea:TiO_2 molar ratio increased. Their activity was quite different from those of the N-doped mesoporous TiO_2 ones. It seems to be that the pore size is very important, greatly affecting the photocatalytic activity. As previously mentioned, the pore size of the commercial TiO_2 is mostly in the macropore region, having a pore size much greater than 50 nm in diameter. Because of the extremely large pore size of the commercial TiO_2, it is much more capable of allowing the reactants to have access into and the products to leave from the pore structure than the mesoporous TiO_2. This might lead to a much easier conversion of biuret (straight chain compound) to cyanuric acid (cyclic compound) according to Eq. (2.6). This effect is relatively dominant at high temperatures (250 and 300°C) because biuret can be easily transformed to cyanuric acid or even released into gas phase, consequently resulting in lowering the photocatalytic H_2 production activity of the N-doped commercial TiO_2 prepared at these conditions. At a calcination temperature of 300°C, in addition to the previous reason, the surface N content is another important parameter, which could be related to the constant photocatalytic activity. From the results of surface N content (Table 2.2), for any given urea:TiO_2 molar ratio at 300°C, the surface N content was lower than those at the other calcination temperatures with little difference between the urea:TiO_2 molar ratios of 0.5:1 and 1:1, resulting in the almost unchanged H_2 production activity. Moreover, even though the surface N content of the commercial photocatalyst with a urea:TiO_2 molar ratio of 3:1 was much higher than those at the other two molar ratios, the photocatalytic H_2 production activity remained almost constant. The results suggest that the addition of nitrogen on the photocatalyst surface has to be optimized for a maximum H_2 production activity over both TiO_2 photocatalysts because the specific surface area can be significantly reduced with a higher amount of doped nitrogen.

As experimentally observed that the N-doped mesoporous TiO_2 prepared at a urea:TiO_2 molar ratio of 1:1 at a calcination temperature of 250°C exhibited the comparatively high photocatalytic activity, the effect of Pt loading onto such the TiO_2 photocatalyst was preliminarily studied. It was found that the H_2 production activity significantly increased with increasing Pt loading content up to 1.3 wt.%, then after this optimum point, the H_2 production activity

decreased, as shown in Table 2.3. This result can be related to surface Pt content, which was analyzed by XPS, and it was found that the surface Pt content also reached the maximum at the Pt content of 1.3 wt.%. The possible explanation is that TiO_2 particles may carry more Pt nanoclusters, which are very important for the removal of photogenerated electrons from TiO_2 for the reduction reaction and lead to an increase of the photocatalytic activity. After reaching a maximum, the H_2 production activity decreased due to too much Pt nanoclusters and their agglomeration on TiO_2 surface. These clusters would shield the photosensitive TiO_2 surface, and subsequently reduce the surface concentration of the electrons and holes available for the reactions. Another explanation is that at high metal loadings, the deposited metal particles may act as the recombination centers for the photoinduced species. Detailed experiments are required in order to logically explain the effect of Pt loading.

Table 2.3 Summary of the effect of Pt loading onto N-doped mesoporous TiO_2 prepared at a urea:TiO_2 molar ratio of 1:1 at a calcination temperature of 250°C on surface Pt content and photocatalytic H_2 production (Reaction conditions: 0.2 g photocatalyst, 150 ml distilled water, 50 ml methanol, and 5 h irradiation time)

Nominal Pt loading (wt.%)	Surface Pt content (wt.%)	H_2 production ($\mu l h^{-1}$)
0	0	6.23
0.4	0.80	8.05
0.8	3.69	15.19
1.0	3.23	17.89
1.1	3.30	17.95
1.3	4.73	26.40
1.4	3.25	11.75
1.6	3.71	8.04

Conclusions

Two types of N-doped TiO_2 photocatalysts, namely synthesized mesoporous TiO_2 and non-mesoporous commercial TiO_2, were comparatively studied for their photocatalytic H_2 production activity under visible light irradiation. To modify the visible light absorption ability of the TiO_2 photocatalysts, N-doping was performed. The urea, as a source of N, was mixed with both TiO_2 photocatalysts at various urea:TiO_2 molar ratios and calcined at various calcination

temperatures. The obtained N-doped TiO_2 photocatalysts could subsequently absorb visible light. The optimum preparation conditions of the N-doped mesoporous TiO_2 and N-doped commercial TiO_2 for achieving the highest photocatalytic H_2 production activity were a urea:TiO_2 molar ratio of 1:1 at a calcination temperature of 250°C and 0.5:1 at a calcination temperature of 250°C, respectively. However, the N-doped mesoporous TiO_2 prepared at such the optimum conditions exhibited relatively the best photocatalytic activity.

Recommendations

The effect of Pt loading on the enhancement of photocatalytic H_2 production activity of the N-doped mesoporous TiO_2 should be further investigated in details. Other techniques for modifying the TiO_2-containing system to be able to utilize visible light region, such as sensitization technique, is also interesting and should be studied with the Pt-loaded mesoporous TiO_2 photocatalyst.

Output ที่ได้จากโครงการ

==========

Output ที่ได้จากโครงการนี้ ได้แก่

1. International Publications

1.1 Published paper (ภาคผนวก ก)

Thammanoon Sreethawong, Tarawipa Puangpetch, Sumaeth Chavadej, and Susumu Yoshikawa, "Quantifying Influence of Operational Parameters on Photocatalytic H_2 Evolution over Pt-Loaded Nanocrystalline Mesoporous TiO_2 Prepared by Single-Step Sol-Gel Process with Surfactant Template", Journal of Power Sources, 2007, 165(2), 861-869. (Impact Factor: 3.521)

1.2 Submitted manuscript (ภาคผนวก ข)

Thammanoon Sreethawong, Siriporn Laehsalee, and Sumaeth Chavadej, "Comparative Investigation of Mesoporous and Non-Mesoporous TiO_2 Nanocrystals for Photocatalytic H_2 Production over N-Doped TiO_2 under Visible Light Irradiation", Submitted for Publication in International Journal of Hydrogen Energy. (Impact Factor: 2.612)

2. International Presentations

2.1 The 4^{th} Asia Pacific Congress on Catalysis (ภาคผนวก ค)

Thammanoon Sreethawong, Tarawipa Puangpetch, Sumaeth Chavadej, and Susumu Yoshikawa, "Probing Factors Affecting Photocatalytic H_2 Evolution over Nanocrystalline Mesoporous Pt/TiO_2 Prepared by Single-Step Sol-Gel Process with Surfactant Template", The 4^{th} Asia Pacific Congress on Catalysis (APCAT 4), 6-8 December 2006, Singapore.

2.2 The 2^{nd} International Conference on Advances in Petrochemicals and Polymers (ภาคผนวก ง)

Siriporn Laehsalee, Sumaeth Chavadej, Susumu Yoshikawa, and Thammanoon Sreethawong, "Use of Pt/N-Doped Titania for Photocatalytic Hydrogen Evolution from Water under Visible Light Irradiation", The 2^{nd} International Conference on Advances in Petrochemicals and Polymers (ICAPP 2007), 25-28 June 2007, Bangkok, Thailand.

3. International Proceedings

3.1 Chemeca 2007 Conference (ภาคผนวก จ)

Siriporn Laehsalee, Thammanoon Sreethawong, Sumaeth Chavadej, and Susumu Yoshikawa, "Photocatalytic Production of Hydrogen from Water over Pt/N-Doped Titania under Visible Light Irradiation", Chemeca 2007 Conference (Academia and Industry Strengthening the Profession), 23-26 September 2007, Melbourne, Victoria, Australia.

ภาคผนวก

==========

ภาคผนวก ก : Paper published in Journal of Power Sources

ภาคผนวก ข : Manuscript submitted for publication in International Journal of Hydrogen Energy

ภาคผนวก ค : Extended abstract of The 4th Asia Pacific Congress on Catalysis

ภาคผนวก ง : Abstract of The 2nd International Conference on Advances in Petrochemicals and Polymers

ภาคผนวก จ : Proceedings of Chemeca 2007 Conference

ภาคผนวก ก

Paper published in Journal of Power Sources

Available online at www.sciencedirect.com
ScienceDirect
Journal of Power Sources 165 (2007) 861–869
JOURNAL OF POWER SOURCES
www.elsevier.com/locate/jpowsour

Quantifying influence of operational parameters on photocatalytic H_2 evolution over Pt-loaded nanocrystalline mesoporous TiO_2 prepared by single-step sol–gel process with surfactant template

Thammanoon Sreethawong [a,*], Tarawipa Puangpetch [a], Sumaeth Chavadej [a], Susumu Yoshikawa [b]

[a] *The Petroleum and Petrochemical College, Chulalongkorn University, Soi Chula 12, Phyathai Road, Pathumwan, Bangkok 10330, Thailand*
[b] *Institute of Advanced Energy, Kyoto University, Uji, Kyoto 611-0011, Japan*

Received 6 November 2006; received in revised form 16 December 2006; accepted 20 December 2006
Available online 22 January 2007

Abstract

The photocatalytic evolution of hydrogen from water was investigated under various conditions over 0.6 wt% Pt-loaded nanocrystalline mesoporous TiO_2 photocatalyst prepared by a single-step sol–gel process with a surfactant template. The highly crystalline photocatalyst possessed a mesoporous characteristic with high surface area and narrow monomodal pore size distribution. More specifically, the influence of the following operational parameters, namely sacrificial reagent type, initial solution pH, photocatalyst concentration, initial sacrificial reagent concentration (of the best sacrificial reagent studied), and irradiation time, was the main focus. The hydrogen evolution was experimentally found to be strongly affected by all of the above parameters. The optimum values of initial solution pH, photocatalyst concentration, and sacrificial reagent concentration, as well as the appropriate type of sacrificial reagent, were obtained. The results showed that the utilization of the photocatalyst with the proper selection of optimum operational conditions could lead to considerably high photocatalytic hydrogen evolution activity.

Keywords: Photocatalysis; Hydrogen evolution; Pt/TiO_2; Single-step sol–gel; Surfactant template; Mesoporous material

1. Introduction

From the beginning of the last century, the scientific community has recognized hydrogen (H_2) as a potential source of fuel. Current uses of H_2 are generally in industrial processes, as well as in rocket fuels and spacecraft propulsion. With further research and development, this hydrogen fuel is believed to be able to effectively serve as an alternative source of energy for generating electricity and fueling motor vehicles. Therefore, it is of significant interest in the development of fuel processing technologies and catalysts/photocatalysts to produce H_2 from an abundantly available resource; water.

Efforts are currently underway to improve photochemical methods for H_2 production. Heterogeneous photocatalysis is one of the most promising approaches in this regard [1–6]. This technique is based on the photoexcitation of a semiconductor photocatalyst with the absorption of photons of energy equal to or greater than the band gap, leading to better oxidation (formation of photogenerated holes, h_{vb}^+) and reduction (formation of photogenerated electrons, e_{cb}^-). The potential levels of the valence band (V_{vb}) and conduction band (V_{cb}) edges play a vital role in predicting the type of reactions that can occur at the surface of the semiconductor photocatalyst. The magnitude of these potentials depends on the nature of the solvent and the pH of the system. Another important factor that makes photocatalysis productive is the ability of the solvent to suppress the undesired electron–hole recombination, either by capturing the valence band holes or the conduction band electrons. Water is the most commonly used solvent in photocatalysis and is the most readily available chemical feedstock, as mentioned earlier, for photocatalytic H_2 evolution through water splitting. But the main associated problem is the low H_2 yield. To resolve this hindrance, primarily oxygenated hydrocarbons, such as methanol and ethanol, have been frequently employed in this water splitting

* Corresponding author. Tel.: +66 2 218 4132; fax: +66 2 215 4459.
E-mail address: thammanoon.s@chula.ac.th (T. Sreethawong).

0378-7753/$ – see front matter © 2007 Elsevier B.V. All rights reserved.
doi:10.1016/j.jpowsour.2006.12.050

reaction [7–16]. Due to the presence of polarity and its ability to donate the lone-pair electron, these kinds of hydrocarbons behave as a sacrificial reagent, also widely known as hole scavenger or electron donor, to prevent an unfavorable electron–hole recombination during the photoexcitation process.

Since the discovery of the photoelectrochemical splitting of water on a titanium dioxide (TiO_2) electrode [17], TiO_2 semiconductor-based photocatalysis has attracted a great deal of study, owing to its high photocatalytic activity, good stability, and non-toxic property. Although TiO_2 is superior to other semiconductors in a variety of practical uses, it still possesses a serious defect that limits its photocatalytic activity; the electron–hole recombination subsequent to the band gap excitation. The high rate of the electron–hole recombination of TiO_2 particles results in a low efficiency of photocatalysis [18]. Many attempts have been made to overcome this weak point of TiO_2; for example, the depositing of noble metals, especially platinum (Pt), the mixing of metal oxides with TiO_2, and the doping of selective metal ions into the TiO_2 lattice [19–26]. The advantage of depositing noble metals is the trapping of the photogenerated charge carriers by the metal particles and thus the inhibition of their recombination during migration from inside the material to the surface. The effect of metal deposition depends on many factors, such as the metal concentration and the distribution of the metal particles [20]. For the photocatalytic H_2 evolution from water, the deposition of Pt particles on the TiO_2 surface has been shown to greatly enhance the photocatalytic production of H_2 from water/sacrificial reagent solutions, since Pt particles not only help the separation of the photogenerated species in illuminated TiO_2 but also act as H_2 evolution sites [7,18,27,28]. There have been a multitude of studies on Pt deposition onto commercially available TiO_2 powders, especially Degussa P-25, which normally possess a non-mesoporous characteristic. However, to our knowledge, investigations on Pt-deposited mesoporous TiO_2 and their photocatalytic activity for H_2 evolution have not been extensively reported.

Since the discovery by Antonelli and Ying [29] of mesoporous TiO_2 synthesized by a sol–gel process with phosphorous surfactants as templates, various methods of surfactant templating have been developed for the preparation of mesoporous structures of TiO_2 [30–32]. Since mesoporous materials normally possess large surface area and narrow pore size distribution, which advantageously make them a versatile candidate in the catalysis field, the utilization of mesoporous TiO_2 in many catalytic reactions becomes very attractive. It is generally anticipated that the use of a high surface area mesoporous oxide support rather than a commercial support for noble or transition metals has some beneficial effects on the catalytic performance. The mesoporous support would give rise to well-dispersed and stable metal particles on its surface after the steps of calcination and reduction, and as a consequence it would show an improved catalytic performance [33]. To achieve such high catalytic activity of the TiO_2 photocatalyst, attempts to focus on the synthesis step are needed, since the light harvesting capability and the reactant accessibility can be enhanced as a result of multiple scattering and high surface area, as well as uniform pore structure of the synthesized TiO_2.

In our previous work [34], the Pt-loaded nanocrystalline mesoporous TiO_2 photocatalyst with 0.6 wt% optimum Pt loading prepared by a single-step sol–gel (SSSG) process with a surfactant template was verified for the first time to possess a superior photocatalytic performance for H_2 evolution to those prepared by conventional incipient wetness impregnation and photochemical deposition processes. The photocatalytic H_2 evolution activity of the SSSG photocatalyst was enhanced in average by about 18% in comparison with the other two processes. Following this accomplishment in the synthesis of highly photocatalytic active Pt-loaded mesoporous TiO_2, it is essential to optimize all relevant reaction conditions, aiming at obtaining maximum H_2 evolution activity. In this contribution, the influence of various operational parameters on photocatalytic H_2 evolution was quantitatively investigated and optimized over the SSSG-prepared 0.6 wt% Pt-loaded mesoporous TiO_2 photocatalyst.

2. Experimental

2.1. Materials

Tetraisopropyl orthotitanate (TIPT, Tokyo Chemical Industry Co. Ltd.), hydrogen hexachloroplatinate (IV) hydrate (Nacalai Tesque Inc.), laurylamine hydrochloride (LAHC, Tokyo Chemical Industry Co. Ltd.), acetylacetone (ACA, Nacalai Tesque Inc.) and methanol (Nacalai Tesque Inc.) were used for the synthesis of Pt-loaded mesoporous TiO_2. LAHC was used as a surfactant template, behaving as a mesopore-directing agent. ACA, serving as a modifying agent, was applied to moderate the hydrolysis and condensation processes of titanium precursor. HCl and NaOH (Nacalai Tesque Inc.) were used for the adjustment of the reaction solution pH. Various sacrificial reagents, including methanol, ethanol, 1-propanol, 2-propanol, 1-butanol, acetic acid, acetone, ethylene glycol, diethylene dioxide (1,4-dioxane), and dimethyl formamide (Nacalai Tesque Inc.) were comparatively utilized for the photocatalytic reaction study. All chemicals were analytical grade and were used without further purification.

2.2. Photocatalyst synthesis procedure

Single-step sol–gel (SSSG)-made 0.6 wt% Pt-loaded nanocrystalline mesoporous TiO_2 photocatalyst was synthesized via a combined sol–gel with surfactant-assisted templating mechanism in the LAHC/TIPT modified with ACA system [34]. In a typical synthesis, a specified amount of analytical grade ACA was first introduced into TIPT with a molar ratio of unity. The mixed solution was then gently shaken until homogeneous mixing. Afterwards, a 0.1 M LAHC aqueous solution of pH 4.2 was added to the ACA-modified TIPT solution, in which the molar ratio of TIPT to LAHC was tailored to a value of 4:1. The mixture was continuously stirred at room temperature for an hour and was then aged at 40 °C for 10 h to obtain transparent yellow sol-containing solution as a result of the complete hydrolysis of the TIPT precursor. To the aged TiO_2 sol solution, a specific amount of hydrogen hexachloroplatinate (IV) hydrate

in methanol was incorporated for a desired Pt loading of 0.6 wt%, and the final mixture was further aged at 40 °C for 1 day to acquire a homogeneous solution. Then, the condensation reaction-induced gelation was allowed to proceed by placing the sol-containing solution into an oven at 80 °C for a week to ensure complete gelation. Subsequently, the gel was dried overnight at 80 °C to eliminate the solvent, which was mainly the distilled water used in the preparation of the surfactant aqueous solution. The dried sample was calcined at 500 °C for 4 h to remove the LAHC template and to consequently produce the desired photocatalyst.

2.3. Photocatalyst characterizations

X-ray diffraction (XRD) was used to identify the crystalline phases present in the sample. A Rigaku RINT-2100 rotating anode XRD system generating monochromated Cu Kα radiation with a continuous scanning mode at a rate of $2^\circ\,min^{-1}$ and operating conditions of 40 kV and 40 mA was used to obtain an XRD pattern. A nitrogen adsorption system (BEL Japan BELSORP-18 Plus) was employed to create adsorption–desorption isotherm at the liquid nitrogen temperature of −196 °C. The Brunauer–Emmett–Teller (BET) approach, using adsorption data over the relative pressure ranging from 0.05 to 0.35, was utilized to determine the surface area of the photocatalyst sample. The Barrett–Joyner–Halenda (BJH) approach was used to determine pore size distribution from the desorption data. The sample was degassed at 200 °C for 2 h to remove physisorbed gases prior to the measurement. The sample morphology was observed by a transmission electron microscope (TEM, JEOL JEM-200CX) and a scanning electron microscope (SEM, JEOL JSM-6500FE) operated at 200 and 15 kV, respectively. The elemental mappings over the desired region of the photocatalyst were detected by an energy-dispersive X-ray spectrometer (EDS) attached to the SEM.

2.4. Photocatalytic activity testing

The photocatalytic H_2 evolution reaction was performed in a closed gas-circulating system. In a typical run, a specified amount of the photocatalyst was suspended in an aqueous sacrificial reagent solution by using a magnetic stirrer within an inner irradiation reactor made of Pyrex glass. A high-pressure Hg lamp (300 W, λ_{max} of 365 nm) was utilized as the light source. The initial solution pH was adjusted to a desired value by adding a few drops of either HCl or NaOH aqueous solution with an appropriate concentration. Prior to the reaction, the mixture was left in the dark while being simultaneously thoroughly deaerated by purging the system with Ar gas for 30 min. Afterwards, the photocatalytic reaction system was closed, and the reaction was started by exposing the photoreactor to the light irradiation. To avoid heating of the solution during the course of the reaction, water was circulated through a cylindrical Pyrex jacket located around the light source. The gaseous H_2 evolved was collected at different intervals of irradiation time and was analyzed by an on-line gas chromatograph (Shimadzu GC-8A, Molecular sieve 5 Å, Ar gas), which was connected to a circulation line and equipped with a thermal conductivity detector (TCD). Different operational parameters were quantitatively varied in order to obtain the optimum conditions for the maximum photocatalytic H_2 evolution over the Pt-loaded mesoporous TiO_2 photocatalyst. These operational parameters included sacrificial reagent type, initial solution pH, photocatalyst concentration, initial sacrificial reagent concentration (of the best sacrificial reagent), and irradiation time.

3. Results and discussion

3.1. Photocatalyst characterizations

Fig. 1 shows the nitrogen adsorption–desorption isotherm and pore size distribution of the 0.6 wt% Pt-loaded mesoporous TiO_2 photocatalyst. The isotherm in Fig. 1(a) is of typical type IV pattern with hysteresis loop, which is a marked characteristic of mesoporous materials, according to the IUPAC classification [35]. The well-defined hysteresis loop with a sloping adsorption branch and a relatively steep desorption branch belongs to H2 type. It is well known that a distribution of various sized cavities, but with the same entrance diameter, would be attributed to this

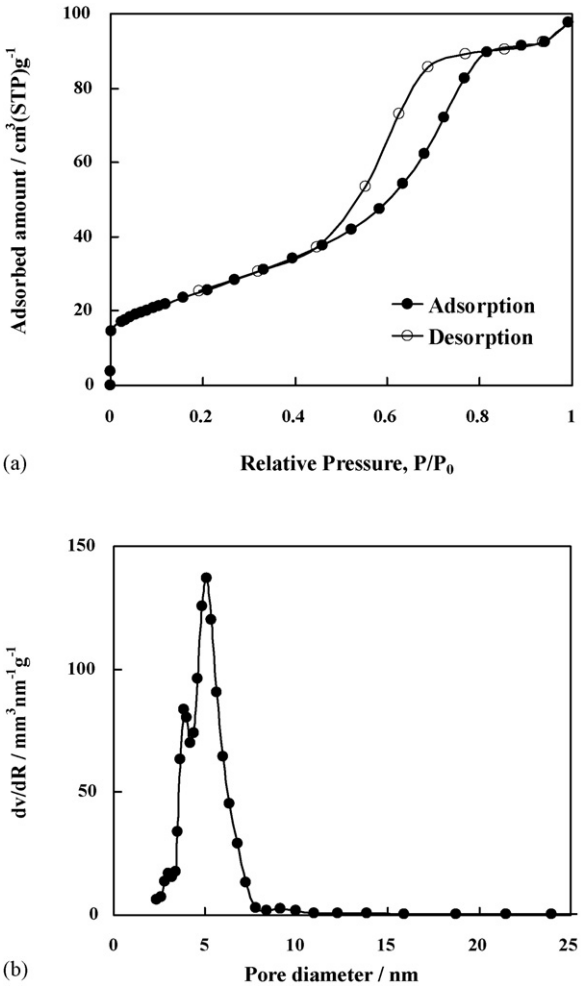

Fig. 1. N_2 adsorption–desorption isotherm (a) and pore size distribution (b) of the synthesized mesoporous Pt/TiO_2 photocatalyst.

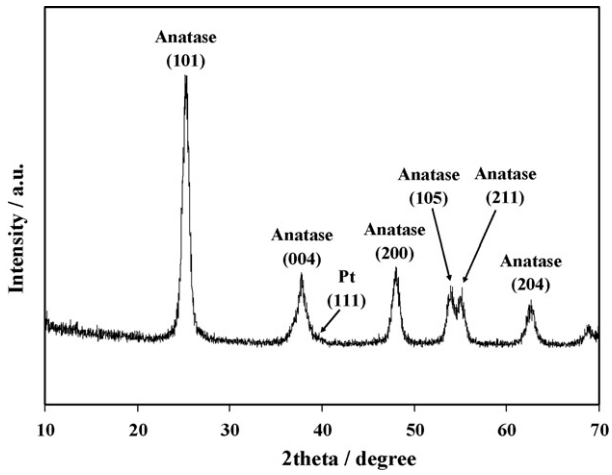

Fig. 2. XRD pattern of the synthesized mesoporous Pt/TiO_2 photocatalyst.

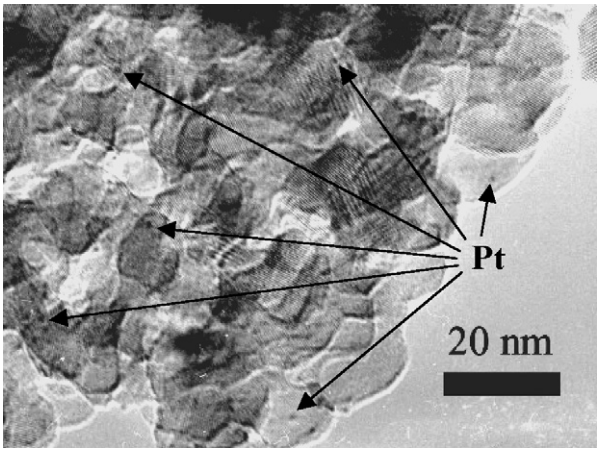

Fig. 3. TEM image of the synthesized mesoporous Pt/TiO_2 photocatalyst.

type of hysteresis loop. As can be seen from Fig. 1(b), a narrow monomodal pore size distribution, centered at a pore diameter in the mesopore region of 2–50 nm, can be obtained from the material synthesized by the synthesis system, suggesting its exquisite quality. The textural properties of the photocatalyst are listed as follows: BET surface area = 89 $m^2\ g^{-1}$, mean pore diameter = 5.06 nm, and total pore volume = 0.162 $cm^3\ g^{-1}$.

The crystalline structure of the synthesized mesoporous Pt/TiO_2 photocatalyst revealed by XRD analysis is shown in Fig. 2. The diffractrogram is indexed to pure anatase TiO_2 (JCPDS Card no. 21-1272) [36] with high crystallinity. From the XRD result, the indistinguishable presence of the diffraction peaks of Pt indicates that the Pt particles were in a very high dispersion degree. As the minimum detection limit of the XRD technique is around 5 nm, it is inferred that the crystallite size of the Pt particles was below that value. The crystallite size of TiO_2 particles, estimated from line broadening of anatase (1 0 1) diffraction peak using Sherrer formula [37], was approx-

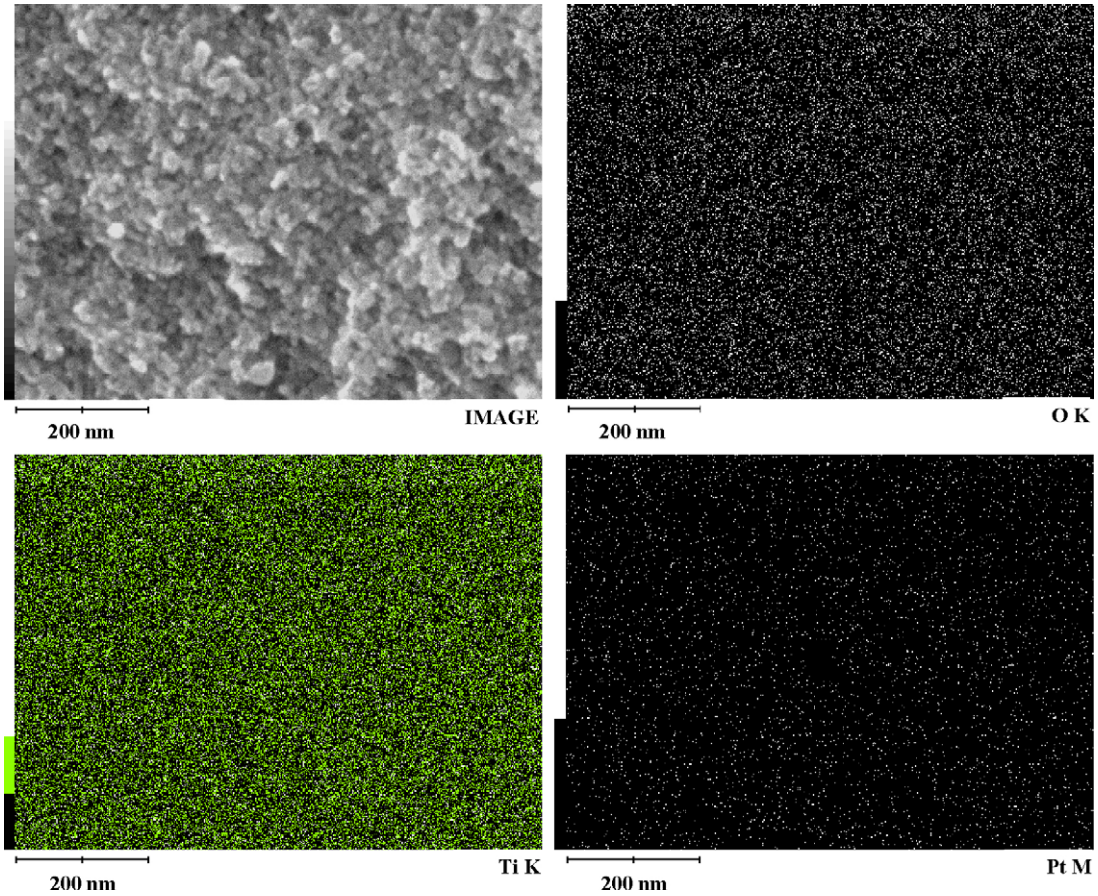

Fig. 4. SEM image and elemental mappings of the synthesized mesoporous Pt/TiO_2 photocatalyst.

imately 11 nm. The particle sizes of Pt and TiO_2 from the TEM analysis are in the region of 1–2 and 10–15 nm, respectively, as depicted by the TEM image in Fig. 3. The observed particle size of TiO_2 is in good accordance with the crystallite size calculated from the XRD result. In addition, homogeneously dispersed Pt nanoparticles on the TiO_2 surface are clearly seen from the TEM image.

The surface morphology of the synthesized photocatalyst was further investigated by using SEM. The acquired image is presented in Fig. 4. In the photocatalyst micrograph, particles with quite uniform size can be observed in aggregated clusters consisting of many nanoparticles. It can be seen that the photocatalyst was highly mesoporous, which is apparent by the SEM image. EDS analysis also provided useful information about the elemental distribution on the photocatalyst, as included in Fig. 4 by the elemental mapping of each component. The existence of dots in the elemental mapping images reveals the presence of all the investigated (Ti, O, and Pt) species. The EDS mappings reveal that all elements in the Pt-loaded TiO_2 were well distributed throughout the bulk photocatalyst, especially the investigated Pt species. This is another good verification of the high dispersion state of the deposited Pt nanoparticles. According to the N_2 adsorption–desorption, TEM, and SEM results, it is additionally worthwhile to emphasize that the mesoporous structure of the synthesized photocatalyst can be attributed to the pores formed between the nanocrystalline TiO_2 particles due to their aggregation, which is in the same line as the mesoporous TiO_2 reported in literature [38–43].

3.2. Photocatalytic H_2 evolution activity

3.2.1. Effect of sacrificial reagent type

In photocatalytic water splitting for H_2 evolution, the oxidation of water by holes is a much slower process than the reduction by electrons. In order to smooth the progress of the oxidation, sacrificial reagents or hole scavengers are often introduced, especially for the principal purpose of preventing the mutual electron–hole recombination process. Once the holes are scavenged from the photocatalyst surface, the longer decay time of surface electrons would certainly facilitate the reduction of protons in the solution to form hydrogen on the Pt active sites [44–46]. It is also definitely important to first mention that no hydrogen evolution activity was experimentally observed for the blank tests (without photocatalyst or without sacrificial reagent).

Initially, various types of sacrificial reagents were tested for the photocatalytic H_2 evolution to find which type of sacrificial reagent is the most effective in assisting the photocatalytic reaction. An aqueous solution containing the same amount of various sacrificial reagents was thus illuminated under identical reaction conditions. Table 1 shows the photocatalytic H_2 evolution activity of the synthesized nanocrystalline mesoporous Pt/TiO_2 photocatalyst using various sacrificial reagents, and Fig. 5 also shows the photocatalytic H_2 evolution profiles and activity using different sacrificial reagent types in an alcohol series. The results show that among the investigated sacrificial reagents, those in the alcohol series exhibited considerably higher photocatalytic activity than others. This might be attributable to the ease in donating lone-pair electrons to the valence band hole upon the photocatalyst excitation [47], as compared to other types of sacrificial reagents. Among the alcohol series itself, methanol was found to be the most effective and strongest sacrificial reagent to yield the highest photocatalytic H_2 evolution activity. It appears that compounds possessing very high polarity, such as acids and ketones, are unable to effectively suppress the electron–hole recombination, probably due to their stable electronic configuration. Apart from that, the carbon-to-carbon bond breaking also plays an important role in differentiating photocatalytic activity, since it directly involves the lone-pair electron donation. The extent of the carbon-to-carbon bond breaking decreases with the increase in chain elongation and complexity, as these factors contribute to enhance the steric hindrance in the molecule [47]. Since methanol was experimentally verified to be the most effective sacrificial reagent for the investigated system using the synthesized mesoporous Pt/TiO_2 photocatalyst, it was used as the main studied sacrificial reagent in further experiments.

3.2.2. Effect of initial solution pH

One of the important parameters affecting the photocatalytic reactions taking place on the photocatalyst surfaces is the solution pH, since it primarily dictates the surface charge properties

Table 1
Effect of various sacrificial reagent types on photocatalytic H_2 evolution activity of the synthesized mesoporous Pt/TiO_2 photocatalyst (reaction conditions: photocatalyst amount, 0.2 g; distilled water amount, 200 ml; sacrificial reagent amount, 20 ml; irradiation time, 5 h)

Type of sacrificial reagent	Molecular structure of sacrificial reagent	H_2 evolution activity (μmol h^{-1})
Methanol	CH_3OH	1385
Ethanol	CH_3CH_2OH	1123
1-Propanol	$CH_3CH_2CH_2OH$	775
2-Propanol	$CH_3CH(OH)CH_3$	599
1-Butanol	$CH_3CH_2CH_2CH_2OH$	629
Acetic acid	CH_3COOH	78
Acetone	CH_3COCH_3	22
Ethylene glycol	$OHCH_2CH_2OH$	451
Diethylene dioxide (1,4-dioxane)	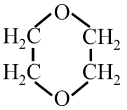	292
Dimethyl formamide	$HCON(CH_3)_2$	87

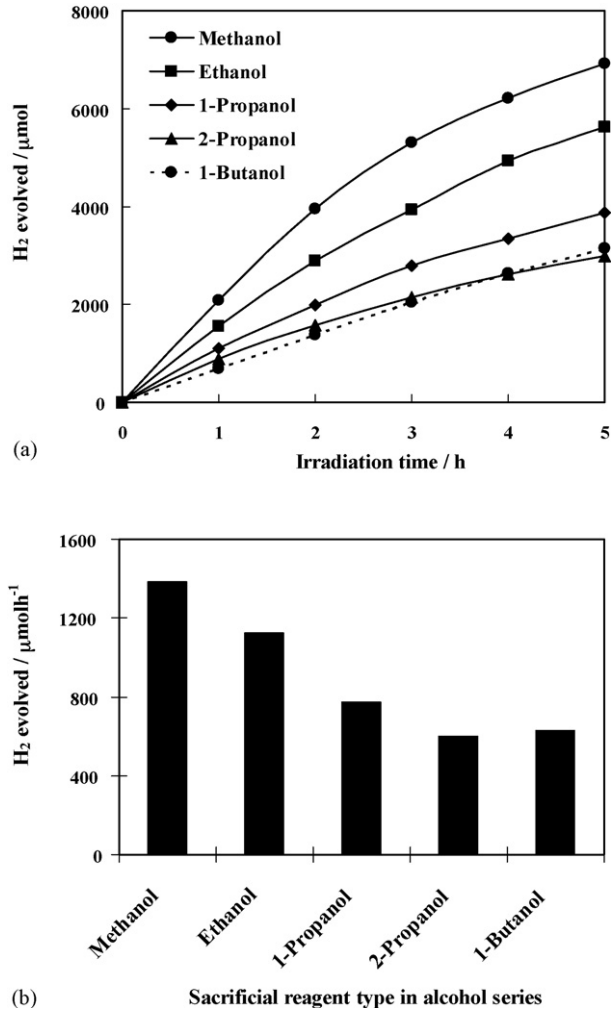

Fig. 5. Effect of sacrificial reagent type in alcohol series on (a) time course of H_2 evolved and (b) dependence of photocatalytic H_2 evolution activity of the synthesized mesoporous Pt/TiO_2 photocatalyst (reaction conditions: photocatalyst amount, 0.2 g; distilled water amount, 200 ml; sacrificial reagent amount, 20 ml; irradiation time, 5 h).

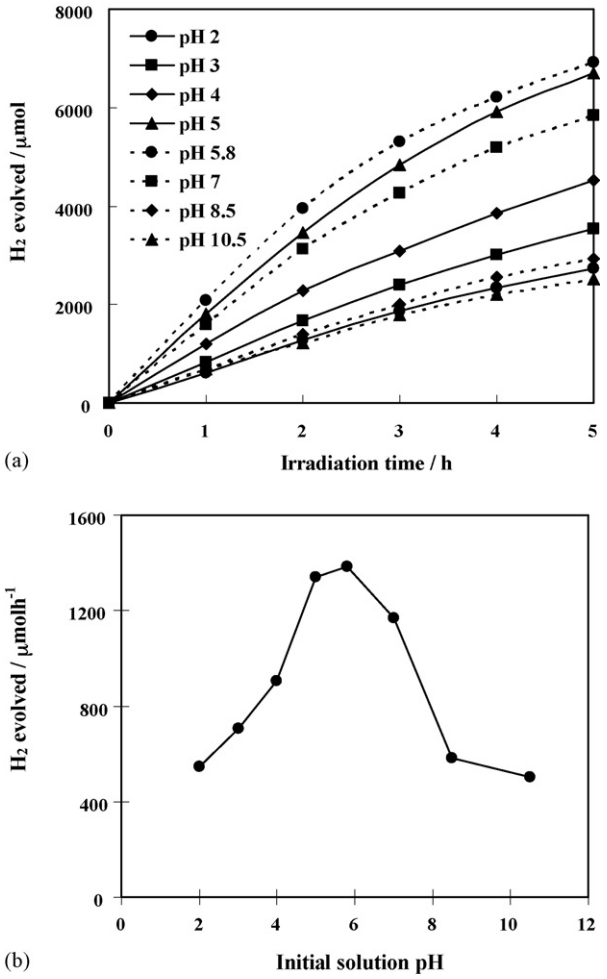

Fig. 6. Effect of initial solution pH on (a) time course of H_2 evolved and (b) dependence of photocatalytic H_2 evolution activity of the synthesized Pt/TiO_2 photocatalyst (reaction conditions: photocatalyst amount, 0.2 g; distilled water amount, 200 ml; sacrificial reagent type, methanol; sacrificial reagent amount, 20 ml; irradiation time, 5 h).

of the photocatalyst. In addition, the solution pH can affect the states of both reactant in solution and photocatalyst surface, which ultimately changes the electrostatic interaction between the reactant and the TiO_2 surface [48–50]. The role of initial solution pH on the photocatalytic H_2 evolution activity was studied over a broad pH range of 2–10.5 using methanol as a sacrificial reagent, noting that the initial pH of the original solution containing 200 ml distilled water and 20 ml methanol (2.25 M) is 5.8, and insignificant changes of solution pH were observed after the course of the photocatalytic reaction. The experimental results shown in Fig. 6 indicate that the efficiency of the H_2 evolution activity increases with an increase in solution pH from 2 to a range of 5–6, and a further increase in solution pH greater than 6 led to a drastic decrease in the H_2 evolution activity. The results imply that the H_2 evolution activity of the studied photocatalyst is favorable at mild acidic conditions, and the optimum initial solution pH is around 6.

The effect of solution pH on the efficiency of the photocatalytic H_2 evolution process is quite complicated since it contributes to several roles. It is first related to the ionization state of the photocatalyst surface according to the following reactions:

$$Ti^{IV}\text{–}OH + H^+ \rightarrow Ti^{IV}\text{–}OH_2{}^+, \quad pH < pH_{PZC} \tag{1}$$

$$Ti^{IV}\text{–}OH + OH^- \rightarrow Ti^{IV}\text{–}O^- + H_2O, \quad pH > pH_{PZC} \tag{2}$$

As known, a pH change can influence the adsorption of these species onto the TiO_2 photocatalyst surfaces, an important step for the photocatalytic reactions to take place. The point of zero charge (PZC) of the TiO_2 is approximately at pH 5.8–6.0 [51–53]. Therefore, at a $pH < pH_{PZC}$, the TiO_2 surface is positively charged, whereas at a $pH > pH_{PZC}$, the TiO_2 surface is negatively charged. At acidic pHs ($pH < 5$), an electrostatic repulsion between the positively charged surface of the photocatalyst and the hydronium cations (H^+) present in the solution retards the adsorption of the hydronium cations so as to accordingly be reduced to form hydrogen, resulting in a lower photocatalytic H_2 evolution activity. In the opposite manner, at alkaline pHs ($pH > 7$), an electrostatic repulsion between the negatively charged surface of the photocatalyst

and the molecules of the sacrificial reagent (lone-pair electron donor) also inhibits the adsorption of the sacrificial reagent as to scavenge the valence band holes for preventing electron–hole recombination. Besides, the photogenerated electrons cannot easily transfer to the photocatalyst surface, plausibly because of the negative charge repulsion, and subsequently transfer to outer system via the photocatalytic reduction reaction. Therefore, the electrons moving inside the bulk photocatalyst have high probability to recombine with holes at both bulk trap and defect sites. A higher rate of mutual recombination also consequently results in a lower photocatalytic H_2 evolution activity. These basically imply that complicated interactions between the species/molecules and the photocatalyst are taking place at acidic or alkaline conditions. When the photocatalyst contains no charge, the species/molecules are probably allowed to much more easily reach the photocatalyst surface and achieve higher photocatalytic reaction activity [54,55], thus experimentally obtaining the highest H_2 evolution activity at the initial solution pHs near the point of zero charge.

The TiO_2 particles, moreover, tend to agglomerate under acidic conditions [56]. This agglomeration can result in a lower surface area available for reactant adsorption and photon absorption, leading to a decrease in the photocatalytic activity; whereas another reason for the decrease in the photocatalytic activity under alkaline conditions can be attributed to the UV screening of the TiO_2 particles due to a higher concentration of OH^- present in the solution [57]. Hence, the solution pH plays an important role both in the characteristics of reactant species-containing solutions and in the reaction mechanisms that can contribute to the H_2 evolution.

3.2.3. Effect of photocatalyst concentration

The effect of the concentration of the synthesized nanocrystalline mesoporous Pt/TiO_2 photocatalyst on the photocatalytic H_2 evolution was investigated in the range of 0–1.82 g l^{-1} by varying the amount of photocatalyst added to the reactor containing an original aqueous 2.25 M methanol solution (pH 5.8) without pH adjustment. Fig. 7 illustrates the photocatalytic H_2 evolution activity as a function of photocatalyst concentration. The H_2 evolution activity first increased and then decreased with an increase in the photocatalyst amount added to the reactor. A higher concentration of the photocatalyst is expected to correspond to a greater absorption of UV energy, leading to a higher photocatalytic H_2 evolution activity. However, the activity began to decline when the concentration of the photocatalyst exceeded 0.91 g l^{-1}, indicating that the addition of the photocatalyst has to be optimized. The obtained experimental results can be rationalized in terms of the availability of active sites on the TiO_2 surface and the light penetration of photoactivating light into the suspension. The availability of active sites increases with the increase in photocatalyst concentration in the suspension, but the light penetration and the consequent photoactivated volume of the suspension shrink [58]. The penetration of light is cloaked in the reactor by the large quantity of the photocatalyst in the aqueous solution. When the photocatalyst concentration is very high, after traveling a certain distance on an optical path, turbidity impedes the further penetration of light in the reactor, indicating

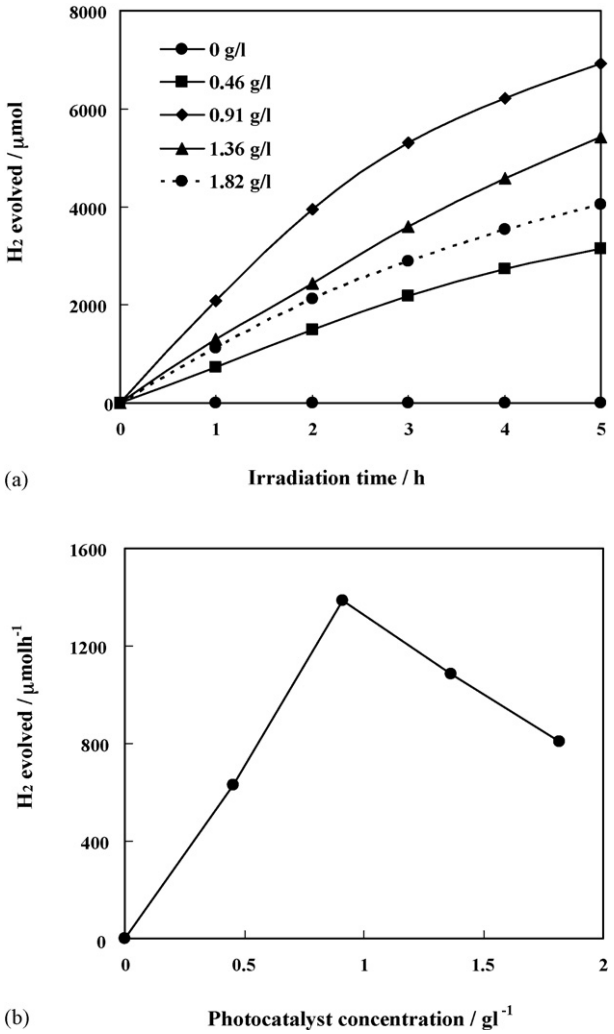

Fig. 7. Effect of photocatalyst concentration on (a) time course of H_2 evolved and (b) dependence of photocatalytic H_2 evolution activity of the synthesized mesoporous Pt/TiO_2 photocatalyst (reaction conditions: distilled water amount, 200 ml; sacrificial reagent type, methanol; sacrificial reagent amount, 20 ml; initial solution pH, 5.8; irradiation time, 5 h).

the block of the illuminating light. Although the light absorption of the outer photocatalyst increases, the capability of generating hydrogen from the inner photocatalyst decreases due to the lack of photoexcitation, signifying the screening effect of excess photocatalyst particles in the solution [49,59]. Consequently, the overall H_2 evolution activity decreases with a very high concentration of the photocatalyst. Moreover, the decrease in the photocatalytic activity at a higher photocatalyst concentration may be due to the deactivation of activated TiO_2 molecules by the collision with ground-state TiO_2 molecules (inactive TiO_2). The deactivation due to the shielding by TiO_2 can be explained according to the following reaction:

$$TiO_2{}^* + TiO_2 \rightarrow TiO_2{}^\# + TiO_2 \quad (3)$$

where $TiO_2{}^*$ is the TiO_2 with active species adsorbed on its surface, and $TiO_2{}^\#$ is the deactivated form of TiO_2 [60]. At a considerably high photocatalyst concentration, agglomeration and sedimentation of the photocatalyst particles have also been

reported. Under this condition, it leads to a reduction of the photocatalyst surface available for photon absorption and reactant adsorption, thus bringing lower stimulation to the photocatalytic reaction. An optimum photocatalyst concentration also greatly depends on the photoreactor geometry, the working conditions of the photoreactor, the degree of mixing, the UV lamp power, and the lamp geometry. The optimum amount of the photocatalyst has to be introduced into the system in order to avoid unnecessary excess photocatalyst and also to ensure total absorption of light photons for the efficient photocatalytic H_2 evolution reaction.

3.2.4. Effect of initial methanol concentration

It is important, both from mechanistic and application points of view, to study the dependence of the photocatalytic H_2 evolution reaction on the concentration of methanol, the most effective sacrificial reagent. The influence of initial methanol concentration on the photocatalytic H_2 evolution activity over the synthesized photocatalyst is shown in Fig. 8. With an increase in the methanol concentration, the photocatalytic activity dramatically increased and reached a maximum at the methanol concentration of 2.25 M. Beyond this optimum methanol concentration, a further increase in methanol concentration led to a decrease in the photocatalytic activity. Under the studied conditions, the optimum methanol concentration was about 2.25 M. At relatively high concentrations of methanol beyond the optimum point, although the surface active sites remain constant for a fixed catalyst concentration, the number of adsorbed methanol molecules accommodated on the photocatalyst surface increases [50,61]. Because the generation of valence band holes on the surface of the photocatalyst required for reacting with methanol molecules does not increase as the intensity of light and amount of catalyst are unchanged, there was an observed decrease in the photocatalytic H_2 evolution activity, probably due to the blockage of the adsorption of hydronium cations at surface active sites, so as to be reduced to produce hydrogen. Besides, as the photocatalytic reaction is an ion and radical reaction, and methanol can also somewhat behave as a quenching agent of ions and radicals [62], more ions and radicals can be quenched with the increase in methanol concentration. These mentioned reasons consequently lead to the decrease of H_2 evolution activity, after methanol concentration is over the optimum level.

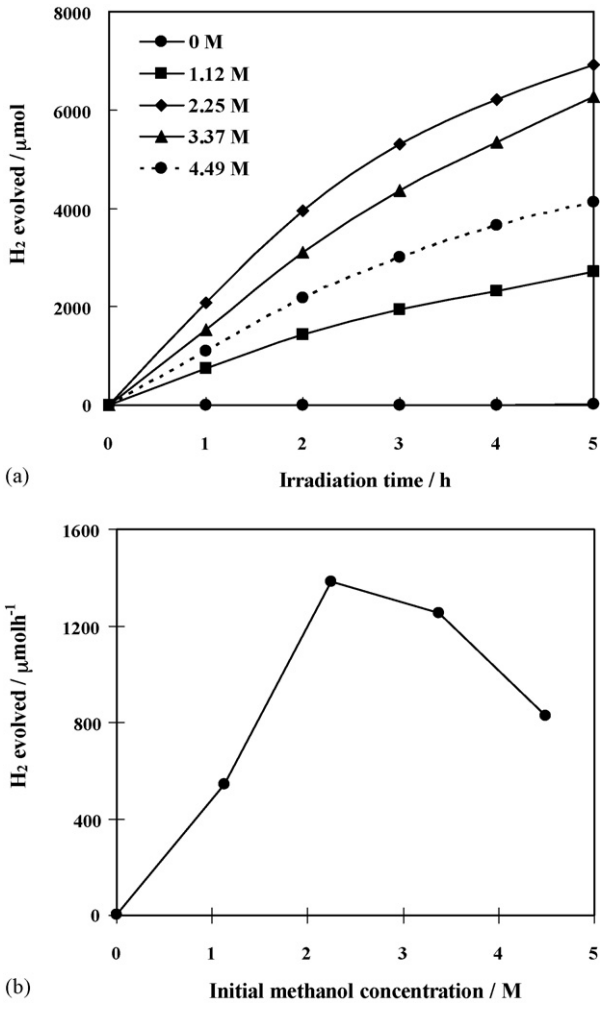

Fig. 8. Effect of initial methanol concentration on (a) time course of H_2 evolved and (b) dependence of photocatalytic H_2 evolution activity of the synthesized mesoporous Pt/TiO_2 photocatalyst (reaction conditions: photocatalyst amount, 0.2 g; solvent: distilled water; sacrificial reagent type, methanol; total solution volume, 220 ml; initial solution pH, 5.8; irradiation time, 5 h).

3.2.5. Effect of irradiation time

The time courses of the photocatalytic H_2 evolution over the synthesized mesoporous Pt/TiO_2 photocatalyst at various reaction conditions are given in part (a) of Figs. 5–8. It can be clearly seen that under light radiation, with increasing the time of irradiation up to 5 h, the amount of H_2 evolved increased almost proportionally to the irradiation time in the investigated period. This is because, with an increase in irradiation time, the photons absorbed on the surface of the photocatalyst become greater, which, in turn, helps in the photocatalytic process. However, a slight decrease in the H_2 evolution rate at a long irradiation time was observed. This can be explained that in a photocatalytic batch system, a long irradiation time regularly causes a progressive decline in the H_2 evolution rate due to the back reactions of products generated in the reaction system, as well as the pressure buildup in the gas phase [63]. Additionally, the active site deactivation due to the strong absorption of some molecular species might also be another cause of the decrease in the H_2 evolution activity after a long illumination time [58].

4. Conclusions

The use of SSSG-prepared 0.6 wt% Pt-loaded nanocrystalline mesoporous TiO_2 photocatalyst with high surface area and narrow monomodal pore size distribution for photocatalyzing H_2 evolution from water was studied under various reaction conditions. Several operational parameters were investigated in order to determine the optimum conditions exhibiting the maximum H_2 evolution activity. The experimental results showed that methanol was found to be the most efficient sacrificial reagent among several types of sacrificial reagents investigated. Mild acidic pH values in the range of 5–6 were favorable for the reaction. The optimum photocatalyst and initial methanol concentration were found to be 0.91 g l^{-1} and 2.25 M, respectively.

Acknowledgements

This work was financially supported by grants provided to the first/corresponding author by the Thailand Research Fund (TRF) (Contract/Grant No. MRG4980030) and by Chulalongkorn University, Thailand, through the Grants for Development of New Faculty Staff under the Ratchadapisek Somphot Endowment Fund (Contract/Grant No. 100/2549). The partial supports from the Petroleum and Petrochemical Consortium under the Ministry of Education, Thailand, and the Research Unit of Petrochemical and Environmental Catalysis under the Ratchadapisek Somphot Endowment Fund, Chulalongkorn University, Thailand, are also greatly acknowledged.

References

[1] M.A. Fox, M.T. Dulay, Chem. Rev. 93 (1993) 341–357.
[2] O. Legrini, E. Oliveros, A.M. Braun, Chem. Rev. 93 (1993) 671–698.
[3] J.C. Amphlett, K.A.M. Creber, J.M. Davis, R.F. Mann, B.A. Peppley, D.M. Stokes, Int. J. Hydrogen Energy 19 (1994) 131–137.
[4] M.R. Hoffmann, S.T. Martin, W. Choi, D. Bahnemann, Chem. Rev. 95 (1995) 69–96.
[5] K. Rajashwer, J. Appl. Electrochem. 25 (1995) 1067–1082.
[6] M.I. Litter, Appl. Catal. B: Environ. 23 (1999) 89–114.
[7] T. Sakata, T. Kawai, K. Hashimoto, Chem. Phys. Lett. 88 (1982) 50–54.
[8] J. Abrahams, R.S. Davidson, C.L. Morrison, J. Photochem. 29 (1985) 353–361.
[9] G.R. Bamwenda, S. Tsubota, T. Nakamura, M. Haruta, J. Photochem. Photobiol. A: Chem. 89 (1995) 177–189.
[10] T. Abe, E. Suzuki, K. Nagoshi, K. Miyashita, M. Kaneko, J. Phys. Chem. B 103 (1999) 1119–1123.
[11] Y. Li, G. Lu, S. Li, Chemosphere 52 (2003) 843–850.
[12] N.L. Wu, M.S. Lee, Int. J. Hydrogen Energy 29 (2004) 1601–1605.
[13] T. Sreethawong, Y. Suzuki, S. Yoshikawa, J. Solid State Chem. 178 (2005) 329–338.
[14] T. Sreethawong, Y. Suzuki, S. Yoshikawa, Int. J. Hydrogen Energy 30 (2005) 1053–1062.
[15] T. Sreethawong, S. Ngamsinlapasathian, Y. Suzuki, S. Yoshikawa, J. Mol. Catal. A: Chem. 235 (2005) 1–11.
[16] T. Sreethawong, S. Yoshikawa, Catal. Commun. 6 (2005) 661–668.
[17] A. Fujishima, K. Honda, Nature 238 (1972) 37–38.
[18] A. Linsebigler, G. Lu, J.T. Yates, Chem. Rev. 95 (1995) 735–758.
[19] E. Borgarello, J. Kiwi, M. Graetzel, E. Pelizzetti, M. Visca, J. Am. Chem. Soc. 104 (1982) 2996–3002.
[20] W. Choi, A. Termin, M.R. Hoffmann, J. Phys. Chem. 98 (1994) 13669–13679.
[21] X. Fu, L.A. Clark, Q. Yang, M.A. Anderson, Environ. Sci. Technol. 30 (1995) 647–653.
[22] C. Anderson, A.J. Bard, J. Phys. Chem. 99 (1995) 9882–9885.
[23] K.T. Ranjit, H. Cohen, I. Willner, S. Bossmann, A. Braun, J. Mater. Sci. 34 (1999) 5273–5280.
[24] J. Moon, H. Takagi, F. Fujishiro, M. Awano, J. Mater. Sci. 36 (2001) 949–955.
[25] V. Vamathevan, R. Amal, D. Beydoun, G. Low, S. Mcevoy, J. Photochem. Photobiol. A: Chem. 148 (2002) 233–245.
[26] Y. Li, T. Wang, S. Peng, G. Lu, S. Li, Acta Phys.-Chim. Sin. 20 (2004) 1434–1439.
[27] N. Serpone, E. Pelizzetti, Photocatalysis: Fundamentals and Applications, Wiley, New York, 1989.
[28] N. Serpone, R.F. Khairutdinov, Semiconductor Nanoclusters, Physical, Chemical, and Catalytic Aspects, Elsevier Science, Amsterdam, 1997.
[29] D.M. Antonelli, Y.J. Ying, Angew. Chem. Int. Ed. Engl. 34 (1995) 2014–2017.
[30] D.M. Antonelli, Micropor. Mesopor. Mater. 30 (1999) 315–319.
[31] P. Yang, D. Zhao, D.I. Margolese, B.F. Chmelka, G.D. Stucky, Chem. Mater. 11 (1999) 2813–2826.
[32] H. Yoshitake, T. Sugihara, T. Tatsumi, Chem. Mater. 14 (2002) 1023–1029.
[33] V. Idakiev, T. Tabakova, Z.Y. Yuan, B.L. Su, Appl. Catal. A: Gen. 270 (2004) 135–141.
[34] T. Sreethawong, S. Yoshikawa, Int. J. Hydrogen Energy 31 (2006) 786–796.
[35] F. Rouquerol, J. Rouquerol, K. Sing, Adsorption by Powders and Porous Solids: Principles, Methodology and Applications, Academic Press, San Diego, 1999.
[36] J.V. Smith (Ed.), X-ray Powder Data File, American Society for Testing Materials, 1960.
[37] B.D. Cullity, Elements of X-ray Diffraction, Addison-Wesley Publication Company, Massachusetts, 1978.
[38] J. Yu, J.C. Yu, M.K.P. Lueng, W. Ho, B. Cheng, X. Zhao, J. Zhao, J. Catal. 217 (2003) 69–78.
[39] J.C. Yu, J. Yu, W. Ho, L. Zhang, Chem. Commun. 19 (2001) 1942–1943.
[40] Y. Zhang, A. Weidenkaff, A. Reller, Mater. Lett. 54 (2002) 375–381.
[41] Y. Zhang, H. Zhang, Y. Xu, Y. Wang, J. Solid State Chem. 177 (2004) 3490–3498.
[42] Y.V. Kolen'ko, V.D. Maximov, A.V. Garshev, P.E. Meskin, N.N. Oleynikov, B.R. Churagulov, Chem. Phys. Lett. 388 (2004) 411–415.
[43] Q. Sheng, Y. Cong, S. Yuan, J. Zhang, M. Anpo, Micropor. Mesopor. Mater. 95 (2006) 220–225.
[44] J. Kiwi, M. Grätzel, J. Phys. Chem. 88 (1984) 6146–6152.
[45] A. Mills, S. Le Hunte, J. Photochem. Photobiol. A: Chem. 108 (1997) 1–35.
[46] D.W. Hwang, H.G. Kim, J. Kim, K.Y. Cha, Y.G. Kim, J.S. Lee, J. Catal. 193 (2000) 40–48.
[47] A. Hameed, M.A. Gondal, J. Mol. Catal. A: Chem. 233 (2005) 35–41.
[48] F.L. Palmer, B.R. Eggins, H.M. Coleman, J. Photochem. Photobiol. A: Chem. 148 (2002) 137–143.
[49] S. Lathasree, A.N. Rao, B. Sivasankar, V. Sadasivam, K. Rengaraj, J. Mol. Catal. A: Chem. 223 (2004) 101–105.
[50] D.P. Das, K. Parida, B.R. De, J. Mol. Catal. A: Chem. 240 (2005) 1–6.
[51] G.A. Parks, Chem. Rev. 65 (1965) 177–198.
[52] W.H. Van Riemsdijk, G.H. Bolt, L.K. Koopal, J. Blaakmeer, J. Colloid Interf. Sci. 109 (1986) 219–228.
[53] Colloidal Dynamics Inc., ZetaProbe Application, Determining the Isoelectric Point (IEP), Colloidal Dynamics, Colloidal Dynamics Inc., Warwick, Rhode Island, USA, 2002 (available at http://www.colloidal-dynamics.com).
[54] D.S. Bhatkhande, V.G. Pangarkar, A.A.M.C. Beenackers, J. Chem. Technol. Biotechnol. 77 (2001) 102–116.
[55] E. Evgenidou, K. Fytianos, I. Poulios, J. Photochem. Photobiol. A: Chem. 175 (2005) 29–38.
[56] M.H. Habibi, A. Hassanzadeh, S. Mahdavi, J. Photochem. Photobiol. A: Chem. 172 (2005) 89–96.
[57] A. Mills, R.H. Davies, D. Worsley, Chem. Soc. Rev. 22 (1993) 417–425.
[58] I.K. Konstantinou, T.A. Albanis, Appl. Catal. B: Environ. 49 (2004) 1–14.
[59] T. Sehili, P. Boule, J. Lemaire, J. Photochem. Photobiol. A: Chem. 50 (1989) 117–127.
[60] B. Neppolian, H.C. Choi, S. Sakthevel, B. Arabindoo, V. Murugesan, J. Hazard. Mater. 89 (2002) 303–317.
[61] M. Qamar, M. Muneer, J. Hazard. Mater. 120 (2005) 219–227.
[62] W. Cui, L. Feng, C. Xu, S. Lü, F. Qiu, Catal. Commun. 5 (2004) 533–536.
[63] K.E. Karakitsou, X.E. Verykios, J. Catal. 134 (1992) 629–634.

ภาคผนวก ข

Manuscript submitted for publication in International Journal of Hydrogen Energy

Comparative Investigation of Mesoporous and Non-Mesoporous TiO_2 Nanocrystals for Photocatalytic H_2 Production over N-Doped TiO_2 under Visible Light Irradiation

Thammanoon Sreethawong*, Siriporn Laehsalee, and Sumaeth Chavadej

The Petroleum and Petrochemical College, Chulalongkorn University,

Soi Chula 12, Phyathai Road, Pathumwan, Bangkok 10330, Thailand

---

*Corresponding author. Tel.: +66-2-218-4144; fax: +66-2-215-4459.

E-mail address: thammanoon.s@chula.ac.th (T. Sreethawong).

Abstract

In this paper, N-doped mesoporous TiO_2 and N-doped non-mesoporous commercial TiO_2 (Degussa P-25) nanocrystals were comparatively investigated for photocatalytic H_2 production from water splitting under visible light irradiation. The mesoporous TiO_2 photocatalyst with nanocrystalline and narrow monomodal pore size distribution characteristics was synthesized by a sol-gel process with the aid of structure-directing surfactant under mild conditions. The N-doping technique was directly performed by calcining the mixture of the TiO_2 photocatalysts and urea, as a N source, at different N contents and calcination temperatures. All prepared photocatalysts were systematically characterized by N_2 adsorption-desorption, Brunauer-Emmett-Teller (BET) surface area analysis, Barrett-Joyner-Halenda (BJH) pore size distribution analysis, UV-visible spectroscopy, X-ray diffraction (XRD), and X-ray photoelectron microscopy (XPS). From the experimental results, it was found that N-doped mesoporous TiO_2 prepared at a urea:TiO_2 molar ratio of 1:1 and a calcination temperature of 250°C exhibited relatively high photocatalytic activity toward hydrogen production. For the N-doped commercial TiO_2, the preparation conditions of a molar ratio of 0.5:1 and a temperature of 250°C showed the best photocatalytic activity, but was still less photocatalytically active than N-doped mesoporous TiO_2 prepared at the optimum conditions. The results indicated the importance of the mesoporous characteristic of the photocatalyst in enhancing the photocatalytic activity by increasing the specific surface area and N-doping capability.

Keywords: N-doping; Mesoporosity; Titania; Visible light; Photocatalysis; Hydrogen production

1. Introduction

H_2 is considered to be a future fuel for replacing conventional energy resources, such as coal, natural gas, and fossil fuel, which are gradually depleting [1]. H_2 is a clean-burning fuel, unlike conventional ones, which unavoidably produce a large amount of CO_2, causing global warming upon their combustion. The combustion of H_2 can generate a huge amount of energy, and the only by-product is water or water vapor. Since it does not involve CO_2 emission, it introduces no pollutants to the environment. Moreover, it can be potentially used in several applications, such as for automobiles, airplanes, and furnaces. Although H_2 is a simple molecule, it can be found in very small quantities in the atmosphere. Because hydrogen atoms are mostly present in the associating forms of hydrocarbons and water, the production of H_2 has to be done by extracting it from these molecules.

Photocatalytic water splitting is a promising process for producing H_2 since water is used as a reactant, which is an abundantly available substance. Also, no pollutants are generated from the photocatalytic water splitting reaction because the reaction produces only H_2 and O_2. Moreover, solar energy, a renewable energy resource, is very appropriate to be used for the photocatalytic H_2 production from water, which occurs when a photocatalyst directly absorbs light with energy equal to or higher than its energy band gap, and the electrons are then excited from the valance band (VB) to the conduction band (CB) and reduce the protons to H_2 molecules [2]. After Fujishima and Honda [3] discovered the photochemical water splitting for H_2 generation using TiO_2 semiconductor electrodes in 1972, a multitude of research on water splitting and semiconductor development has been extensively done. TiO_2 has always been the most investigated semiconductor photocatalyst because it is chemically stable, non-corrosive, environmentally friendly, and cost-effective. Despite the positive attributes of TiO_2, there are two drawbacks associated with its use: (i) charge carrier (e^-/h^+) recombination

occurs easily due to its wide band gap and (ii) the light absorption ability of its band gap does not allow the utilization of visible light, which accounts for 42% of the solar energy exposed to the earth's surface, or in other words, only a small UV light fraction, 8%, can be absorbed and utilized [4].

In order to solve the aforementioned problem, the combination with other technologies, such as electron donor or hole scavenger addition, is necessary for preventing the mutual charge recombination. The addition of primarily oxygenated hydrocarbon electron donors in the photocatalytic H_2 production system, such as methanol and ethanol, has been found to greatly improve photocatalytic activity far more than the pure water system [5-7]. To improve the visible light absorption ability of TiO_2, anion doping, such as nitrogen-doped TiO_2 (N-doped TiO_2), is an effective method to enhance its visible light response. Subsequent to the report of Asahi et al. [8] for the preparation of N-doped TiO_2 in an atmosphere of N_2 or NH_3 with its improved light absorption ability into the visible light region, a number of attempts have focused on the synthesis and development of visible light-sensitive N-doped TiO_2 photocatalysts by using several techniques, which include thermal oxidation in N_2 and NH_3 atmospheres, thermal decomposition of N-containing compounds (such as urea, ammonia, ammonium hydroxide, ammonium carbonate, melamine, and quanidine), mechanochemical processes with thermal treatment, N_2-plasma treatment, sol-gel process with ammonia solution, solvothermal process, anodization, chemical vapor deposition, and supercritical NH_3/alcohol fluid process [9-26]. However, most of these techniques inevitably require a special apparatus, which are a major drawback. Since it is evident that the use of urea as a nitrogen source is more environmentally friendly than other N-containing compounds, especially NH_3 gas, due to safety and air pollution concerns, as well as the fact that the preparation of N-doped TiO_2 by thermal decomposition of urea is much more straightforward, this technique was used for

doping nitrogen onto TiO_2 photocatalysts in this study.

Although several research works have been done to synthesize N-doped TiO_2 photocatalysts and to examine their photocatalytic activity under visible light irradiation, most of them were carried out to use the N-doped TiO_2 photocatalysts for other probe photocatalytic reactions, such as photocatalytic degradation/decomposition of methylene blue [8-14], 2-propanol [15-17], nitrous oxide [18-21], phenol [22-24], azo dyes [25], and trichloroethylene [26], but not for the photocatalytic H_2 production from water. However, only a few investigations were conducted for photocatalytic H_2 production [27], no any study has ever reported the use of nanocrystalline mesoporous-structured TiO_2 for such the purpose.

Nanocrystalline TiO_2 generally possesses high photocatalytic efficiency because of the unique properties conferred by its very small physical dimensions. The large specific surface area and high volume fraction of atoms located both on the surface and at the grain boundaries result in an increased surface energy [28–30]. Therefore, nanocrystalline TiO_2 particles with a mesoporous structural network will be more promising because light absorption can be further improved owing to the enlarged surface area and multiple scattering. They can also facilitate better accessibility of reactants, leading to the enhancement of photocatalytic reactions [31]. Among various techniques, sol-gel is an effective route for the synthesis of mesoporous-structured materials under mild conditions with an excellent chemical homogeneity of the resulting products. Additionally, in conjunction with a structure-directing surfactant, the sol-gel process enables the formation of mesoporous-structured materials with successfully controlled porosity [32].

In this study, the N-doped mesoporous TiO_2 and N-doped non-mesoporous commercial TiO_2 (Degussa P-25) photocatalysts were directly prepared by calcining a mixture of TiO_2 photocatalysts and urea, and used for the photocatalytic H_2 production

from water under visible light irradiation. The mesoporous TiO_2 nanocrystal was synthesized via a sol-gel process with the aid of structure-directing surfactant, according to our previous work [32]. The main influences of the urea:TiO_2 molar ratio and the calcination conditions on the N-doping capability and consequent photocatalytic activity for both mesoporous- and non-mesoporous TiO_2 photocatalysts were also investigated.

2. Experimental

2.1 Materials

Tetraisopropyl orthotitanate (TIPT, $Ti(OCH(CH_3)_2)_4$, Merck) as a Ti precursor and acetylacetone (ACA, $CH_3COCH_2COCH_3$, Rasayan) as a modifying ligand were used for synthesizing a mesoporous TiO_2 photocatalyst. Laurylamine hydrochloride (LAHC, $CH_3(CH_2)_{11}NH_2{\cdot}HCl$, Merck) was used as a structure-directing surfactant to control the mesoporosity of the synthesized TiO_2 photocatalyst. Urea (NH_2CONH_2, Unilab) was used as a N source for doping on the TiO_2 photocatalyst. Methanol (CH_3OH, Lab-Scan Analytical Sciences) was used as a hole scavenger or electron donor for the photocatalytic H_2 production. All chemicals were analytical grade and were used as received without further purification. Commercial Degussa P-25 TiO_2 was selected for the comparative studies of the photocatalytic H_2 production.

2.2 Synthesis procedure of mesoporous TiO_2 and preparation of N-doped TiO_2

A nanocrystalline mesoporous TiO_2 photocatalyst was synthesized via a sol-gel process with the aid of structure-directing surfactant for a system of LAHC/TIPT modified with ACA [32]. In the typical synthesis, a specified amount of ACA was first introduced into TIPT with a molar ratio of unity. The mixed solution was then gently shaken until it was homogeneously mixed. Afterwards, a 0.1 M LAHC aqueous solution with a pH of 4.2 was added into the ACA-modified TIPT solution, in which the molar ratio of TIPT to LAHC in the mixed solution was tailored to 4:1. The mixture was

continuously stirred at room temperature for 1 h and was further aged at 40°C overnight to obtain a transparent yellow sol. Then, the condensation reaction-induced gelation was allowed to proceed by placing the sol-containing solution into an oven at 80ºC for a week to ensure complete gelation. The gel was subsequently dried at 80°C overnight to eliminate the solvent, which was mainly the distilled water used in the preparation of the surfactant aqueous solution, and the dried gel was further calcined at 500°C for 4 h to remove the LAHC template and to consequently produce the nanocrystalline mesoporous TiO_2 photocatalyst. Afterwards, the synthesized mesoporous TiO_2 was thoroughly mixed with urea at various urea:TiO_2 molar ratios, and the mixture was ground by using an agate mortar. The resulting powder was finally calcined at different temperatures, between 200 and 300°C, for 2 h to acquire N-doped TiO_2 photocatalysts. The same procedure was also used to prepare N-doped commercial TiO_2 photocatalysts.

2.3 Photocatalyst characterizations

A nitrogen sorption system (Quantachrome, Autosorb 1) was employed to measure the adsorption–desorption isotherms at a liquid nitrogen temperature of -196°C. The photocatalyst sample was degassed at 150°C for 2 h to remove the physisorbed gases prior to measurement. The Brunauer–Emmett–Teller (BET) approach using adsorption data over the relative pressure ranging from 0.05 to 0.35 was utilized to determine the specific surface areas of all studied photocatalysts. The Barrett–Joyner–Halenda (BJH) approach was used for the calculation of the mean pore sizes and pore size distributions of the photocatalyst samples. X-ray diffraction (XRD) was used to identify the crystalline structure and composition of the photocatalysts. A Rigaku RINT-2100 rotating anode XRD system generating monochromated CuKα radiation with continuous scanning mode at a rate of 2°/min and operating at 40 kV and 40 mA was used to obtain the XRD patterns of all the photocatalysts. A Shimadzu UV-2550 UV-visible spectrophotometer was used to record the diffuse reflectance spectra of the

photocatalyst samples at room temperature with $BaSO_4$ as the reference. The oxidation state and surface composition were analyzed by an X-ray photoelectron spectroscope (XPS). A MgKα source emitting an X-ray energy of 1,253.6 eV was used as the X-ray source. The relative surface charging of the samples was removed by referencing all the energies to the C1s level as an internal standard at 285 eV.

2.4 Photocatalytic H_2 production experiments

Photocatalytic H_2 production experiments were performed in a closed-gas system. In a typical run, a specified amount of all prepared photocatalysts (0.2 g), namely N-doped synthesized TiO_2 and N-doped commercial TiO_2, was suspended in an aqueous methanol solution (CH_3OH 50 ml and distilled water 150 ml) by using a magnetic stirrer within a reactor made of Pyrex glass. The mixture was initially deaerated by purging with Ar gas for 45 min in a dark environment. The photocatalytic reaction was then started by exposing the mixture with visible light irradiation from a 300 W Xe arc lamp (Wacom Electric, KXL-300F) emitting light with a wavelength longer than 400 nm using a UV cut-off glass filter (ATG, B-48S). The gaseous samples from the headspace of the reactor were periodically collected and analyzed for hydrogen by a gas chromatograph (Perkin Elmer/Arnel, HayeSep D, Ar gas) equipped with a thermal conductivity detector (TCD).

3. Results and discussion

3.1 Mesoporous TiO_2 photocatalyst synthesis results

In this study, the nanocrystalline mesoporous TiO_2 photocatalyst was synthesized via the sol-gel process with the aid of structure-directing surfactant by using TIPT as the Ti precursor modified with an ACA agent and LAHC as the structure-directing surfactant. Firstly, TIPT was mixed with ACA, resulting in a change of the co-ordination number of the Ti atoms from 4 to 5 [33], as shown in Eq. (1). This also

causes the change of solution color from colorless to yellow. The obtained ACA-modified TIPT is comparatively less active to the moisture in air than the TIPT itself, and is more suitable for the sol-gel synthesis.

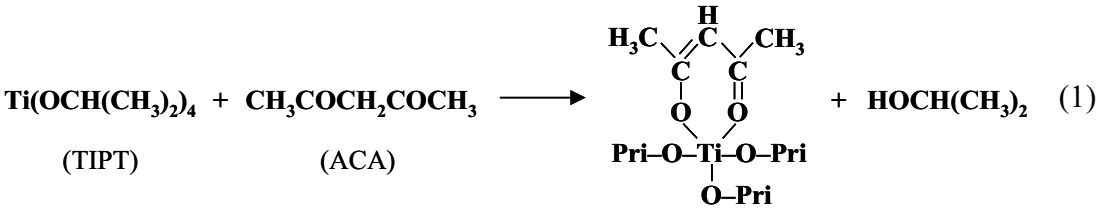

(1)

Ti coordination number: 4 Ti coordination number: 5

In order to control the mesoporous structure of the TiO_2, the LAHC aqueous solution was added into the TIPT/ACA solution. The precipitation of a yellow solution occurred immediately after the aqueous solution addition, owing to the partial hydrolysis of the modified TIPT molecules. Then, the solution was continuously stirred at 40°C to dissolve the precipitates. Consequently, a transparent yellow sol was obtained, which resulted from the interaction between the hydrolyzed TIPT molecules and the hydrophilic head groups of micellar LAHC and the suspension of these interacted species in the solution as infinitesimally colloidal solid particles. After placing the transparent yellow sol in an oven at 80°C, a white gel was formed via the condensation process of the modified TIPT molecules attached to the LAHC head groups, and ACA was eliminated, as evidenced by the existence of a transparent yellow liquid layer on the gel. Complete gel formation was observed after a week, and the gel was then dried at 80°C to obtain dried TiO_2 (zero gel). The mesoporous TiO_2 photocatalyst was eventually obtained when the dried gel was calcined at 500°C, which was a sufficiently high temperature for both removing the LAHC template and crystallizing the photocatalyst [32].

3.2 Photocatalyst characterization results

To improve the visible light absorption ability of the TiO_2 photocatalysts, N-

doping was carried out by mixing urea, a simple N-containing molecule, with the synthesized TiO_2 and the commercial TiO_2 at various urea:TiO_2 molar ratios and various calcination temperatures. It was experimentally found that after the N-doping, the color of both TiO_2 photocatalysts clearly changed from white to yellow.

3.2.1 Pore structures of photocatalysts

The N_2 adsorption-desorption isotherms of the as-synthesized TiO_2 and N-doped synthesized TiO_2 exhibit the typical IUPAC type IV pattern with the presence of a hysteresis loop [34], as shown in Fig. 1. The hysteresis loop is ascribed to the existence of the mesoporous structure (mesopore size between 2-50 nm) in the sample. A sharp increase in the adsorption volume of N_2 was observed and located in the P/P_0 range of 0.5-0.9. This sharp increase can be assigned to the capillary condensation, indicating good homogeneity of the samples and fairly small pore sizes, since the P/P_0 position of the inflection point is pertaining to pore dimension. As illustrated in the inset of Fig. 1, the pore size distribution of the sample is quite narrow and monomodal, owing to the single hysteresis loop, implying that the synthesis technique used in this study can yield a mesoporous TiO_2 nanocrystal with a narrow pore size distribution. In contrast, for the commercial TiO_2 and N-doped commercial TiO_2, the N_2 adsorption-desorption isotherms corresponded to the IUPAC type II pattern [34], as depicted in Fig. 2. It is apparent that the commercial TiO_2 exhibits non-mesoporous characteristic due to the absence of the hysteresis loop. No capillary condensation of N_2 into the pore was observed since the desorption isotherm was insignificantly different from the adsorption one. The pore size distribution of the commercial TiO_2, as shown in the inset of Fig. 2, is quite broad. The average pore sizes of the commercial TiO_2 and N-doped commercial TiO_2 are quite large, and their pore size distributions not only exist in the mesoporous region but also mostly cover the macropore region (macropore size > 50 nm).

3.2.2 Textural properties of photocatalysts

The experimental results of the textural property characterization of the photocatalysts, including BET surface area, mean pore diameter, and total pore volume, are shown in Table 1. For any given N-doped mesoporous or N-doped commercial TiO_2 photocatalyst, the surface area tended to decrease with increasing urea:TiO_2 molar ratio at all calcination temperatures. For the N-doped mesoporous TiO_2, of which the isotherm exhibited typical IUPAC type IV, the mean pore diameter was quite similar to the pure mesoporous TiO_2, however the total pore volume decreased with increasing urea:TiO_2 molar ratio. For the commercial TiO_2, the mean pore diameter and total pore volume are usually not reported because it contains a large portion of macropores, which has a very broad pore size distribution with the pore diameters larger than 50 nm up to 200-250 nm.

3.2.3 Light absorption capability of photocatalysts

UV-visible spectroscopy was used to investigate the light absorption capability of the studied photocatalysts. The changes in the absorption spectra of N-doped mesoporous TiO_2 nanocrystal with different urea:TiO_2 molar ratios are exemplified in Fig. 3. The absorption band of pure mesoporous TiO_2 is in the range of 200-400 nm. The high light absorption band at low wavelengths in the spectra indicates the presence of the Ti species as tetrahedral Ti^{4+}. This light absorption band is generally associated with the electronic excitation of the valence band O2p electron to the conduction band Ti3d level [35]. Its light absorption onset is approximately at 385 nm, which corresponds to the energy band gap of anatase TiO_2, 3.2 eV. For the N-doped mesoporous TiO_2, as also shown in Fig. 3, the light absorption band shifts to a wavelength longer than 400 nm (red shift), which is in the range of the visible light region. From the light absorption results, the N-doping technique can improve the visible light absorption capability of the mesoporous TiO_2 synthesized in this study. The

light absorption spectra of the N-doped commercial TiO_2 at different urea:TiO_2 molar ratios are shown in Fig. 4. The light absorption onset of the pure commercial TiO_2 begins at the wavelength longer than 400 nm, indicating that it can absorb visible light by itself without N-doping. This is because the commercial TiO_2 possesses both anatase and rutile phases, as shown by XRD patterns in the next part. Their energy band gap is approximately 3.2 and 3.0 eV for anatase and rutile TiO_2, respectively, which can originally absorb both UV and visible ranges. It was therefore experimentally found that the N-doping cannot much enhance the visible light absorption capability of the commercial TiO_2. As shown later from the XPS results, because the commercial TiO_2 possesses less capability of allowing the N-doping owing to its comparatively low surface N content, its visible light absorption is not obviously improved. By comparing between Fig. 3 and 4, the N-doping process gave the positive effect on the absorbance intensity, especially in UV light region, for the synthesized TiO_2 while giving the negative effect for the commercial TiO_2, however the absorption of UV light with wavelength shorter than 400 nm requires no extensive consideration due to the utilization of only visible light for photocatalytic study. As shown later for the photocatalytic activity results, since both N-doped TiO_2 photocatalysts showed potential performance for photocatalytic H_2 production under visible light irradiation, it means that the photocatalysts can effectively capture the irradiated visible light for generating the excited electrons necessary for reducing protons to H_2 molecules. The possible reasons for these observations of absorbance intensity changes are still in doubt and need further clarified investigation.

3.2.4 Crystallinity and purity of photocatalysts

The XRD patterns of the N-doped mesoporous TiO_2 nanocrystal prepared at different urea:TiO_2 molar ratios and calcination temperatures are shown in Fig. 5, compared with that of the pure mesoporous TiO_2 photocatalyst, whereas those of the N-

doped commercial TiO_2 prepared at different urea:TiO_2 molar ratios and calcination temperatures are shown in Fig. 6, also compared with that of the pure commercial TiO_2 . As shown in Fig. 5, all samples of N-doped mesoporous TiO_2 prepared at a urea:TiO_2 molar ratio of 0.5:1, regardless of calcination temperature, show quite a similar XRD diffractogram with the pure mesoporous TiO_2. The dominant peaks at 2θ at about 25.2, 37.9, 47.8, 53.8, and 55.0°, which represent the indices of (101), (004), (200), (105), and (211) planes (JCPDS Card No. 21-1272) [36], respectively, conform to the crystalline structure of anatase TiO_2. At a temperature of 200°C, the biuret formation was first clearly observed at a urea:TiO_2 molar ratio of 3:1, as shown in Fig. 5. The biuret was also found at the urea:TiO_2 molar ratio of 1:1 in a very small amount due to the comparatively low peak intensity at this temperature ((c) in Fig. 5). A similar tendency of biuret formation was observed at a temperature of 250°C for the urea:TiO_2 molar ratios of both 1:1 and 3:1 ((f) and (g) in Fig. 5), but in extremely low amounts at the molar ratio of 1:1. In addition, cyanuric acid was apparently formed at this temperature. At 300°C, biuret formation was not observed at a molar ratio of 1:1 ((i) in Fig. 5), suggesting that biuret is decomposed at this temperature. At a molar ratio of 3:1 ((j) in Fig. 5), a large amount of cyanuric acid was observed, and biuret was observed in relatively low amounts when compared to 250°C at the same molar ratio. These results indicate that biuret starts to decompose to form cyanuric acid at temperatures higher than 200°C. Schaber et al. [37] explained about the decomposition of urea to produce many compounds depending on temperature. Two main products are biuret and cyanuric acid. Upon increasing temperature, biuret is formed at approximately 150 to 250°C. Cyanuric acid then appears in consecutive order at approximately 190 to 350°C. The formation of biuret and cyanuric acid due to the urea composition is shown in the following decomposition reactions.

At temperatures between 150 and 250°C,

$H_2N\text{-}CO\text{-}NH_2$ (l) + heat ⟶ $NH_4^+NCO^-$ (l) (2)

urea ammonium iso-cyanate

$NH_4^+NCO^-$ (l) ⟷ NH_3 (g) + HNCO (g) (3)

ammonium iso-cyanate ammonia iso-cyanic acid

$H_2N\text{-}CO\text{-}NH_2$ (l) + HNCO (g) ⟷ $H_2N\text{-}CO\text{-}NH\text{-}CO\text{-}NH_2$ (s) (4)

urea iso-cyanic acid biuret

and, at temperatures between 190 and 350°C,

3HNCO (g) ⟶ $C_3O_3N_3H_3$ (s) (5)

iso-cyanic acid cyanuric acid

$2H_2N\text{-}CO\text{-}NH\text{-}CO\text{-}NH_2$ (l) ⟶ $C_3O_3N_3H_3$ (s) + HNCO (g) + NH_3 (g) (6)

biuret cyanuric acid iso-cyanic acid ammonia

where s, l, and g represent solid, liquid, and gas phases, respectively.

The decomposition reactions of urea as described above exactly correspond to the effect of calcination temperature on the formation of impurities (biuret and cyanuric acid) at a high urea:TiO_2 molar ratio of 3:1 where the peak responsible for biuret formation was first observed at 200°C, and its intensity increased when increasing the calcination temperature to 250°C. With further increasing to 300°C, the amount of biuret formed was found to decrease substantially. In the meantime, cyanuric acid was first denoted at 250°C and increased significantly at 300°C. For the XRD patterns of N-

doped commercial TiO_2, as shown in Fig. 6, the dominant peaks at 2θ of about 27.4, 36.1, 41.2, and 54.3°, which represent the indices of (110), (101), (111), and (211) planes (JCPDS Card No. 21-1276) [36], respectively, indicate the presence of the rutile phase, in addition to the presence of the anatase phase. Both biuret and cyanuric acid were observed in the same trend as the N-doped mesoporous TiO_2. The main difference between the mesoporous TiO_2 and the commercial TiO_2 photocatalysts was that the synthesized mesoporous TiO_2 is in only anatase form, whereas the commercial TiO_2 possesses the mixed phases of anatase (76.5%) and rutile (23.5%), of which the phase composition is calculated by the following equations [38]:

$$W_R = [1 + 0.8I_A/I_R]^{-1} \quad (7)$$

$$W_A = 1 - W_R \quad (8)$$

where I_A and I_R represent integrated intensities of anatase (101) and rutile (110) diffraction peaks, respectively, and W_A and W_R represent phase compositions of anatase and rutile, respectively.

3.2.5 Oxidation state and surface N content of photocatalysts

The oxidation states and surface compositions of N, O, and Ti of the N-doped mesoporous TiO_2 and N-doped commercial TiO_2 nanocrystals were analyzed by XPS. The XPS results of the N-doped mesoporous TiO_2 prepared at a urea:TiO_2 molar ratio of 1:1 and calcination temperature of 250°C are exemplified in Fig. 7. Fig. 7(a) represents a typical XPS spectrum of Ti. The peaks of the Ti2p spectrum appeared with their centers at 458.4 and 464.0 eV, which correspond to the $Ti2p_{3/2}$ and $Ti2p_{1/2}$ levels, respectively. The peaks can denote the Ti^{4+} oxidation state, which agree well with the light absorption results. Fig. 7(b) shows the peak of the N1s spectrum centered at 400.8 eV, which can be ascribed to the molecularly chemisorbed nitrogen. Many recent

literatures also reported the presence of a broad N1s peak between 397 and 403 eV for N-doped TiO_2 photocatalysts prepared by various techniques [39-42]. Fig. 7(c) shows the deconvoluted peaks of the O1s (mesoporous TiO_2) spectrum with one centered at 529.7 eV, which is typical for the Ti-O-Ti environment and agrees with the O1s binding energy for TiO_2 molecule [43], and the other centered at 532.5 eV, which is typical for the Ti-O-H environment of the hydroxyl group on the photocatalyst surface [44]. Nosaka et al. [15] also investigated the N-doped TiO_2 photocatalyst with the XPS technique and observed that the peaks of the N1s spectrum appeared with their centers approximately at both 396 and 401 eV, correspondingly representing atomically substitutional nitrogen and molecularly chemisorbed nitrogen with comparatively low signal for the former. Although the N1s with a binding energy centered at 396 eV was not clearly observed for the samples in this study, it is believed to exist in a low amount. It has been analyzed that the peak centered at 396 eV is typical for N bound to Ti atoms, and the signal centered at 401 eV is typical for N bound to O, C, or N atoms. In combining with the light absorption results, it can be inferred that the molecularly chemisorbed nitrogen could contribute to the extended absorption into visible light region. The surface nitrogen compositions of all the investigated N-doped TiO_2 samples are summarized in Table 2. The presence of surface nitrogen on the as-synthesized mesoporous TiO_2 may be due to the imperfect removal of LAHC used as the surfactant template during the calcination step. For the pure commercial TiO_2, the presence of surface nitrogen is plausibly because of their production technique via spray combustion. During the combustion step, which is generally carried out with air, the commercial TiO_2 can inevitably be N-doped. For the N-doped mesoporous TiO_2 prepared at any given urea:TiO_2 molar ratio, the surface N content increases with increasing calcination temperature from 200 to 250°C, but decreases with further increasing to 300°C, as shown in Table 2. The trend of the surface N content for N-

doped mesoporous TiO_2 is quite different from that for N-doped commercial TiO_2, of which at all urea:TiO_2 molar ratios, the surface N content tended to decrease with increasing the calcination temperature from 200 to 300°C. These results can probably be related to their pore characteristics. As the pore size of the synthesized TiO_2 exists entirely in the mesopore region, the formed N-containing compounds at 250°C, i.e. biuret and cyanuric acid, are easily trapped inside the pores due to the pore size limitation. However, with increasing the temperature to 300°C, biuret further decomposes to smaller compounds, and so they can be more thermally released from the pore structure at this high temperature. In contrast to the pore size of the commercial TiO_2, which is mostly in the large macropore region, any compounds formed can be simultaneously released by the thermal removal process. At a higher temperature, this thermal removal phenomenon becomes more significant due to the greater amount of applied energy, resulting in less surface N content. Moreover, at any given calcination temperature, the surface N content increased with increasing urea:TiO_2 molar ratio for both the mesoporous TiO_2 and commercial TiO_2, due to the presence of a higher amount of available urea molecules so as to increase the doping capability. When comparing these two types of TiO_2, it is obvious that the surface N content of the mesoporous TiO_2 was considerably higher than that of the commercial TiO_2 at all preparation conditions, because of the higher surface area of the mesoporous TiO_2, as well as other physical surface properties originating from the specific preparation technique.

3.3 Photocatalytic H_2 production activity results

The results of photocatalytic H_2 production over the photocatalysts are shown in Fig. 8. The photocatalytic activity in the absence of either light irradiation, photocatalyst, or methanol was also comparatively studied. It was found that there was no detectable H_2 production in their absence, indicating that all of them are very important for the photocatalytic H_2 production from water splitting. Moreover, without

N-doping, on both types of TiO_2 photocatalysts, extremely poor photocatalytic H_2 production activity was observed. As shown in Fig. 8, the N-doped mesoporous TiO_2 prepared at a urea:TiO_2 molar ratio of 1:1 and a calcination temperature of 250°C exhibits the highest H_2 production activity. For the series of the widely-known high photocatalytic activity commercial TiO_2, the best N-doping conditions were at a urea:TiO_2 molar ratio of 0.5:1 and a calcination temperature of 250°C.

At both calcination temperatures, 200 and 250°C, the photocatalytic H_2 production activity of the N-doped mesoporous TiO_2 tended to increase with increasing urea:TiO_2 molar ratio from 0.5:1 to 1:1 and then to decrease with further increasing molar ratio. It seems that for the N-doped mesoporous TiO_2 with a urea:TiO_2 molar ratio of 3:1, a huge amount of urea was decomposed to biuret (at 200 and 250°C) and further to cyanuric acid (250°C), and they could not be completely removed; consequently they remained inside the mesoporous structure, as shown in the XRD patterns (Fig. 5). Since both biuret and cyanuric acid are comparatively large molecules, they are easily trapped inside the pores of the synthesized mesoporous TiO_2, resulting in the decreased H_2 production activity due to less accessibility of the reactants to the photocatalyst surface (Table 1 and Fig. 8) despite the higher surface N content (Table 2). For any given urea:TiO_2 molar ratio, the photocatalytic activity of the N-doped mesoporous TiO_2 prepared at 300°C was different from those prepared at the other two calcination temperatures, 200 and 250°C. The H_2 production reached a maximum at a urea:TiO_2 molar ratio of 0.5:1 and gradually decreased as the molar ratio further increased. A possible explanation might be that at this high temperature, the biuret formed can be easily decomposed to cyanuric acid, iso-cyanic acid, and ammonia (Eq. (6)). The surface nitrogen may then also be released more, resulting in less surface N content (Table 2) and subsequently lowering the photocatalytic activity, as shown in Fig. 8. In addition, although the cyanuric acid formation at a molar ratio of 1:1 was not observed

from XRD, the decreased pore volume and increased amount of surface N content can be confirmed, as shown in Tables 1 and 2.

For the N-doped commercial TiO_2 photocatalyst calcined at 200°C, the photocatalytic H_2 production activity tended to increase with increasing urea:TiO_2 molar ratio from 0.5:1 to 1:1 and then to decrease with further increasing the molar ratio. At 250°C, the photocatalytic activity reached a maximum at a urea:TiO_2 molar ratio of 0.5:1 and gradually decreased as the urea:TiO_2 molar ratio further increased. At 300°C, the photocatalytic activity remained almost unchanged, even though the urea:TiO_2 molar ratio increased. Their activity was quite different from those of the N-doped mesoporous TiO_2 ones. It seems to be that the pore size is very important, greatly affecting the photocatalytic activity. As previously mentioned, the pore size of the commercial TiO_2 is mostly in the macropore region, having a pore size much greater than 50 nm in diameter. Because of the extremely large pore size of the commercial TiO_2, it is much more capable of allowing the reactants to have access into and the products to leave from the pore structure than the mesoporous TiO_2. This might lead to a much easier conversion of biuret (straight chain compound) to cyanuric acid (cyclic compound) according to Eq. (6). This effect is relatively dominant at high temperatures (250 and 300°C) because biuret can be easily transformed to cyanuric acid or even released into gas phase, consequently resulting in lowering the photocatalytic H_2 production activity of the N-doped commercial TiO_2 prepared at these conditions. At a calcination temperature of 300°C, in addition to the previous reason, the surface N content is another important parameter, which could be related to the constant photocatalytic activity. From the results of surface N content (Table 2), for any given urea:TiO_2 molar ratio at 300°C, the surface N content was lower than those at the other calcination temperatures with little difference between the urea:TiO_2 molar ratios of 0.5:1 and 1:1, resulting in the almost unchanged H_2 production activity. Moreover, even

though the surface N content of the commercial photocatalyst with a urea:TiO_2 molar ratio of 3:1 was much higher than those at the other two molar ratios, the photocatalytic H_2 production activity remained almost constant. The results suggest that the addition of nitrogen on the photocatalyst surface has to be optimized for a maximum H_2 production activity over both TiO_2 photocatalysts because the specific surface area can be significantly reduced with a higher amount of doped nitrogen.

In summary, the combination of porous structure and N-doping with their proper controls is definitely required for achieving the highest photocatalytic H_2 production activity over the TiO_2 photocatalyst.

4. Conclusions

Two types of N-doped TiO_2 photocatalysts, namely synthesized mesoporous TiO_2 and non-mesoporous commercial TiO_2, were comparatively studied for their photocatalytic H_2 production activity under visible light irradiation. The nanocrystalline mesoporous TiO_2 photocatalyst was synthesized by the surfactant-assisted tempting sol-gel method using TIPT as the Ti precursor modified with the ACA agent and LAHC as the surfactant template to control its porosity structure. To modify the visible light absorption ability of the TiO_2 photocatalysts, N-doping was performed. The urea, as a source of N, was mixed with both TiO_2 photocatalysts at various urea:TiO_2 molar ratios and calcined at various calcination temperatures. The obtained N-doped TiO_2 photocatalysts could subsequently absorb visible light. The optimum preparation conditions of the N-doped mesoporous TiO_2 and N-doped commercial TiO_2 for achieving the highest photocatalytic H_2 production activity were a urea:TiO_2 molar ratio of 1:1 at a calcination temperature of 250°C and 0.5:1 at a calcination temperature of 250°C, respectively. However, the N-doped mesoporous TiO_2 prepared at such the optimum conditions exhibited relatively the best photocatalytic activity.

Acknowledgments

This work was financially supported by the grants obtained from both the Thailand Research Fund (TRF) (Contract/Grant No. MRG4980030) and Chulalongkorn University, Thailand, through the Grants for Development of New Faculty Staff under the Ratchadapisek Somphot Endowment Fund (Contract/Grant No. 100/2549) to the first/corresponding author. The partial supports from the National Excellence Center for Petroleum, Petrochemicals, and Advanced Materials under the Ministry of Education, Thailand, and the Research Unit of Petrochemical and Environmental Catalysis under the Ratchadapisek Somphot Endowment Fund, Chulalongkorn University, Thailand, are also greatly acknowledged. Indebted appreciation is also forwarded to the National Synchrotron Research Center, Thailand for the support of the use of XPS apparatus. In addition, the authors would like to express sincere gratitude to Prof. Susumu Yoshikawa, Institute of Advanced Energy, Kyoto University, Japan, for his invaluable advice.

References

1. Bak T, Nowotny J, Rekas M, Sorrell CC. Photo-electrochemical hydrogen generation from water using solar energy. Int J Hydrogen Energy 2002;27:991-1022.
2. Hoffmann MR, Martin ST, Choi W, Bahnemann DW. Environmental applications of semiconductor photocatalysis. Chem Rev 1995;95:69-96.
3. Fujishima A, Honda K. Electrochemical photolysis of water at a semiconductor electrode. Nature 1972;238:37-8.
4. Park JH, Kim S, Bard AJ. Novel carbon-doped TiO_2 nanotube arrays with high aspect ratios for efficient solar water splitting. Nano Lett 2006;6:24-8.
5. Bamwenda GR, Tsubota S, Nakamura T, Haruta M. Photoassisted hydrogen production from a water-ethanol solution: a comparison of activities of Au-TiO_2 and Pt-TiO_2. J Photochem Photobiol A: Chem 1995;89:177–89.
6. Abe T, Suzuki E, Nagoshi K, Miyashita K, Kaneko M. Electron source in photoinduced hydrogen production on Pt-supported TiO_2 particles. J Phys Chem B 1999;103:1119-23.
7. Sreethawong T, Puangpetch T, Chavadej S, Yoshikawa S. Quantifying influence of operational parameters on photocatalytic H_2 evolution over Pt-loaded nanocrystalline mesoporous TiO_2 prepared by single-step sol–gel process with surfactant template. J Power Sources 2007;165:861-9.
8. Asahi R, Morikawa T, Ohwaki T, Aoki K, Taga Y. Visible-light photocatalysis in nitrogen-doped titania oxides. Science 2001;293:269-71.
9. Burda C, Lou Y, Chen X, Samia ACS, Stout J, Gole JL. Enhanced nitrogen doping in TiO_2 nanoparticles. Nano Lett 2003;3:1049-51.

10. Gandhe AR, Naik SP, Fernandes JB. Selective synthesis of N-doped mesoporous TiO_2 phases having enhanced photocatalytic activity. Micropor Mesopor Mater 2005;87:103-9.

11. Suda Y, Kawasaki H, Ueda T, Ohshima T. Preparation of high quality nitrogen doped TiO_2 thin film as a photocatalyst using a pulsed laser deposition method. Thin Solid Films 2004;453-454:162-6.

12. Sathish M, Viswanathan B, Viswanath RP, Gopinath CS. Synthesis, characterization, electronic structure, and photocatalytic activity of nitrogen-doped TiO_2 nanocatalyst. Chem Mater 2005;17:6349-53.

13. Yamada K, Nakamura H, Matsushima S, Yamane H, Haishi T, Ohira K, Kumada K. Preparation of N-doped TiO_2 particles by plasma surface modification. C R Chim 2006;9:788-93.

14. Sathish M, Viswanathan B, Viswanath RP. Characterization and photocatalytic activity of N-doped TiO_2 prepared by thermal decomposition of Ti–melamine complex. Appl Catal B: Environ 2007;74:308-13.

15. Nosaka Y, Matsushita M, Nishino J, Nosaka AY. Nitrogen-doped titanium dioxide photocatalysts for visible response prepared by using organic compounds. Sci Technol Adv Mater 2005;6:143-148.

16. Jang JS, Kim HG, Ji SM, Bae SW, Jung JH, Shon BH, Lee JS. Formation of crystalline $TiO_{2-x}N_x$ and its photocatalytic activity. J Solid State Chem 2006;179:1067-75.

17. Huang C, Chen L, Cheng K, Pan G. Effect of nitrogen-plasma surface treatment to the enhancement of TiO_2 photocatalytic activity under visible light irradiation. J Mol Catal A: Chem 2007;261:218-24.

18. Yin S, Zhang Q, Saito F, Sato T. Preparation of visible light-activated titania photocatalyst by mechanochemical method. Chem Lett 2003;32:358-9.

19. Aita Y, Komatsu M, Yin S, Sato T. Phase-compositional control and visible light photocatalytic activity of nitrogen-doped titania via solvothermal process. J Solid State Chem 2004;177:3235-8.

20. Yin S, Yamaki H, Zhang Q, Komatsu M, Wang J, Tang Q, Saito F, Sato T. Mechanochemical synthesis of nitrogen-doped titania and its visible light induced NO_x destruction ability. Solid State Ionics 2004;172:205-9.

21. Kang I, Zhang Q, Kano J, Yin S, Sato T, Saito F. Synthesis of nitrogen doped TiO_2 by grinding in gaseous NH_3. J Photochem Photobiol A: Chem 2007;189:232-8.

22. Silveyra R, Saenz LDLT, Flores WA, Martinez VC, Elguezabal AA. Doping of TiO_2 with nitrogen to modify the interval of photocatalytic activation towards visible radiation. Catal Today 2005;107-108:602-5.

23. Li H, Li J, Huo Y. Highly active TiO_2N photocatalysts prepared by treating TiO_2 precursors in NH_3/ethanol fluid under supercritical conditions. J Phys Chem B 2006;110:1559-65.

24. Fu H, Zhang L, Zhang S, Zhu Y, Zhao J. Electron spin resonance spin-trapping detection of radical intermediates in N-doped TiO_2-assisted photodegradation of 4-chlorophenol. J Phys Chem B 2006;110:3061-5.

25. Liu Y, Chen X, Li J, Burda C. Photocatalytic degradation of azo dyes by nitrogen-doped TiO_2 nanocatalysts. Chemosphere 2005;61:11-8.

26. Joung X, Amemiya T, Murabayashi M, Itoh K. Relation between photocatalytic activity and preparation conditions for nitrogen-doped visible light-driven TiO_2 photocatalysts. Appl Catal A: Gen 2006;312:20-6.

27. Yuan J, Chen M, Shi J, Shangguan W. Preparations and photocatalytic hydrogen evolution of N-doped TiO_2 from urea and titanium tetrachloride. Int J Hydrogen Energy 2006;31:1326-31.

28. Hagfeldt A, Graetzel M. Light-induced redox reactions in nanocrystalline systems. Chem Rev 1995;95:49-68.

29. Zhang Z, Wang CC, Zakaria R, Ying YJ. Role of particle size in nanocrystalline TiO_2-based photocatalysts. J Phys Chem B 1998;102:10871-8.

30. Almquist CB, Biswas P. Role of synthesis method and particle size of nanostructured TiO_2 on its photoactivity. J Catal 2002;212:145-56.

31. Antonelli DM, Ying YJ. Synthesis of hexagonally packed mesoporous TiO_2 by a modified sol-gel method. Angew Chem Int Ed Engl 1995;34:2014-7.

32. Sreethawong T, Suzuki Y, Yoshikawa S. Synthesis, characterization, and photocatalytic activity for hydrogen evolution of nanocrystalline mesoporous titania prepared by surfactant-assisted templating sol-gel process. J Solid State Chem 2005;178:329-38.

33. Brinker CJ, Scherer GW. Sol-Gel Science. Academin Press, 1989.

34. Rouquerol F, Rouquerol J, Sing K. Adsorption by Powders and Porous Solid: Principle, Methodology and Applications, Academic Press, San Diego, 1999.

35. Fuerte A, Hernández-Alonso MD, Maira AJ, Martínez-Arias A, Fernández-García M, Conesa JC, Soria J, Munuera G. Nanosize Ti–W mixed oxides: effect of doping level in the photocatalytic degradation of toluene using sunlight-type excitation. J Catal 2002;212:1-9.

36. Smith JV. X-ray Powder Data File, American Society for Testing Materials, 1960.

37. Schaber PM, Colson J, Higgins S, Thielen D, Anspach B, Brauer J. Study of the urea thermal decomposition (pyrolysis) reaction and importance to cyanuric acid production. American Lab 1999;13-21.

38. Spurr RA, Myers H. Quantitative analysis of anatase-rutile mixtures with an X-ray diffractometer. Anal Chem 1957;29:760-2.

39. Gole JL, Stout JD, Burda C, Lou Y, Chen X. Highly efficient formation of visible light tunable $TiO_{2-x}N_x$ photocatalysts and their transformation at the nanoscale. J Phys Chem B 2004;108:1230-40.

40. Sakthivel S, Janczarek M, Kisch H. Visible light activity and photoelectrochemical properties of nitrogen-doped TiO_2. J Phys Chem B 2004;108:19384-7.

41. Sato S, Nakamura R, Abe S. Visible-light sensitization of TiO_2 photocatalysts by wet-method N doping. Appl Catal A: Gen 2005;284:131-7.

42. Cong Y, Zhang JL, Chen F, Anpo M. Synthesis and characterization of nitrogen-doped TiO_2 nanophotocatalyst with high visible light activity. J Phys Chem C 2007;111:6976-82.

43. Zhang X, Zhang F, Chan KY. The synthesis of Pt-modified titanium dioxide thin films by microemulstion templating, their characterization, and visible-light photocatalytic properties. Mater Chem Phys 2006;97:384-9.

44. Yu J, Xiong J, Cheng B, Liu S. Fabrication and characterizaton of Ag-TiO_2 multiphase nanocomposite thin films with enhanced photocatalytic activity. Appl Catal B: Environ 2005;60:211-21.

Table 1 Summary of textural properties of the TiO_2 photocatalysts without and with N-doping prepared at various conditions

Calcination temperature (°C)	**Urea:TiO_2 molar ratio**	**BET surface area (m^2g^{-1})**	**Mean pore diameter (nm)**	**Total pore volume (cm^3g^{-1})**
-	Pure mesoporous TiO_2	110.30	6.114	0.185
200	0.5:1	78.14	6.150	0.136
	1:1	35.36	6.156	0.070
	3:1	22.12	4.619	0.044
250	0.5:1	82.83	6.146	0.155
	1:1	38.52	6.129	0.080
	3:1	23.45	6.140	0.049
300	0.5:1	75.78	6.150	0.147
	1:1	73.98	6.161	0.137
	3:1	22.86	6.104	0.053
-	Pure Degussa P-25 TiO_2	69.35	- [(a)]	- [(a)]
200	0.5:1	54.96	- [(a)]	- [(a)]
	1:1	53.26	- [(a)]	- [(a)]
	3:1	17.63	- [(a)]	- [(a)]
250	0.5:1	50.66	- [(a)]	- [(a)]
	1:1	44.63	- [(a)]	- [(a)]
	3:1	20.77	- [(a)]	- [(a)]
300	0.5:1	51.40	- [(a)]	- [(a)]
	1:1	26.21	- [(a)]	- [(a)]
	3:1	24.22	- [(a)]	- [(a)]

[(a)] N_2 adsorption-desorption isotherms correspond to IUPAC type II pattern.

Table 2 Summary of surface N content of the TiO_2 photocatalysts prepared at different

conditions

Calcination temperature (°C)	**Urea:TiO_2 molar ratio**	**Surface N content (wt.%)**	
		Mesoporous TiO_2	**Commercial TiO_2**
-	0:1	4.72 [(a)]	2.59 [(a)]
200	0.5:1	5.77	3.96
	1:1	20.11	5.01
	3:1	21.28	7.73
250	0.5:1	8.70	3.21
	1:1	26.23	4.68
	3:1	32.61	7.93
300	0.5:1	7.11	2.35
	1:1	11.23	2.91
	3:1	30.25	7.17

[(a)] Pure TiO_2

Figure Captions

Fig. 1. N_2 adsorption-desorption isotherm and pore size distribution (inset) of (a) the as-synthesized mesoporous TiO_2 and (b) the N-doped synthesized TiO_2 prepared at a urea:TiO_2 molar ratio of 1:1 and calcined at 250°C.

Fig. 2. N_2 adsorption-desorption isotherm and pore size distribution (inset) of (a) the commercial TiO_2 and (b) the N-doped commercial TiO_2 prepared at a urea:TiO_2 molar ratio of 0.5:1 and calcined at 250°C.

Fig. 3. UV-visible spectra of (a) pure nanocrystalline mesoporous TiO_2 and (b)-(d) N-doped mesoporous TiO_2 with different urea:TiO_2 molar ratios of 0.5:1, 1:1, and 3:1, respectively, prepared at a calcination condition of 250°C.

Fig. 4. UV-visible spectra of (a) commercial TiO_2 and (b)-(d) N-doped commercial TiO_2 with different urea:TiO_2 molar ratios of 0.5:1, 1:1, and, 3:1, respectively, prepared at calcination condition of 250°C.

Fig. 5. XRD patterns of (a) pure mesoporous TiO_2, and (b)-(d) N-doped mesoporous TiO_2 with different urea:TiO_2 molar ratios of 0.5:1, 1:1, and, 3:1, respectively, prepared at a calcination condition of 200°C, (e)-(g) urea:TiO_2 molar ratios of 0.5:1, 1:1, and, 3:1, respectively, at 250°C, and (h)-(j) urea:TiO_2 molar ratios of 0.5:1, 1:1, and, 3:1, respectively, at 300°C (A: Anatase TiO_2, B: Biuret, C: Cyanuric acid).

Fig. 6. XRD patterns of (a) commercial TiO_2, (b)-(d) N-doped commercial TiO_2 with different urea:TiO_2 molar ratios of 0.5:1, 1:1, and, 3:1, respectively, prepared at a calcination condition of 200°C, (e)-(g) urea:TiO_2 molar ratios of 0.5:1, 1:1, and, 3:1, respectively, at 250°C, and (h)-(j) urea:TiO_2 molar ratios of 0.5:1, 1:1, and, 3:1, respectively, at 300°C (A: Anatase TiO_2, R: Rutile TiO_2, B: Biuret, C: Cyanuric acid).

Fig. 7. XPS spectra of (a) Ti2p, (b) N1s, and (c) O1s of N-doped mesoporous TiO_2 prepared at a urea:TiO_2 molar ratio of 1:1 and a calcination temperature of 250°C.

Fig. 8. Photocatalytic H_2 production activity of (a) N-doped mesoporous TiO_2 and (b) N-doped commercial TiO_2 prepared with different urea:TiO_2 molar ratios of 0.5:1, 1:1, and, 3:1 and at different calcination temperatures of 200, 250, and 300°C (Reaction conditions: 0.2 g photocatalyst, 150 ml distilled water, 50 ml methanol, and 5 h irradiation time).

(a)

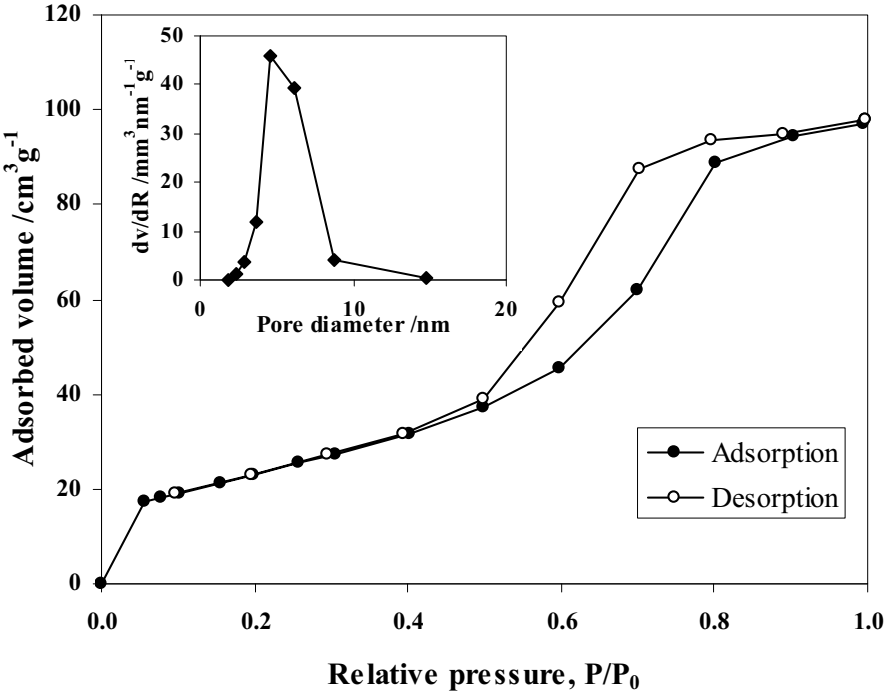

(b)

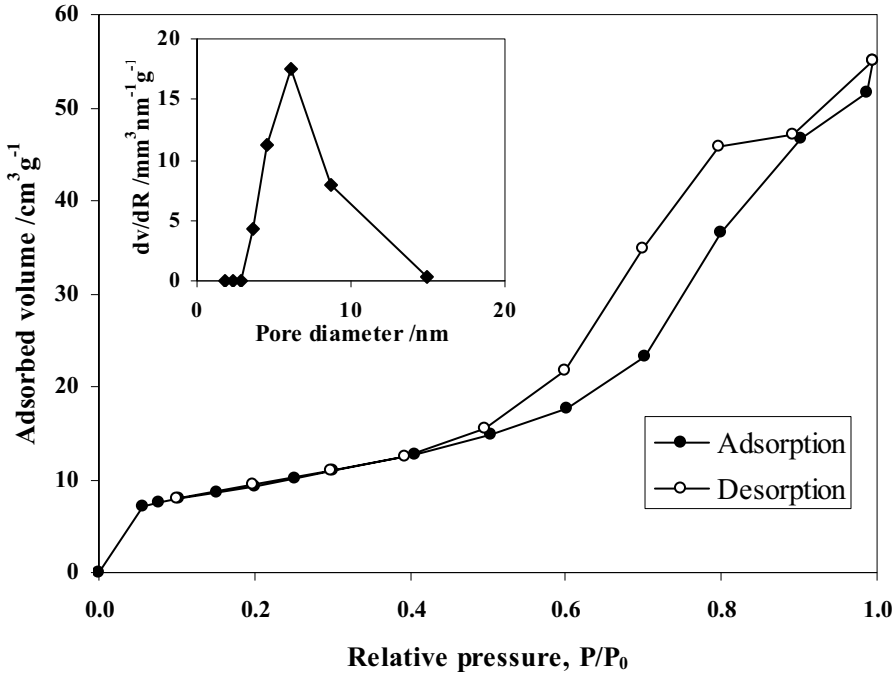

Fig. 1. N_2 adsorption-desorption isotherm and pore size distribution (inset) of (a) the as-synthesized mesoporous TiO_2 and (b) the N-doped synthesized TiO_2 prepared at a urea:TiO_2 molar ratio of 1:1 and calcined at 250°C.

(a)

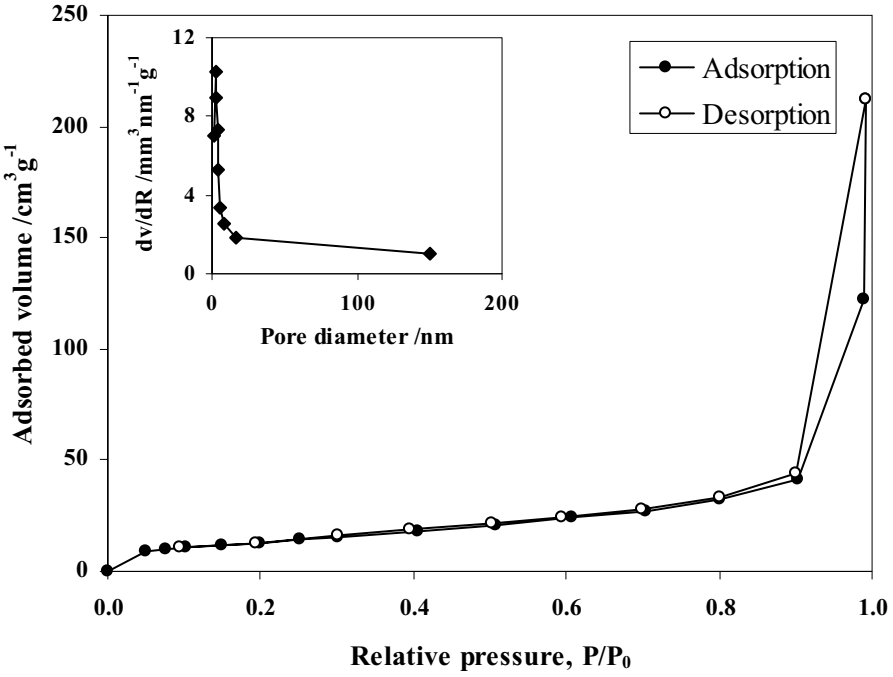

(b)

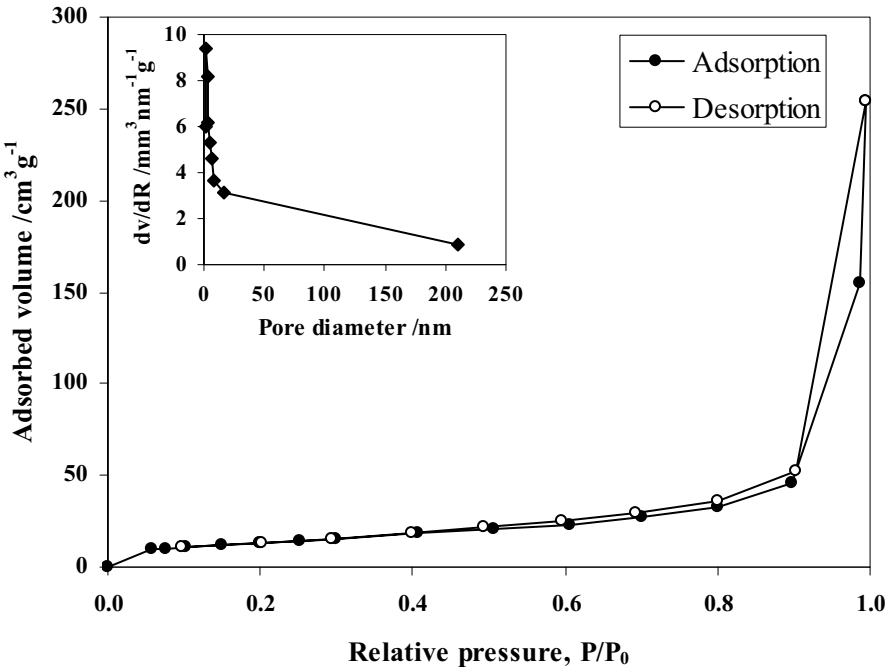

Fig. 2. N_2 adsorption-desorption isotherm and pore size distribution (inset) of (a) the commercial TiO_2 and (b) the N-doped commercial TiO_2 prepared at a urea:TiO_2 molar ratio of 0.5:1 and calcined at 250°C.

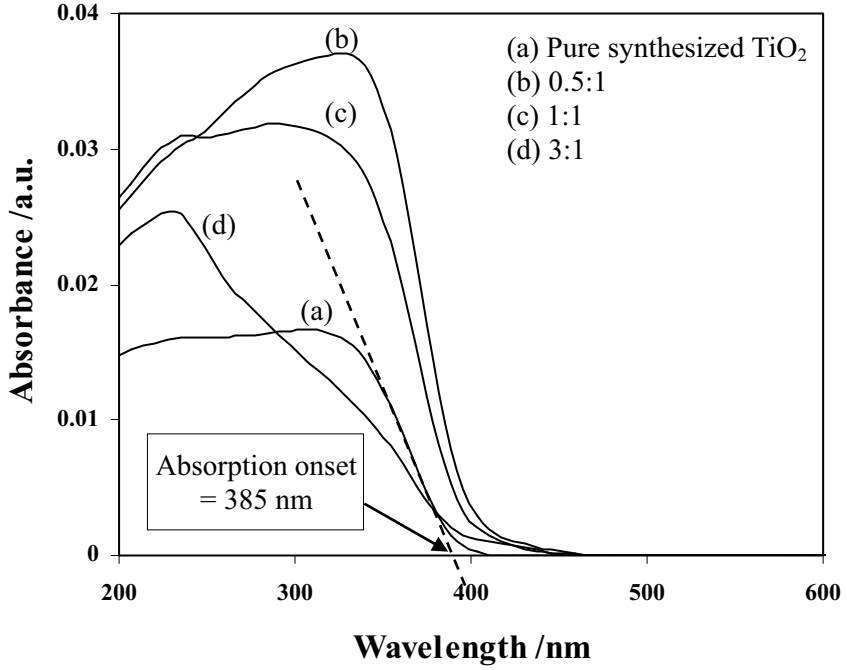

Fig. 3. UV-visible spectra of (a) pure nanocrystalline mesoporous TiO_2 and (b)-(d) N-doped mesoporous TiO_2 with different urea:TiO_2 molar ratios of 0.5:1, 1:1, and 3:1, respectively, prepared at a calcination condition of 250°C.

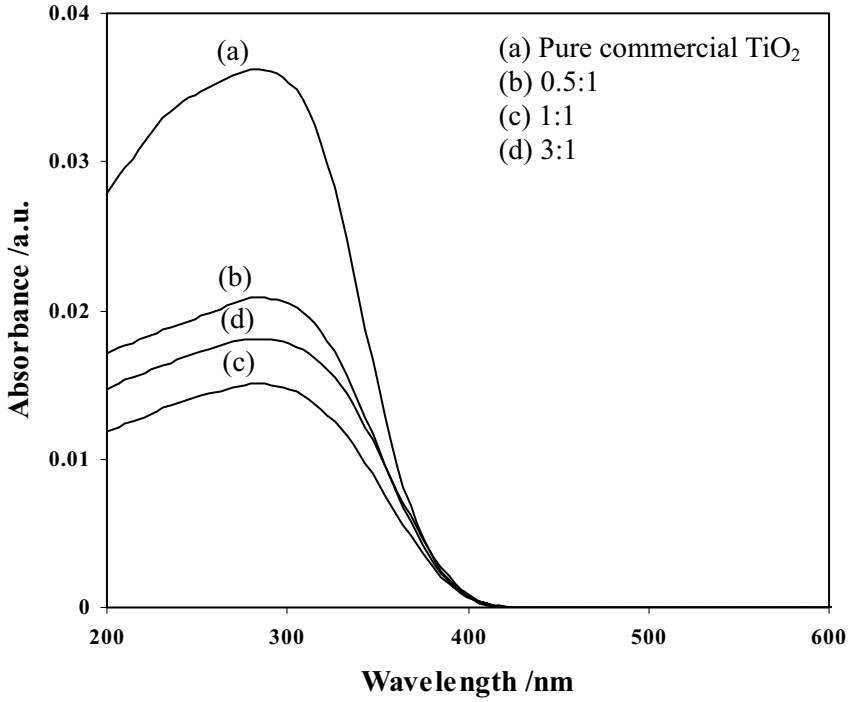

Fig. 4. UV-visible spectra of (a) commercial TiO_2 and (b)-(d) N-doped commercial TiO_2 with different urea:TiO_2 molar ratios of 0.5:1, 1:1, and, 3:1, respectively, prepared at a calcination condition of 250°C.

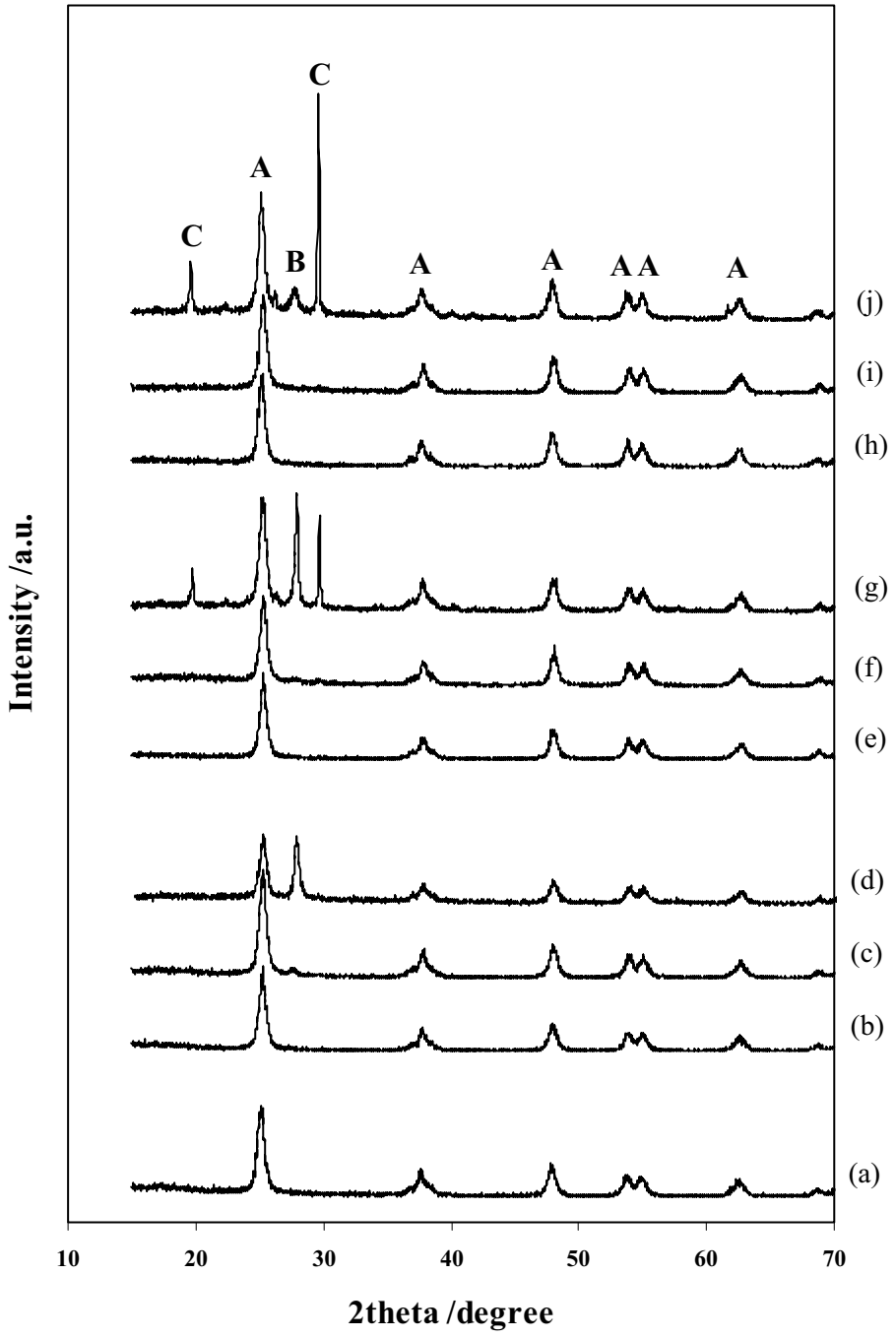

Fig. 5. XRD patterns of (a) pure mesoporous TiO_2, and (b)-(d) N-doped mesoporous TiO_2 with different urea:TiO_2 molar ratios of 0.5:1, 1:1, and, 3:1, respectively, prepared at a calcination condition of 200°C, (e)-(g) urea:TiO_2 molar ratios of 0.5:1, 1:1, and, 3:1, respectively, at 250°C, and (h)-(j) urea:TiO_2 molar ratios of 0.5:1, 1:1, and, 3:1, respectively, at 300°C (A: Anatase TiO_2, B: Biuret, C: Cyanuric acid).

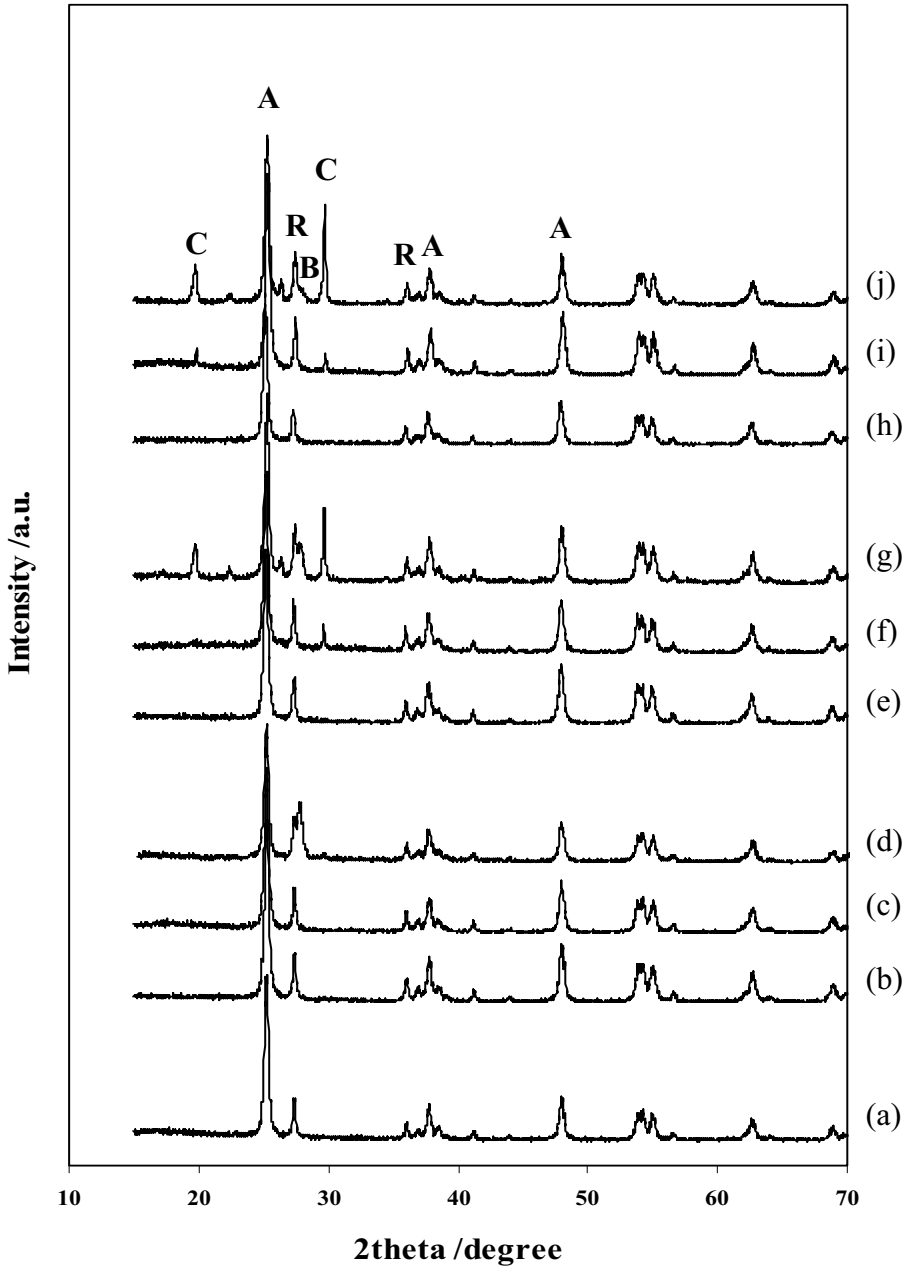

Fig. 6. XRD patterns of (a) commercial TiO_2, (b)-(d) N-doped commercial TiO_2 with different urea:TiO_2 molar ratios of 0.5:1, 1:1, and, 3:1, respectively, prepared at a calcination condition of 200°C, (e)-(g) urea:TiO_2 molar ratios of 0.5:1, 1:1, and, 3:1, respectively, at 250°C, and (h)-(j) urea:TiO_2 molar ratios of 0.5:1, 1:1, and, 3:1, respectively, at 300°C (A: Anatase TiO_2, R: Rutile TiO_2, B: Biuret, C: Cyanuric acid).

(a)

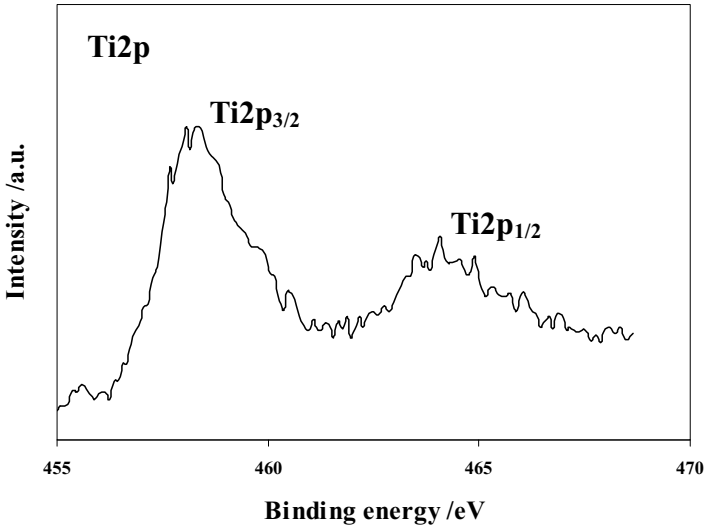

(b)

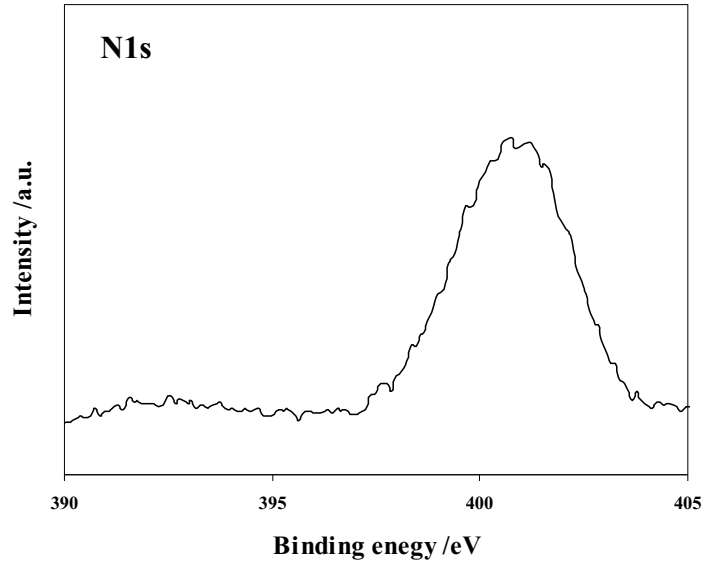

(c)

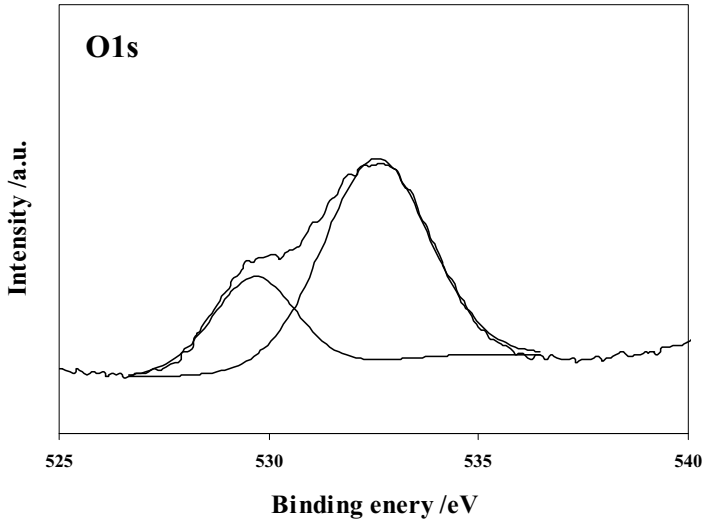

Fig. 7. XPS spectra of (a) Ti2p, (b) N1s, and (c) O1s of N-doped mesoporous TiO_2 prepared at a urea:TiO_2 molar ratio of 1:1 and a calcination temperature of 250°C.

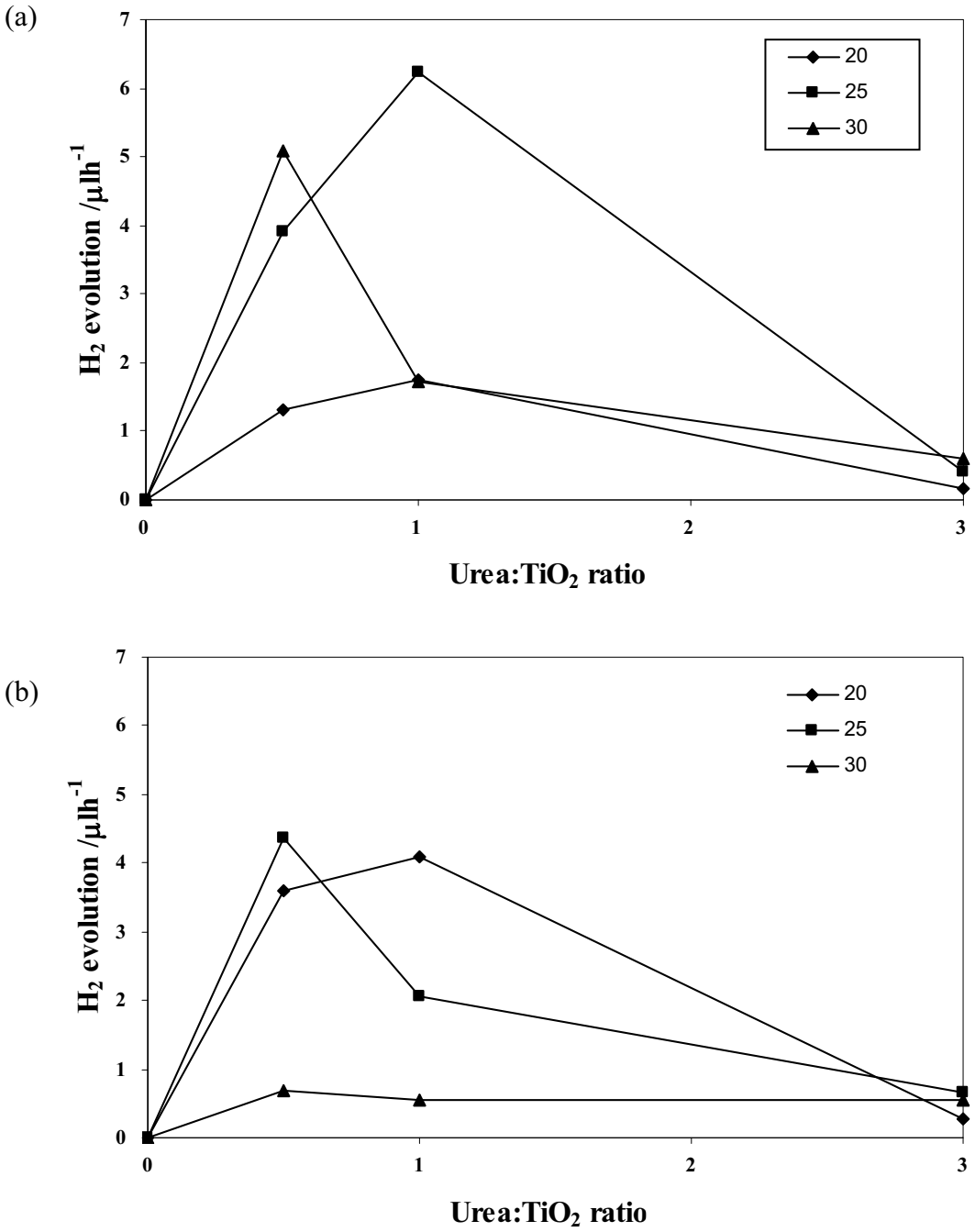

Fig. 8. Photocatalytic H_2 production activity of (a) N-doped mesoporous TiO_2 and (b) N-doped commercial TiO_2 prepared with different urea:TiO_2 molar ratios of 0.5:1, 1:1, and, 3:1 and at different calcination temperatures of 200, 250, and 300°C (Reaction conditions: 0.2 g photocatalyst, 150 ml distilled water, 50 ml methanol, and 5 h irradiation time).

ภาคผนวก ค

Extended abstract of The 4th Asia Pacific Congress on Catalysis

Probing factors affecting photocatalytic H_2 evolution over nanocrystalline mesoporous Pt/TiO_2 prepared by single-step sol-gel process with surfactant template

Thammanoon Sreethawong*, Tarawipa Puangpetch, Sumaeth Chavadej
The Petroleum and Petrochemical College, Chulalongkorn University
Soi Chula 12, Phyathai Road , Pathumwan, Bangkok 10330, Thailand
Email address: thammanoon.s@chula.ac.th,
tarawipa_p@yahoo.com, sumaeth.c@chula.ac.th

Susumu Yoshikawa
Institute of Advanced Energy, Kyoto University
Uji, Kyoto 611-0011, Japan
Email address: s-yoshi@iae.kyoto-u.ac.jp

ABSTRACT

Nanocrystalline Pt/TiO_2 photocatalyst possessing mesoporous characteristic and narrow monomodal pore size distribution was synthesized and utilized to study photocatalytic H_2 evolution from water. A single-step sol-gel process with surfactant template acting as mesopore-directing agent was employed to load Pt onto the mesoporous TiO_2. The effects of various operational parameters, including solution pH, photocatalyst concentration, sacrificial reagent type, and sacrificial reagent concentration on the photocatalytic H_2 evolution activity over the mesoporous TiO_2 loaded with optimum Pt content were studied. The optimum values of solution pH, photocatalyst concentration, and sacrificial reagent concentration, as well as appropriate type of sacrificial reagent were experimentally obtained.

1. INTRODUCTION

Direct production of hydrogen from photocatalytic splitting of water over semiconductors utilizing solar light energy has attracted much attention aiming to searching a suitable source of hydrogen for future clean energy supply. TiO_2 has been intensively used in photocatalysis including photocatalytic H_2 evolution. Noble metals behaving as cocatalysts have been used to disperse on TiO_2 surface in order to expedite the photoinduced electron transport upon band gap excitation. A multitude of interests have been focused on Pt loading on TiO_2 to enhance photocatalytic H_2 evolution activity [1]. In this study, nanocrystalline mesoporous TiO_2 was prepared by a surfactant-assisted templating sol-gel process. Single-step sol-gel method was used to load Pt cocatalyst onto TiO_2 photocatalyst during sol-gel preparation. The nanocrystalline mesoporous Pt/TiO_2 was applied for photocatalytic H_2 evolution. The effects of several operational parameters on photocatalytic H_2 evolution activity were mainly investigated.

2. EXPERIMENTAL

For the photocatalyst synthesis procedure [2], a specified amount of tetraisopropyl orthotitanate (TIPT) was mixed with acetylacetone (ACA) and 0.1 M laurylamine hydrochloride (LAHC) aqueous solution in an orderly manner. The mixed solution was stirred at 40ºC until obtaining transparent yellow sol. Then, a necessary amount of hydrogen hexachloroplatinate(IV) hydrate in methanol was added into the sol, and

the final mixture was further aged at 40ºC. Afterwards, the gel was formed by placing the sol-containing solution into an oven at 80ºC for a few days, dried overnights at 80ºC, and calcined at 500ºC. The photocatalyst was methodically characterized by XRD, N_2 adsorption-desorption analysis, and TEM. Studies of the photocatalytic H_2 evolution reaction over the synthesized photocatalyst was carried out in a closed-gas system. A specified amount of photocatalyst was suspended in an aqueous solution of sacrificial reagents under various reaction conditions within a Pyrex glass reactor. The reaction was started by exposing the photocatalytic system with light irradiated from 300 W high-pressure Hg lamp. The gaseous H_2 evolved was periodically collected and analyzed by a gas chromatograph equipped with thermal conductivity detector.

3. RESULTS AND DISCUSSION

The XRD pattern of the synthesized photocatalyst shows that the diffractogram was indexed to anatase TiO_2. The absence of diffraction peaks of Pt indicates that Pt was in a very high dispersion degree. The particle sizes of both Pt and TiO_2 from TEM analysis are in the region of 1-2 and 10-15 nm, respectively. The N_2 adsorption-desorption isotherm exhibited IUPAC type IV pattern with single hysteresis loop, which is a prevalent characteristic of mesoporous material [3]. The pore size distribution was also very narrow and monomodal, suggesting a good quality of the sample.

The photocatalytic H_2 evolution results over the nanocrystalline mesoporous TiO_2 loaded with various Pt contents show that optimum Pt loading was 0.6 wt%. The optimization results over the reveal that the mild acidic pH values in the range of 5-6 were favorable for the photocatalytic H_2 evolution reaction. Methanol was found to be the most efficient sacrificial reagent among several types of sacrificial reagent investigated. The optimum concentrations photocatalyst and methanol were found to be 0.91 g/l and 2.25 M, respectively.

4. CONCLUSIONS

Photocatalytic activity for H_2 evolution was investigated over nanocrystalline mesoporous TiO_2 photocatalyst loaded with Pt cocatalyst by the single-step sol-gel process with surfactant template. The optimum conditions for obtaining the highest photocatalytic activity over the nanocrystalline mesoporous TiO_2 loaded with 0.6 wt% Pt were at solution pH of 5-6, photocatalyst concentration of 0.91 g/l, and methanol concentration of 2.25 M.

Acknowledgements

This work was financially supported by grants provided by Thailand Research Fund (TRF) (Contract/Grant No. MRG4980030) and by Chulalongkorn University, Thailand, through the Grants for Development of New Faculty Staff under the Ratchadapisek Somphot Endowment Fund (Contract/Grant No. 100/2549).

References

[1] **Linsebigler, A., Lu, G., and Yates, J.T.** (1995). *Photocatalysis on TiO_2 surfaces: principles, mechanisms, and selected results*. Chem. Rev. **95(3)**, 735-758.

[2] **Sreethawong, T. and Yoshikawa, S.** (2006). *Enhanced photocatalytic hydrogen evolution over Pt supported on mesoporous TiO_2 prepared by single-step sol-gel process with surfactant template*. Int. J. Hydrogen Energy **31(6)**, 786-796.

[3] **Rouquerol, F., Rouquerol, J., and Sing, K.** (1999). *Adsorption by Powders and Porous Solids: Principles, Methodology and Applications*, Academic Press, San Diego.

ภาคผนวก ง

Abstract of The 2nd International Conference on Advances in Petrochemicals and Polymers

Use of Pt/N-Doped Titania for Photocatalytic Hydrogen Evolution from Water under Visible Light Irradiation

Laehsalee Siriporn ,[1] *Chavadej Sumaeth,*[1] *Yoshikawa Susumu,*[2] *and Sreethawong Thammanoon**[1]

[1]The Petroleum and Petrochemical College, Chulalongkorn University, Bangkok, Thailand
[2]Institute of Advanced Energy, Kyoto University, Japan

To date, there have been a multitude of studies on the production of hydrogen from direct water splitting using the most investigated semiconductor photocatalyst, titania (TiO_2), because hydrogen has been considered as a clean-burning fuel. Moreover, this process takes advantage of the utilization of available and abundant resources, water and sunlight, which is believed to be a sustainable source of future energy supply. However, TiO_2-composed systems require some modifications in order to improve the photocatalytic activity under visible light, which is the main portion of sunlight exposing the earth surface, such as anion doping of TiO_2. In this study, N-doped mesoporous TiO_2 and N-doped non-mesoporous commercial TiO_2, Degussa P-25, prepared at different N-doping content and calcination temperatures, as well as the effect of Pt loading were investigated for photocatalytic H_2 evolution under visible light irradiation. It was experimentally found that N-doped mesoporous TiO_2 prepared at a urea:TiO_2 molar ratio of 1:1 and a calcination temperature of 250°C exhibited the highest efficiency. For the N-doped P-25, the preparation conditions of the molar ratio of 0.5:1 and the temperature of 250°C is the best, but still less photocatalytically active than such the N-doped mesoporous TiO_2 prepared at optimum conditions. Pt loading onto the N-doped mesoporous TiO_2 via incipient wetness impregnation method was performed to improve the photocatalytic activity, exhibiting the optimum Pt loading content of 1.3 wt.%.

*thammanoon.s@chula.ac.th

ภาคผนวก จ

Proceedings of Chemeca 2007 Conference

MRG4980030

Photocatalytic Production of Hydrogen from Water over Pt/N-Doped Titania under Visible Light Irradiation

S. Laehsalee[a], T. Sreethawong[a*], S. Chavadej[a], and S. Yoshikawa [b]
[a]The Petroleum and Petrochemical College, Chulalongkorn University, Bangkok, Thailand
[b]Institute of Advanced Energy, Kyoto University, Kyoto, Japan
*E-mail: thammanoon.s@chula.ac.th

Abstract

To date, there have been a multitude of studies on the production of hydrogen from direct water splitting using the most investigated semiconductor photocatalyst, titania (TiO_2), because hydrogen has been considered as a clean-burning fuel. Moreover, this process takes advantage of the utilization of available and abundant resources, water and sunlight, which are believed to be sustainable sources of future energy supply. However, TiO_2-composed systems require some modifications in order to improve the photocatalytic activity under visible light, which is the main portion of sunlight exposing the earth surface, such as anion doping of TiO_2. In this study, the preparation of N-doped mesoporous TiO_2 and N-doped non-mesoporous commercial TiO_2, Degussa P-25, prepared at different N-doping content and calcination temperatures, as well as the effect of Pt loading, were investigated for photocatalytic H_2 evolution under visible light irradiation. It was experimentally found that N-doped mesoporous TiO_2 prepared at a urea:TiO_2 molar ratio of 1:1 and a calcination temperature of 250°C exhibited the highest efficiency. For the N-doped P-25, the preparation condition of the molar ratio of 0.5:1 and the temperature of 250°C is the best, but still less photocatalytically active than such the N-doped mesoporous TiO_2 prepared at the optimum conditions. Pt loading onto the N-doped mesoporous TiO_2 via incipient wetness impregnation method was performed to improve the photocatalytic activity, exhibiting the optimum Pt loading content of 1.3 wt.%.

1. INTRODUCTION

H_2 is considered to be an alternative fuel for replacing conventional energy resources, such as coal, natural gas, and fossil fuel, which are gradually depleting, because it is clean energy, unlike the conventional ones, which produce CO_2 that can cause global warming upon their combustion. The combustion of H_2 can generate energy, and the only by product is water or water vapor. Moreover, it can be used in many applications, especially a fuel for fuel cells.

The photocatalytic water splitting is a promising process for producing H_2 since water is used as reactant, which is an abundantly available substrate. Moreover, the solar energy as an energy resource is used for H_2 production from water. It is can be considered as an ideal process since the sunlight is also renewable resource. The photocatalytic H_2 evolution from water over photocatalyst can achieve when the photocatalyst directly absorbs light with energy equal or higher than its energy band gap, and then the electrons are excited from the valance band (VB) to the conduction band (CB) and reduce photons to H_2 molecules (Serpone & Pelizzetti, 1989; Hoffmann *et al*, 1995). Among various semiconductors, TiO_2 is the most investigated photocatalyst because it is chemically stable, non-corrosive, environmentally friendly, and cost-effective. Despite the positive attributes of TiO_2, there are few drawbacks associated with its use: (i) charge carrier recombination occurs easily and (ii) the band gap absorption does not allow the utilization of visible light. In order to solve the former problems, the combination with other technologies, such as noble metal loading and hole scavenger addition, are necessary. To improve visible light absorption ability of TiO_2, anion doping, such as nitrogen-doped TiO_2, is an effective method to enhance visible light response (Asahi *et al*, 2001).

The mesoporous materials have attracted much attention in the area of catalysis because of their large surface area and narrow pore size distribution (Rouquerol *et al*, 1999). The sol-gel process is an effective method for synthesis of mesoporous materials. Moreover, in combination with a surfactant template, the sol-

gel process allows the formation of mesoporous oxide with controlled porosity. In this study, the photocatalytic H_2 evolution from water by comparatively using N-doped mesoporous and N-doped non-mesoporous TiO_2 (commercial Degussa P-25 TiO_2) photocatalysts under visible light irradiation without and with Pt loading was investigated.

2. EXPERIMENTAL PROCEDURE

2.1. Materials

All chemicals/materials used in this research are a follows. Tetraisopropyl orthotitanate (TIPT, $Ti(OCH(CH_3)_2)_4$), (synthesis grade, MERCK), as Ti precursor and acetylacetone (ACA, $CH_3COCH_2COCH_3$), (synthesis grade, Rasayan), as a modifying ligand were used for synthesized TiO_2 photocatalyst. Laurylamine hydrochloride (LAHC, $CH_3(CH_2)_{11}NH_2{\cdot}HCl$), (synthesis grade, MERCK), was used as surfactant template to control porosity. Urea (NH_2CONH_2), (Laboratory Reagent, UNILAB), and hydrogen hexachloroplatinate (IV) hexahydrate ($H_2PtCl_6{\cdot}6H_2O$), (analytical grade, ALDRICH), were used as N and Pt sources, respectively. Methanol (CH_3OH), (Anhydroscan, LAB-SCAN Analytical Sciences), was used as hole scavenger or electron donor for photocatalytic H_2 evolution. Commercial Degussa P-25 TiO_2 was selected for comparative study of photocatalytic H_2 evolution.

2.2. Synthesis procedure

The nanocrystalline mesoporous TiO_2 photocatalyst was synthesized via the surfactant-assisted templating sol-gel method (Sreethawong *et al*, 2005). Firstly, tetraisopropyl orthotitanate (TIPT) as a titanium precursor was mixed with acetylacetone (ACA) at the molar ratio of unity. To control porosity, laurylamine hydrochloride (LAHC) aqueous solution was added into the TIPT/ACA solution with the molar ratio of TIPT to LAHC of 4. The mixture was continuously stirred at 40°C overnight to obtain transparent yellow sol. The gel was formed by placing the sol into the oven at 80°C for a week. Then, the gel was dried overnight at 80°C and then calcined at 500°C for 4 h to remove LAHC template and obtain nanocrystalline mesoporous TiO_2. After that, the synthesized mesoporous TiO_2 and Degussa P-25 TiO_2 powder was mixed with urea at various urea:TiO_2 molar ratios by using an agate mortar. The powders were then calcined at 200-300°C for 2 h. In order to improve the photocatalytic activity, Pt was loaded onto the N-doped TiO_2 photocatalyst via incipient wetness impregnation method and then calcined at 200°C for 6 h.

2.3. Characterization techniques

A nitrogen adsorption system (Quantachrome Autosorb 1) was employed to measure adsorption–desorption isotherms at liquid nitrogen temperature of -196°C. The Brunauer–Emmett–Teller (BET) and Barrett–Joyner–Halenda (BJH) approaches were utilized to determine specific surface area, mean pore size and pore size distribution. The sample was degassed at 150°C for 2 h to remove physisorbed gases prior to measurement. The sample morphology was observed by a transmission electron microscope (JEOL 2000CX) operated at 200 kV. X-ray diffraction (XRD) was used to identify the structure and composition of crystalline photocatalyst. A Rigaku RINT 2000 XRD system generating monochromated CuKα radiation with continuous scanning mode at the rate of 5°/min and operating conditions of 40 kV and 30 mA was used to obtain XRD patterns. A Shimadzu UV-2550 UV-Visible spectrophotometer was exploited to record diffuse reflectance spectra of the samples at room temperature with $BaSO_4$ as the reference. The surface composition was analyzed by an X-ray photoelectron spectroscope (XPS). A MgKα source emitting X-ray energy of 1253.6 eV was used as X-ray source.

2.4. Photocatalytic H_2 evolution system

A specified amount of all prepared photocatalysts (0.2 g), namely N-doped synthesized TiO_2, N-doped Degussa P-25, and Pt-loaded N-doped TiO_2, was suspended in an aqueous methanol solution (50 ml CH_3OH and 150 ml distilled water) by means of magnetic stirrer within a reactor made of Pyrex glass. The mixture was deaerated by purging with Ar gas for 45 min in dark environment. The reaction was started by exposing the mixture with visible light irradiation from a 300 W Xe arc lamp emitting light with wavelength longer than 400 nm. The gaseous H_2 evolved was periodically collected by a gas-tight syringe and analyzed by a gas chromatograph (GC) equipped with a thermal conductivity detector (TCD).

3. RESULTS AND DISCUSSION

3.1. Photocatalyst characterizations

To study mesoporous and non-mesoporous structures of the TiO_2 photocatalysts, N_2 adsorption-desorption analysis was used. The N_2 adsorption-desorption isotherms of the synthesized TiO_2 exhibited typical IUPAC type IV pattern with hysteresis loop, indicating mesoporous structure (Rouquerol *et al*, 1999), as shown in Figure 1. The pore size distribution is quite narrow with mean pore diameter in the mesopore region (pore diameter between 2-50 nm). For the commercial Degussa P-25 TiO_2, N_2 adsorption-desorption isotherms correspond to IUPAC type II pattern (Rouquerol *et al*, 1999), exhibiting non-mesoporous characteristics due to the absence of hysteresis loop, as shown in Figure 1. The pore size distribution is quite broad since their pore size distributions not only exist in the mesoporous region but also mostly cover the macropore with pore diameter larger than 50 nm.

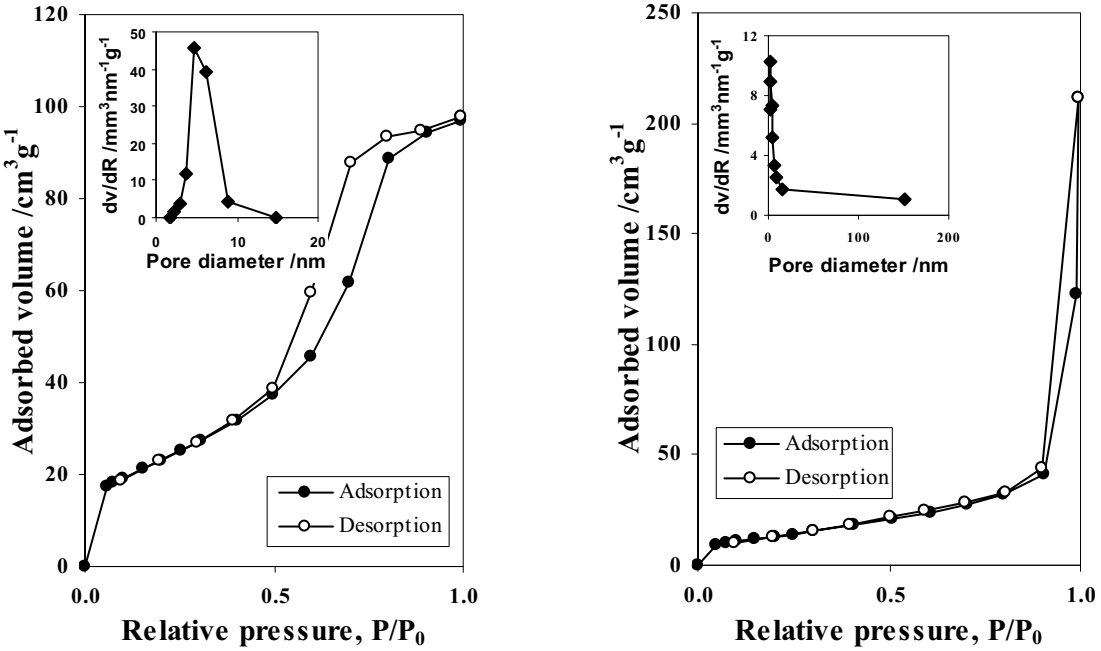

Figure 1 N_2 adsorption-desorption isotherms and (inset) pore size distribution of (left) the synthesized mesoporous TiO_2 calcined at 500°C for 4 h and (right) the commercial Degussa P-25 TiO_2.

To investigate the visible light absorption ability of the photocatalysts, UV-Vis spectroscopy was used. For pure mesoporous TiO_2, its absorption onset is approximately at 385 nm, corresponding to UV region. For the N-doped mesoporous TiO_2, the absorption band shifts to wavelength longer than 400 nm, corresponding to the visible region. So, the N-doping method can improve the visible light absorption ability of TiO_2. For the pure commercial Degussa P-25 TiO_2, the absorption onset begins at the wavelength longer

than 400 nm. Because the commercial Degussa P-25 TiO_2 possesses both anatase and rutile phases, their energy band gaps are approximately 3.2 and 3.0 eV for anatase and rutile TiO_2, respectively, which can help absorb both UV and visible regions. Consequently, the absorption onsets between pure and N-doped commercial Degussa P-25 TiO_2 are slightly different.

Surface area analysis was used to characterize the textural property of photocatalyst, as shown in Table 1. For all mesoporous and commercial Degussa P-25 TiO_2 photocatalysts, the surface area tended to decrease with increasing the urea:TiO_2 molar ratio at different calcination temperatures. The possible explanation is that the urea as N precursor can be decomposed to many components depending on temperature. Two main components are biuret and cyanuric acid (Schaber *et al*, 1999). The appearance of biuret and cyanuric acid affected to the decrease in the surface area. For the N-doped mesoporous TiO_2, the mean pore diameter was quite similar to the pure mesoporous TiO_2, and the total pore volume decreased with increasing urea:TiO_2 molar ratio. For the commercial Degussa P-25 TiO_2, the mean pore diameter and total pore volume are always not reported because it mostly consists of macropore with pore diameter larger than 50 nm.

Table 1. Summary of textural properties of the TiO_2 photocatalysts without and with N-doping prepared at various conditions

Calcination temperature/°C	Urea:TiO_2 molar ratio	BET surface area/m^2g^{-1}	Mean pore diameter/nm	Total pore volume/cm^3g^{-1}
	Pure mesoporous TiO_2	110.30	6.114	0.185
200	0.5:1	78.14	6.150	0.136
	1:1	35.36	6.156	0.070
	3:1	22.12	4.619	0.044
250	0.5:1	82.83	6.146	0.155
	1:1	38.52	6.129	0.080
	3:1	23.45	6.140	0.049
300	0.5:1	75.78	6.150	0.147
	1:1	73.98	6.161	0.137
	3:1	22.86	6.104	0.053
	Pure Degussa P-25 TiO_2	69.35	- [(a)]	- [(a)]
200	0.5:1	54.96	- [(a)]	- [(a)]
	1:1	53.26	- [(a)]	- [(a)]
	3:1	17.63	- [(a)]	- [(a)]
250	0.5:1	50.66	- [(a)]	- [(a)]
	1:1	44.63	- [(a)]	- [(a)]
	3:1	20.77	- [(a)]	- [(a)]
300	0.5:1	51.40	- [(a)]	- [(a)]
	1:1	26.21	- [(a)]	- [(a)]
	3:1	24.22	- [(a)]	- [(a)]

[(a)] N_2 adsorption-desorption isotherm corresponds to IUPAC type II pattern.

The formation of biuret and cyanuric acid was confirmed by XRD analysis, as shown in Figure 2. The dominant peak of all mesoporous TiO_2 is at about 25° (JCPDS Card No. 21-1272) (Smith, 1960), which exhibits anatase phase. For all commercial Degussa P-25 TiO_2, the dominant peaks are about at 25 and 27° (JCPDS Card No. 21-1276) (Smith, 1960), which exhibit both anatase and rutile phases, respectively. At temperature of 200°C, the biuret formation was first clearly observed. At temperature of 250°C, the cyanuric acid was initially formed. At 300°C, the cyanuric acid formation was highly observed, and the biuret formation was observed with relatively less amount when compared to the temperature of 250°C at the same molar ratio of urea to titania. These results indicate that the cyanuric acid was formed at a temperature higher than 200°C, above which the biuret started decomposing.

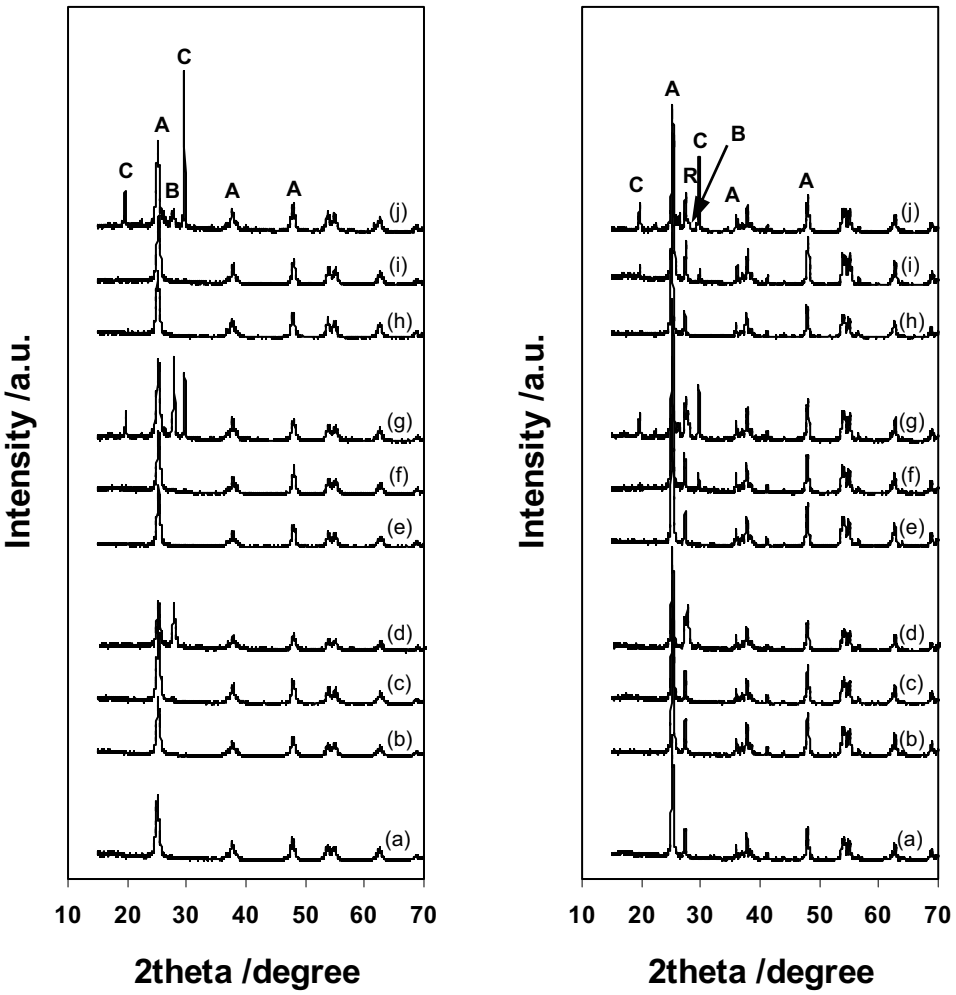

Figure 2 XRD patterns of (left) mesoporous TiO_2 and (right) commercial Degussa P-25 TiO_2: (a) pure TiO_2, and (b)-(d) N-doped TiO_2 with different urea:TiO_2 molar ratios of 0.5:1, 1:1, and, 3:1, respectively, prepared at calcination conditions of 200°C for 2 h, (e)-(g) urea:TiO_2 molar ratios of 0.5:1, 1:1, and, 3:1, respectively, at 250°C for 2 h, (h)-(j) urea:TiO_2 molar ratios of 0.5:1, 1:1, and, 3:1, respectively, at 300°C for 2 h (A: Anatase TiO_2, R: Rutile, B: Biuret, C: Cyanuric acid).

To determine the surface N content and oxidation state, XPS analysis was used. It can be found that the surface N content increased with increasing the urea:TiO_2 molar ratio for both the mesoporous TiO_2 and commercial Degussa P-25 due to the presence of higher amount of urea molecules as to increase the doping capability, as shown in Table 2.

Table 2 The summary of surface N content of N-doped photocatalyst

Calcination temperature/°C	Urea:mesoporous TiO_2 molar ratio	Surface N content/wt%	Urea:Degussa P-25 molar ratio	Surface N content/wt%
	Pure mesoporous TiO_2	4.72	Pure Degussa P-25 TiO_2	2.59
200	0.5:1	5.77	0.5:1	3.96
	1:1	20.11	1:1	5.01
	3:1	21.28	3:1	7.73
250	0.5:1	8.70	0.5:1	3.21
	1:1	26.23	1:1	4.68
	3:1	32.61	3:1	7.93
300	0.5:1	7.11	0.5:1	2.35
	1:1	11.23	1:1	2.91
	3:1	30.25	3:1	7.17

3.2. Photocatalytic H_2 evolution results

For photocatalytic H_2 evolution study, the photocatalytic activity in the absence of light irradiation, photocatalyst, or methanol was initially studied. It was found that there was no detectable H_2 evolution in the absence of them, indicating that all of them are necessarily important for the photocatalytic H_2 evolution. The highest H_2 evolution activities of N-doped mesoporous TiO_2 and N-doped Degussa P-25 TiO_2 were obtained at the urea:TiO_2 molar ratio of 1:1 prepared at a calcination temperature of 250°C and 0.5:1 with a calcination temperature 250°C, respectively, as shown in Figure 3. Interestingly, the mesoporous one gave better photocatalytic activity. So, the mesoporous TiO_2 prepared at this optimum condition was taken to study the effect of Pt cocatalyst loading in order to improve the H_2 evolution activity of the system. The Pt was loaded onto the TiO_2 photocatalyst by using incipient wetness impregnation method. In order to understand the role of Pt, the brief mechanism of photocatalytic H_2 evolution over Pt/TiO_2 is first explained. The reaction is initiated by the photoexcitation of TiO_2 particles, which leads to the formation of electron hole pairs. Photogenerated conduction band electrons can be transferred to electron acceptor, H^+. With Pt on TiO_2 photocatalyst, Pt can rapidly trap electrons, and hydrogen can be produced on Pt by reduction reaction. Likewise, valence band holes can be filled by the electron donor, CH_3OH, resulting in the great prevention of photoinduced charge recombination (Kawai & Sakata, 1980; Bamwenda *et al*, 1995).

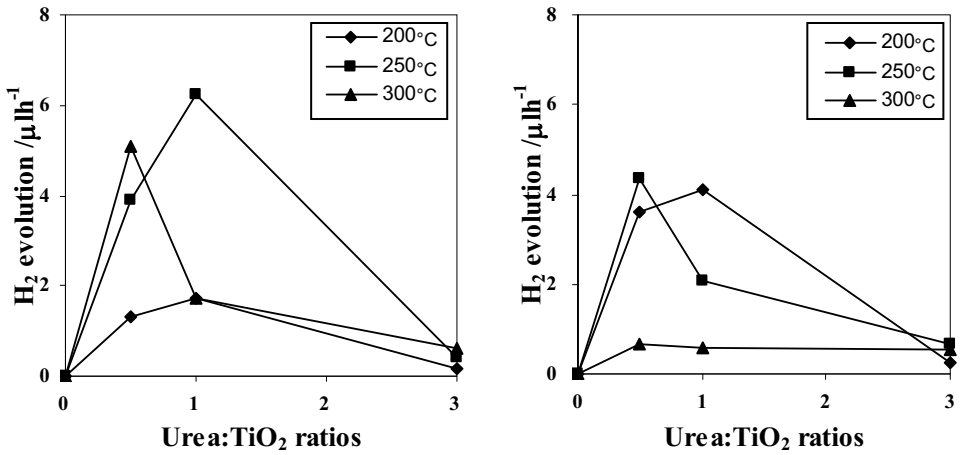

Figure 3 The H_2 evolution of (left) N-doped mesoporous TiO_2 and (right) N-doped commercial Degussa P-25 TiO_2 with different urea:TiO_2 molar ratios of 0.5:1, 1:1, and 3:1 prepared at different calcination temperatures of 200, 250, and 300°C (Reaction conditions: photocatalyst, 0.2 g; distilled water, 150 ml; methanol, 50 ml; and irradiation time, 5 h).

The H_2 evolution activity significantly increased with increasing the nominal Pt loading content up to 1.3 wt.%, then after this optimum point, the H_2 evolution activity decreased, as shown in Table 3. This result can be related to surface Pt content, which was analyzed by XPS, and it was found that the surface Pt content also reached the maximum at the nominal Pt content of 1.3 wt.%. The possible explanation is that TiO_2 particles may carry more Pt nanoclusters, which are very important for the removal of photogenerated electrons from TiO_2 for the reduction reaction and lead to an increase of the photocatalytic activity. After reaching a maximum, the H_2 evolution activity decreased due to too much Pt nanoclusters on TiO_2. These clusters would shield the photosensitive TiO_2 surface, and subsequently reduce the surface concentration of the electrons and holes available for the reactions. Another explanation is that at high metal loadings, the deposited metal particles may act as the recombination centers for the photoinduced species (Courbon *et al*, 1984).

Table 3. Summary of the effect of Pt loading onto N-doped mesoporous TiO_2 on surface Pt content and photocatalytic H_2 evolution (Reaction conditions: photocatalyst, 0.2 g; distilled water, 150 ml; methanol, 50 ml; and irradiation time, 5 h)

Nominal Pt loading/wt%	Surface Pt content/wt%	H_2 evolution/μlh^{-1}
0	0	6.23
0.4	0.80	8.05
0.8	3.69	15.19
1.0	3.23	17.89
1.1	3.30	17.95
1.3	4.73	26.40
1.4	3.25	11.75
1.6	3.71	8.04

4. CONCLUSIONS

In this work, two types of TiO_2 photocatalyst, the mesoporous TiO_2 synthesized by surfactant-assisted tempting sol-gel method and commercial Degussa P-25 TiO_2, were comparatively used for photocatalytic H_2 evolution under visible light irradiation in a form of N-doped TiO_2. The results of N_2 adsorption-desorption analysis revealed that the synthesized TiO_2 photocatalyst possessed mesoporous structure (mesopore size between 2-50 nm), whereas the commercial Degussa P-25 TiO_2 possessed non-mesoporous structure. To modify the visible light absorption ability of TiO_2 photocatalyst, N-doping onto TiO_2 photocatalyst was performed. The urea as a source of N was mixed with the TiO_2 photocatalysts at various urea:TiO_2 molar ratios and calcined at various calcination temperatures. The optimum preparation conditions of the N-doped mesoporous and Degussa P-25 TiO_2 were the urea:TiO_2 molar ratio of 1:1 at calcination temperature of 250°C and 0.5:1 at calcination temperature of 250°C, respectively. However, the N-doped mesoporous TiO_2 prepared at such the optimum condition exhibited the best H_2 evolution activity. To improve the photocatalytic H_2 evolution activity, Pt was loaded onto this N-doped mesoporous TiO_2 by incipient wetness impregnation method. The optimum Pt loading content was 1.3 wt%, providing the highest photocatalytic H_2 evolution activity. It was clearly found that the surface Pt content greatly influenced on the H_2 evolution activity.

5. ACKNOWLEDGMENTS

This work was financially supported by grants provided by Thailand Research Fund (TRF) (Contract/Grant No. MRG4980030) and by Chulalongkorn University, Thailand, through the Grants for Development of New Faculty Staff under the Ratchadapisek Somphot Endowment Fund (Contract/Grant No. 100/2549). Research facilities for this work was provided by the National Excellence Center for Petroleum, Petrochemicals, and Advanced Materials, Thailand, and The Research Unit of Applied surfactants for

Separation and Pollution Control, The Rachadapisek Somphote Fund, Chulalongkorn University, Thailand.

6. REFERENCES

Asahi, R., Morikawa, T., Ohwaki, T., Aoki, K., and Taga, Y. (2001), *Visible-Light Photocatalysis in Nitrogen-Doped Titanium Oxides,* Science, 293, 269–271.

Bamwenda, G.R., Tsubota, S., Nakamura, T., and Haruta, M. (1995), *Photoassisted hydrogen production from a waterethanol solution: a comparison of activities of Au-TiO_2 and Pt-TiO_2*, J. Photochem. Photobiol. A: Photochem., 89, 177–189.

Courbon, H., Herrmann, J.M., and Pichat, P. (1984), *Effect of platinum deposits on oxygen-adsorption and oxygen isotope exchange over variously pretreated, ultraviolet-illuminated powder TiO_2,* J. Phys. Chem. B., 88, 5210-5214.

Hoffmann, M.R., Martin, S.T., Choi, W., and Bahnemann, D.W. (1995), *Environmental applications of semiconductor photocatalysis*, Chem Rev., 95, 69-96.

Kawai, T., and Sakata, T. (1980), *Photocatalytic hydrogen production from liquid methanol and water*, Chem. Commun., 15, 694-695.

Rouquerol, F., Rouquerol, J., Sing, K. (1999), *Adsorption by Powders and Porous Solid: Principle, Methodology and Applications,* Academic Press, San Diego.

Schaber, P.M., Colson, J., Higgins, S., Thielen, D., Anspach, B. and Brauer, J. (1999), *Study of the urea thermal decomposition (pyrolysis) reaction and importance to cyanuric acid production*, Am. Lab., 13-21.

Serpone, N., and Pelizzetti, E. (1989), *Photocatalysis: Fundamentals and Applications*, Wiley, New York.

Smith (Ed.), J.V. (1960), *X-ray Powder Data File*, American Society for Testing Materials.

Sreethawong, T., Suzuki, Y., and Yoshikawa, S. (2005), *Synthesis, characterization, and photocatalytic activity for hydrogen evolution of nanocrystalline mesoporous titania prepared by surfactant-assisted templating sol–gel process*, J. Solid State Chem., 178, 329-338.